POLE PLACEMENT AND REDUCED-ORDER MODELLING FOR TIME-DELAYED SYSTEMS USING GALERKIN APPROXIMATIONS

A Thesis Submitted
in Partial Fulfillment of the Requirements for
the Degree of

Doctor of Philosophy

by

SHANTI SWAROOP KANDALA

भारतीय प्रौद्योगिकी संस्थान हैदराबाद
Indian Institute of Technology Hyderabad

to the

Department of Mechanical and Aerospace Engineering
Indian Institute of Technology Hyderabad

December 2019

Declaration

I declare that this thesis titled ***Pole Placement and Reduced-Order Modelling for Time-Delayed Systems Using Galerkin Approximations*** represents my own ideas and words and where others ideas or words have been included; I have adequately cited and referenced the original sources. I also declare that I have adhered to all principles of academic honesty and integrity and have not misrepresented, fabricated or falsified any idea/data/fact/ source in my submission. I understand that any violation of the above will result in disciplinary action by the Institute and can also evoke penal action from the sources that have not been properly cited or from whom proper permission has not been taken when needed.

Signature of candidate

K. Shanti Swaroop.

Shanti Swaroop Kandala

ME14RESCH01001

Approval Sheet

This thesis entitled ***Pole Placement and Reduced-Order Modelling for Time-Delayed Systems Using Galerkin Approximations*** by ***Mr. Shanti Swaroop Kandala*** is approved for the degree of ***Doctor of Philosophy*** from ***Indian Institute of Technology Hyderabad.***

V.C.Prakash

Dr. Chandrika Prakash Vyasarayani (Supervisor)
Department of Mechanical and Aerospace Engineering
Indian Institute of Technology Hyderabad

R. Prasanth Kumar

Prof. R. Prasanth Kumar (Internal Examiner)
Department of Mechanical and Aerospace Engineering
Indian Institute of Technology Hyderabad

Dr. K. Siva Kumar (Chairman)
Department of Electrical Engineering
Indian Institute of Technology Hyderabad

C.S. Shankaram 20/12/2019

Prof. C. S. Shankar Ram (External Examiner)
Department of Engineering Design
Indian Institute of Technology Madras

Acknowledgements

With the sincerest of regards, I take this opportunity to express my gratitude to my supervisor, Dr. Chandrika Prakash Vyasarayani, for his expert guidance, continuous motivation, and mentorship. He was not only there for me as an advisor, but also there for me whenever I needed any personal suggestion. Today when I look back, I cannot imagine my doctoral journey without him being an integral part of it.

My sincere thanks to all my committee members, Prof. Vinayak Eswaran, Prof. Prasanth Kumar, and Dr. Ketan P. Detroja, for their valuable time, insightful suggestions, and motivation. I also thank Dr. Karri Badarinath for being there with me in troubled times and seeing me grow into a professional. My sincere thanks to Dr. Kishalay Mitra for his constant encouragement and motivational conversations.

I want to acknowledge the financial support received from the Ministry of Human Resource Development, Government of India, during my Ph. D., and the Departments of Mechanical and Aerospace engineering, and Electrical engineering for providing the required resources for hassle-free research.

My journey would have been incomplete without my labmates. I take this opportunity to thank fellow labmates Ajinkya, Dr. Anwar, Ashwanth, Damodar, Junaid, Lala Bahadur, Naresh, Nitish, Sayan, Sumit, Surya, Varun and Zaid for creating a conducive atmosphere for research. In particular, I would like to thank my friends, Dr. Rakesh, Himabindu, Meenu, Dr. Sishir, Dr. Swetha and Akshita who have always been there with me.

Lastly, there are these people in my life who shaped me and influenced me in every walk of life. I want to thank my friend, Dr. Manasa, for always prodding me to come out of my comfort zone and being just a call away. My wife, Sravani, for being a part of my roller-coaster ride and standing by my side through the thick and thin of times. My sisters, Bhavya and Sravya, who always had ears to listen to my journey and have pushed me to take that one extra step every time. My parents, for letting me build a career based on my interests and ensuring that I give my best in all the walks of life.

Nothing is complete without thanking the Lord Venkateshwara for his divine blessings throughout my life.

Shanti Swaroop Kandala

Abstract

The dynamics of time-delayed systems (TDS) are governed by delay differential equations (DDEs), which are infinite dimensional and pose computational challenges. The Galerkin approximation method is one of several techniques to obtain the spectrum of DDEs for stability and stabilization studies. In the literature, Galerkin approximations for DDEs have primarily dealt with second-order TDS (second-order Galerkin method), and the formulations have resulted in *spurious* roots, i.e., roots that are not among the characteristic roots of the DDE. Although these spurious roots do not affect stability studies, they nevertheless add to the complexity and computation time for control and reduced-order modelling studies of DDEs. A refined mathematical model, called the first-order Galerkin method, is proposed to avoid spurious roots, and the subtle differences between the two formulations (second-order and first-order Galerkin methods) are highlighted with examples.

For embedding the boundary conditions in the first-order Galerkin method, a new pseudoinverse-based technique is developed. This method not only gives the exact location of the rightmost root but also, on average, has a higher number of converged roots when compared to the existing pseudospectral differencing method. The proposed method is combined with an optimization framework to develop a pole-placement technique for DDEs to design closed-loop feedback gains that stabilize TDS. A rotary inverted pendulum system apparatus with inherent sensing delays as well as deliberately introduced time delays is used to experimentally validate the Galerkin approximation-based optimization framework for the pole placement of DDEs.

Optimization-based techniques cannot always place the rightmost root at the desired location; also, one has no control over the placement of the next set of rightmost roots. However, one has the precise location of the rightmost root. To overcome this, a pole-placement technique for second-order TDS is proposed, which combines the strengths of the method of receptances and an optimization-based strategy. When the method of receptances provides an unsatisfactory solution, particle swarm optimization is used to improve the location of the rightmost pole. The proposed approach is demonstrated with numerical studies and is validated experimentally using a 3D hovercraft apparatus.

The Galerkin approximation method contains both converged and unconverged roots of the DDE. By using only the information about the converged roots and applying the eigenvalue decomposition, one obtains an r-dimensional reduced-order model (ROM) of the DDE. To analyze the dynamics of DDEs, we first choose an appropriate value for r; we then select the minimum value of the order of the Galerkin approximation method system at which at least r roots converge. By judiciously selecting r, solutions of the ROM and the original DDE are found to match closely. Finally, an r-dimensional ROM of a 3D hovercraft apparatus in the presence of delay is validated experimentally.

List of Publications

Journals

1. **Kandala, S. S.**, Samukham, S., Uchida, T. K., and Vyasarayani, C. P., "Spurious roots of delay differential equations using Galerkin approximations", Journal of Vibration and Control, 2019 (accepted)

2. **Kandala, S. S.**, Uchida, T. K., and Vyasarayani, C. P., "Pole placement for time-delayed systems using Galerkin approximations", *ASME Journal of Dynamic Systems, Measurement and Control*, vol. 141, no. 5, p. 051012, 2019

3. **Kandala, S. S.**, Chakraborty, S., Uchida, T. K., and Vyasarayani, C. P., "Hybrid method-of-receptances and optimization-based technique for pole placement in time-delayed systems", *International Journal of Dynamics and Control*, pp. 1–12, 2019

4. Chakraborty, S., **Kandala, S. S.***, and Vyasarayani, C.P., "Reduced ordered modelling of time delay systems using Galerkin approximations and eigenvalue decomposition", *International Journal of Dynamics and Control*, vol. 7, no. 3, pp. 1065–1083, 2019 (* - equal contribution)

Conferences

1. **Kandala, S. S.**, Chakraborty, S., and Vyasarayani, C. P., "Comparing method of receptances and optimization-based techniques for pole-placement of time-delayed systems", *Indian Control Conference*, New Delhi, India, 2019

2. Chakraborty, S., **Kandala, S. S.***, and Vyasarayani, C. P., "Reduced ordered modelling of time delay systems using Galerkin approximations and eigenvalue decomposition", 5^{th} *IFAC International Conference in Advances in Control and Optimization of Dynamical Systems*, IFACPapersOnLine 51(1), 566-571, Hyderabad, India, 2018

3. **Kandala, S. S.**, and Vyasarayani, C. P., "Pole placement for time-delayed systems using Galerkin approximations", *European Nonlinear Dynamics Conference (ENOC)*, ID 447, (ISBN 978-963-12-9168-1), Hungary, Budapest, 2017

Contents

List of Figures

List of Tables

List of Abbreviations

DDE	Delay differential equation
DPA	Dominant pole algorithm
EVD	Eigenvalue decomposition
FOG	Full-Order Galerkin
FOTF	Full-order transfer function
GETF	Galerkin eigenvalue decomposed transfer function
GEVD	Galerkin eigenvalue decomposed
LTI	Linear time-invariant
MIMO	Multi-input multi-output
MoR	Method of receptances
ODE	Ordinary differential equation
PDE	Partial differential equation
PQEAP	Partial quadratic eigenvalue assignment problem
PSD	Pseudospectral differencing
PSO	Particle swarm optimization
QPmR	Quasi-polynomial root-finder
ROM	Reduced-order model
SISO	Single-input single-output
TAI	Thermoacoustic instability
TDS	Time-delayed system

Chapter 1

Introduction

A control system is a subsystem comprising sensors, actuators, and controllers that helps in obtaining a desired output. Many modern-day applications are unimaginable without the presence of control systems. Some examples include anti-lock braking systems, sorting robots in warehouses, rocket guidance systems, heating systems, and autonomous vehicles.

There are two main kinds of control system configuration, namely open-loop and closed-loop systems. In an open-loop control system, also referred to as a non-feedback system, the input signal is not affected by the output of the system. On the other hand, in a closed-loop control system, also known as a feedback control system, the output of the system is either totally or partially fed back into the system, which influences the input to the controller.

In literature, there are two approaches for the analysis and design of control systems: classical or frequency-domain modelling, and modern or time-domain modelling (also referred to as state-space modelling). With the advent of complex control systems and their demanding nature, time-domain modelling, which has many advantages over frequency-domain modelling, has gained traction. According to [3], "The state-space approach (also referred to as the modern, or time-domain, approach) is a unified method for modelling, analyzing, and designing a wide range of systems."

To control the dynamics of a system effectively, it is necessary to first develop a mathematical model of its behavior. Defining $\mathbf{A}$ as the system/state transition matrix, $\mathbf{B}$ as the input matrix, $\mathbf{C}$ as the output matrix and $\mathbf{D}$ as the feedforward matrix, the linearized system dynamics around an operating point can be represented

in state-space form as follows:

$$\dot{\mathbf{x}}(t) = \mathbf{A}\mathbf{x}(t) + \mathbf{B}\mathbf{u}(t), \tag{1.1a}$$

$$\mathbf{y}(t) = \mathbf{C}\mathbf{x}(t) + \mathbf{D}\mathbf{u}(t), \tag{1.1b}$$

where $\mathbf{x}(t)$ is the state vector, $\dot{\mathbf{x}}(t)$ is its time derivative, $\mathbf{y}(t)$ is the output vector, and $\mathbf{u}(t)$ is the input or control vector. To understand the stability characteristics of the system represented by Eqs. (1.1a) and (1.1b), the eigenvalues of the state matrix $\mathbf{A}$ must be obtained. If the eigenvalues of $\mathbf{A}$ lie in the left half of the complex plane, the system is stable. If at least one of the eigenvalues of $\mathbf{A}$ is in the right half of the complex plane, then the system is unstable.

Consider an n^{th}-order system represented in state-space form as follows:

$$\dot{\mathbf{x}}(t) = \mathbf{A}\mathbf{x}(t) + \mathbf{B}\mathbf{u}(t), \tag{1.2a}$$

$$\mathbf{y}(t) = \mathbf{C}\mathbf{x}(t), \tag{1.2b}$$

where $\mathbf{x}(t) \in \mathbb{R}^{n\times 1}$, $\mathbf{A} \in \mathbb{R}^{n\times n}$, and $\mathbf{B} \in \mathbb{R}^{n\times m}$. In order to stabilize the system represented by Eqs. (1.2a) and (1.2b), it must be controllable. A system is said to be controllable "if an input to a system can be found that takes every state variable from a desired initial state to a desired final state"; otherwise, the system is uncontrollable [3]. If the rank of the controllability matrix $\mathbf{C_M} \triangleq [\mathbf{B} \quad \mathbf{AB} \quad \mathbf{A^2B} \quad \cdots \quad \mathbf{A}^{n-1}\mathbf{B}]$ is n, then the system represented by Eqs. (1.2a) and (1.2b) is controllable. For systems in which $\mathbf{C_M}$ is of rank n, a control vector of the form $\mathbf{u}(t) = -\mathbf{K}^{\mathrm{T}}\mathbf{x}(t)$, where $\mathbf{K}$ is the feedback vector, can be found to control the system. The feedback vector $\mathbf{K}$ can be obtained using the pole-placement (full state feedback) technique or the optimal control technique. In this thesis, the pole-placement technique is employed to obtain $\mathbf{K}$. The pole-placement technique for ordinary differential equations (ODEs) is explained briefly in the next section.

1.1 Pole placement for ODEs

The pole-placement technique forms the basis of this thesis, and is explained here. Consider a spring-mass-damper system as shown in Fig. 1.1.

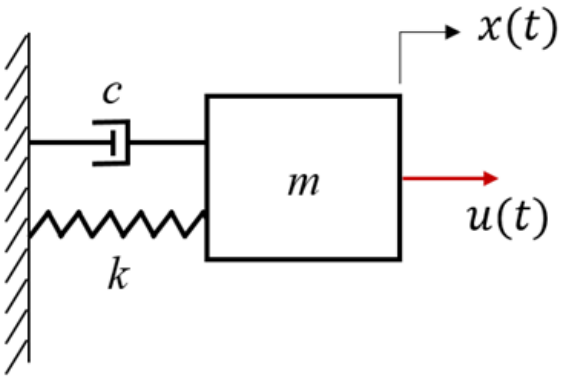

FIGURE 1.1: Spring-mass-damper system.

The linearized dynamics of the spring-mass-damper system shown in Fig. 1.1 are governed by:

$$m\ddot{x}(t) + c\dot{x}(t) + kx(t) = u(t), \tag{1.3}$$

where m is the mass, c is the damping coefficient, and k is the spring constant. Defining $\mathbf{x}(t) \triangleq [x(t),\ \dot{x}(t)]^{\mathrm{T}}$, Eq. (1.3) can be written as a system of two first-order ODEs as follows:

$$\dot{\mathbf{x}}(t) = \begin{bmatrix} 0 & 1 \\ -\frac{k}{m} & -\frac{c}{m} \end{bmatrix} \mathbf{x}(t) + \begin{bmatrix} 0 \\ \frac{1}{m} \end{bmatrix} \mathbf{u}(t) \Longrightarrow \dot{\mathbf{x}}(t) = \mathbf{A}\mathbf{x}(t) + \mathbf{B}\mathbf{u}(t). \tag{1.4}$$

Defining $m = 1$, $c = 0.5$ and $k = 1.5$, Eq. (1.4) can be written as:

$$\dot{\mathbf{x}}(t) = \begin{bmatrix} 0 & 1 \\ -1.5 & -0.5 \end{bmatrix} \mathbf{x}(t) + \begin{bmatrix} 0 \\ 1 \end{bmatrix} \mathbf{u}(t). \tag{1.5}$$

The eigenvalues of $\mathbf{A}$ are located at 1.5 and -1 and, hence, the system is unstable. The system is controllable as the rank of $\mathbf{C_M} = [\mathbf{B}\ \ \mathbf{AB}]$ is 2. We define $\mathbf{K} = [k_1,\ k_2]^{\mathrm{T}}$ such that $\mathbf{u}(t) = -\mathbf{K}^{\mathrm{T}}\mathbf{x}(t)$, where k_1 and k_2 are the feedback gains for the displacement and velocity feedback, respectively. Equation (1.4) can then be written as follows:

$$\dot{\mathbf{x}}(t) = [\mathbf{A} - \mathbf{B}\mathbf{K}^{\mathrm{T}}]\mathbf{x}(t) \Longrightarrow \dot{\mathbf{x}}(t) = \begin{bmatrix} 0 & 1 \\ -1.5 - k_1 & -0.5 - k_2 \end{bmatrix} \mathbf{x}(t). \tag{1.6}$$

Defining the closed-loop pole locations of Eq. (1.6) to be $-1 \pm i$ and using the Ackermann's formula [3], the values of k_1 and k_2 are obtained as 0.5 and 1.5, respectively. The procedure described above is one of the various possible pole-placement techniques for the systems governed by ODEs [3].

Now, consider $u(t)$ of the form $u(t-\tau)$ in Eq. (1.3), where τ is a time delay. The delay τ can arise due to lags in sensing, communication, and actuation. Systems that have a delay are called time-delayed systems (TDS) and their governing equations are delay differential equations (DDEs). TDS are also referred to as systems with aftereffect or dead-time, hereditary systems, equations with deviating argument, or differential-difference equations [4]. Due to the delay τ, the control input now becomes $\mathbf{u}(t-\tau) = -\mathbf{K}^{\mathrm{T}}\mathbf{x}(t-\tau)$.

Substituting $\mathbf{u}(t-\tau)$ in Eq. (1.5), we get:

$$\dot{\mathbf{x}}(t) = \begin{bmatrix} 0 & 1 \\ -1.5 & -0.5 \end{bmatrix} \mathbf{x}(t) + \begin{bmatrix} 0 & 0 \\ -k_1 & -k_2 \end{bmatrix} \mathbf{x}(t-\tau). \tag{1.7}$$

Substituting $\mathbf{x}(t) = \mathbf{x}_0 e^{\lambda t}$ in Eq. (1.7) and equating the determinant to zero, we get:

$$\det\left(\lambda\mathbf{I} - \mathbf{A} - \mathbf{B}\mathbf{K}^{\mathrm{T}} e^{-\lambda\tau}\right) = 0. \tag{1.8}$$

Equation (1.8) has infinitely many roots due to the presence of the transcendental term $e^{-\lambda\tau}$. The infinite dimensionality of Eq. (1.8) can be easily understood by using the Taylor series expansion for the transcendental term $e^{-\lambda\tau}$. Expanding $e^{-\lambda\tau}$ about $\tau = 0$ using the Taylor series, Eq. (1.8) can be written as:

$$\det\left(\lambda\mathbf{I} - \mathbf{A} - \mathbf{B}\mathbf{K}^{\mathrm{T}}\left(1 - \lambda\tau + \frac{\lambda^2\tau^2}{2} - \frac{\lambda^3\tau^3}{6} + \frac{\lambda^4\tau^4}{24} \mp \ldots + (-1)^n \frac{\lambda^n\tau^n}{n!} + \ldots\right)\right) = 0. \tag{1.9}$$

Equation (1.9) has infinitely many roots and, hence, has infinite dimensionality. However, as can be seen from Eq. (1.8), we have only a finite number of parameters k_1 and k_2 to control an infinite-dimensional system using the pole-placement technique. Hence, pole placement for systems governed by DDEs is a challenging and complex task [5–7].

Many practical systems and dynamic processes can be aptly described as time-delayed systems. As shown in Eq. (1.7), for a TDS, time derivatives of the state variables are explicit functions of past states. Some of the problems in which time delays play an important role are control of human balance with reflex delays [8–12], thermoacoustic instability (TAI) in combustion systems [13–17], robotics [18], machining processes [18–23], vibrations of heat-exchanger tubes under cross-flow [24, 25], feedback-controller systems [26–29], population dynamics [30, 31], neural networks [32–34], shimmy dynamics [35–37], and traffic flow dynamics [38–41]. Next, the challenges

associated with pole placement for a TDS are explained using a spring-mass-damper system (see Fig. 1.1) that is governed by a second-order DDE.

1.1.1 Example of a TDS

In the absence of time delay ($\tau = 0$), by selecting $k_1 = 0.5$ and $k_2 = 1.5$, the closed-loop poles of Eq. (1.6) can be placed at $-1 \pm i$. In this section, the effect of delay τ on the system dynamics is explored. Considering $\mathbf{u}(t-\tau) = -\mathbf{K}^{\mathrm{T}}\mathbf{x}(t-\tau)$, Eq. (1.7) can be written as:

$$\dot{\mathbf{x}}(t) = \begin{bmatrix} 0 & 1 \\ -1.5 & -0.5 \end{bmatrix} \mathbf{x}(t) + \begin{bmatrix} 0 & 0 \\ -0.5 & -1.5 \end{bmatrix} \mathbf{x}(t-\tau). \tag{1.10}$$

The characteristic equation is obtained by substituting $\mathbf{x}(t) = \mathbf{x}_0 e^{\lambda t}$ in Eq. (1.10) and equating the determinant to zero as follows:

$$\det\left(\lambda\mathbf{I} - \mathbf{A} - \mathbf{B}\mathbf{K}^{\mathrm{T}} e^{-\lambda\tau}\right) = 0. \tag{1.11}$$

Equation (1.11) is infinite dimensional. Figures 1.2(a) and 1.2(b) show the time responses of Eq. (1.10) for $\tau = 0.5$ and $\tau = 1$ respectively. It can be seen that a small variation in τ affects the stability and dynamics of the system substantially. Figures 1.3(a) and 1.3(b) show the first few rightmost roots of Eq. (1.10) for $\tau = 0.5$ and $\tau = 1$, respectively. The system is stable for $\tau = 0.5$ (see Fig. 1.3(a)) but unstable for $\tau = 1$ (see Fig. 1.3(b)). It should be noted that only k_1 and k_2 can be varied to control the infinite-dimensional system and that, for a DDE to be stable, the rightmost root must be in the left half of the complex plane.

In the above example, the delay τ is constant. However, τ can also be time varying, for instance time periodic. The knowledge of the rightmost root of a DDE is imperative to perform control studies or develop finite-dimensional (reduced-order) models since the DDE is stable only if its rightmost root is in the left half of the complex plane.

The above example clearly illustrates the necessity to obtain the spectrum (characteristic roots) of DDEs for performing control studies; it is also important for developing the reduced-order models (ROMs). The next section focuses on the literature covering various techniques to obtain the spectrum of DDEs, their control strategies, and development of reduced-order models.

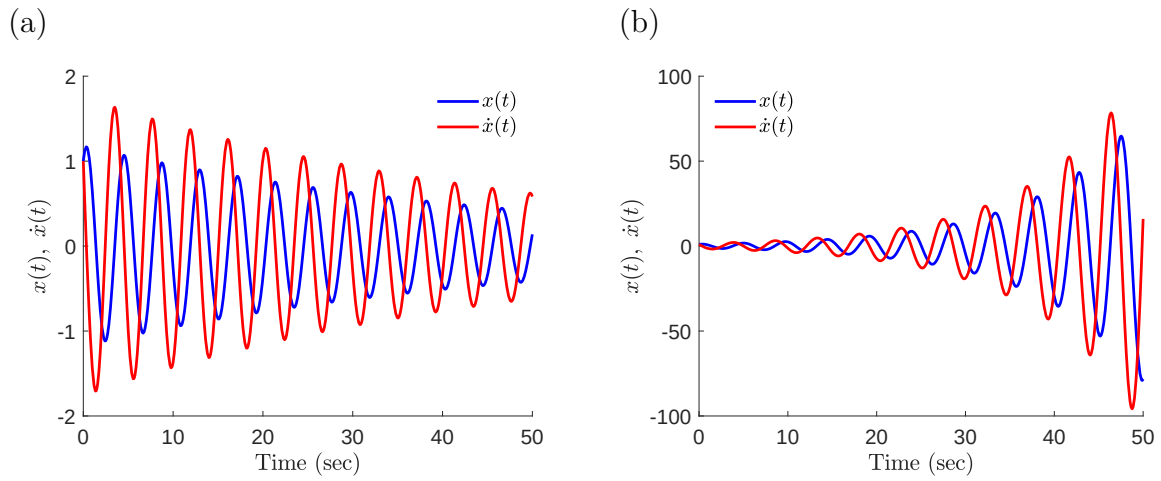

FIGURE 1.2: Time response of the spring-mass-damper system given by Eq. (1.10) with delays (a) $\tau = 0.5$ and (b) $\tau = 1$.

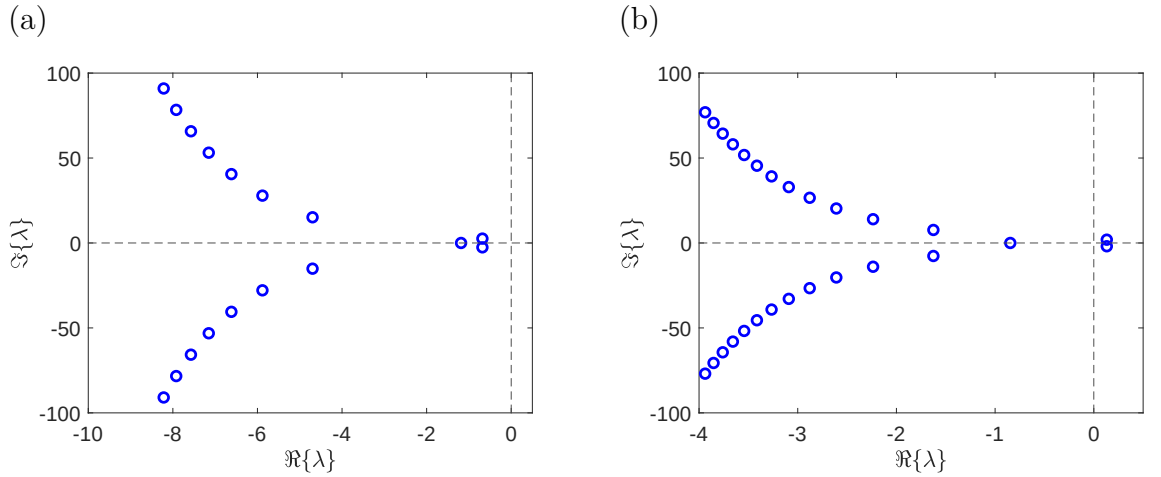

FIGURE 1.3: Characteristic roots of the spring-mass-damper system given by Eq. (1.10) with delays (a) $\tau = 0.5$ and (b) $\tau = 1$.

1.2 Literature review

Over the past few decades, researchers have carried out studies to gain a better understanding of the stability, stabilization, and reduced-order modelling of TDS/DDEs. In this section, we present a review of past work to obtain the characteristic roots of DDEs, to stabilize a DDE (with constant/discrete delays), and to understand the dynamics of DDEs by reducing them to finite-dimensional systems.

1.2.1 Spectrum of DDEs

The spring-mass-damper system, as explained in Section 1.1.1, clearly demonstrates the need to study the spectrum of a DDE to understand its stability characteristics. This section explores the various methods used to obtain the spectrum of DDEs. Several methods exist for analyzing the stability of DDEs with constant/discrete delays, including the Lambert-W function [5, 42–45], Galerkin approximations [46–49], Laplace transforms [50], semi-discretization [51], pseudo-spectral collocation [52–54], time finite elements [55, 56], continuous-time approximation [57, 58], and finite-difference methods [59, 60]. Recently, Pekař and Gao have presented an exhaustive list of various methods to study the stability of DDEs with constant/discrete/distributed delays [61]. The Galerkin approximation and pseudo-spectral collocation methods fall under the broad category of spectral methods. A key advantage of spectral methods is the convergence property of the approximate eigenvalues – specifically, the rightmost characteristic root of the DDE converges first [62]. The location of the rightmost characteristic root is critical when analyzing stability; thus, spectral methods are favorable in this context.

1.2.2 Pole placement for TDS

Time delays can introduce instability or undesirable behavior to an otherwise stable closed-loop system. In the design of closed-loop control systems, delay plays an important role in applying the pole-placement technique to arrive at the final feedback gain parameters. A system governed by DDEs can be stabilized by adjusting the system parameters and/or tuning delays [63–65], using optimization-based [66–68] and non-optimization-based [69] strategies. Michiels et al. [66] proposed a continuous pole-placement technique using the gradient-sampling algorithm [70], which was among the first attempts at applying an eigenvalue optimization approach to infinite-dimensional systems. Optimization strategies were also used by Vanbiervliet et al. [71] for stabilizing time-delayed systems by tuning system parameters, and by Vyhlídal et al. [68] for stabilizing time-delayed systems using state-derivative feedback controllers. Yi et al. [7, 72] solved the eigenvalue assignment problem using the Lambert-W function, which allows one to write the analytical expressions in terms of the system parameters, similar to the state-transition matrix in linear ODE systems. The method of Yi et al. was limited to systems comprising a single discrete delay; Wei et al. [73] extended the Lambert-W function to handle distributed delays. Niu et al. [69] proposed an

eigenvalue assignment technique based on the generalized Runge–Kutta method, but applied their method to DDEs with only a single delay.

1.2.3 Algebraic pole placement frameworks for TDS

The optimization-based framework for the pole placement of DDEs as proposed in [74] focuses on the placement of only the rightmost root of the DDE at the desired location in the left half of the complex plane. Sometimes, however, the rightmost root is not placed at the desired location using optimization-based techniques. Moreover, there is no control over the placement of the next set of rightmost roots. To address this, analytical approaches for the pole placement of DDEs such as the method of receptances (MoR) [75, 76] have been explored. The MoR, a popular algebraic strategy for the pole-placement problem in TDS, was developed by Ram et al. [75, 76]. Ram et al. [75] used MoR to place $2n$ poles (eigenvalues of the characteristic polynomial) of a second-order system with n degrees of freedom—that is, for a system with $2n$ states when written in first-order form. Later, Ram et al. [76] proposed a hybrid method for *partial* pole placement of second-order systems. As its name suggests, this work placed only $m < 2n$ poles at specified locations, leaving the remaining spectrum of $2n - m$ poles undisturbed. Although computationally straightforward, the MoR approach has several drawbacks: the poles placed at the specified locations may not be dominant (referred to as "spillover"), a separate analysis must be carried out to determine whether the resulting closed-loop system is stable, and multiple delays cannot be accommodated. In Ram et al. [75], the time delay was handled using the Taylor series expansion; however, Insperger [77] demonstrated that the results obtained using a Taylor series expansion for time delays are often inaccurate.

Several authors have advanced the field in recent years; here, a brief chronology of these developments is provided. Pratt et al. [78] defined the pole-placement problem for a TDS as a quadratic partial eigenvalue assignment problem with time delay, and proposed a "direct and partial modal" approach for active vibration problems. As with the method of Ram et al. [75], the approach proposed by Pratt et al. [78] was limited by its use of the Taylor series for incorporating the time delay and by the requirement to perform an *a posteriori* analysis to evaluate the stability of the resulting system. Ouyang and Singh [79] used MoR in one of the first applications of pole placement to asymmetric systems with time delay. Once again, this approach has the drawback that stability is not guaranteed.

Singh and Datta [80] obtained a closed-form solution to compute control gains for zero assignment in active vibration control problems. As with the work of Ram et al. [75], an *a posteriori* analysis is required to compute the primary eigenvalues of the system, which increases the complexity of computation. Bai et al. [81] formulated the pole-placement problem for second-order systems as a partial quadratic eigenvalue assignment problem (PQEAP) and proposed a multi-step hybrid method for solving symmetric systems. The proposed approach was applied to a multiple-input system, wherein the system matrices were combined with the measured receptances. A limitation of this approach is that it can be applied only to symmetric systems. Furthermore, the effects of high time delays (i.e., $\tau > 0.1$) were not explored. Bai et al. [82] later proposed an optimization-based approach to solve the PQEAP, extending the single-input hybrid method proposed by Ram et al. [76]. The optimization-based hybrid method of Bai et al. minimizes the feedback norms of the multi-input PQEAP with time delay.

Wang and Zhang [83] proposed a direct method to solve the partial eigenvalue assignment problem for high-order control systems with time delay, without first converting the system into first-order form. The proposed method requires only partial knowledge of the eigenvalues and corresponding eigenvectors of the matrix polynomial; however, the Taylor series was used to address the transcendental terms, which will fail to provide accurate results at higher delays. Mao and Dai [84] analyzed the sensitivity of closed-loop eigenvalues to perturbations in time delay during partial eigenvalue assignment. Li and Chu [85] generalized the well-known Kautsky, Nichols, and Van Dooren algorithm to solve the pole-placement problem for linear and quadratic TDS. They demonstrated that the results for systems with time delay are similar to those without delay, except for the presence of secondary eigenvalues.

Singh and Ouyang [86] proposed a method for assigning complex poles to second-order damped asymmetric systems using a constant-time-delay state-feedback controller. Again, an *a posteriori* analysis was necessary because the eigenvalues that are placed at the desired locations are not guaranteed to be the primary eigenvalues. Mao [87] proposed a partial eigenvalue assignment problem for TDS based on the orthogonality relations of the quadratic pencil (characteristic equation). Mao demonstrated the partial assignment of eigenvalues in a TDS without disturbing the remaining spectrum, obtained the explicit solution for the single-input case, and reported the parametric solution for the multi-input case. Singh et al. [88] defined a pole-placement problem without first transforming a given second-order system into a standard state-space form. Employing a sophisticated mathematical theory, Singh et

al. were able to guarantee that the unassigned eigenvalues do not reside to the right of the assigned poles in the complex plane (i.e., there is no spillover).

Schmid and Nguyen [89] proposed a parametric formula for the feedback-gain matrix that will produce a desired set of closed-loop eigenvalues for a TDS. By considering only small time delays in the input, Schmid and Nguyen used unconstrained optimization to obtain the state-feedback matrix, minimizing the sensitivity of the eigenvalues to input delays. Schmid et al. [90] extended this approach to TDS with multiple time delays by first designing the control law for a non-delayed system, then investigating its applicability to the corresponding TDS. Schmid et al. demonstrated that it is possible to place the poles of a TDS at the same locations as for the system without delay. An *a posteriori* analysis using the quasi-polynomial root-finder (QPmR) algorithm [91] was performed to study the stability of the resulting system.

Zhang [92] proposed an explicit algorithm to assign the eigenvalues for multi-input, high-order control systems with time delay. Zhang demonstrated that this method avoids spillover and can be implemented with only partial information of the eigenvalues and corresponding eigenvectors of the matrix polynomial. Wang and Zhang extended their earlier work on partial assignment [83] and applied it to a multi-input TDS without use of the Sherman–Morrison formula [93]. Ariyatanapol et al. [94] proposed a receptance-based method for partial pole placement in asymmetric TDS that requires no knowledge of the mass, damping, or stiffness matrices. Ariyatanapol et al. used a single-input state-feedback controller and determined the critical stability of the system using the frequency-sweeping test. An *a posteriori* analysis was performed to calculate the first few dominant poles of the resulting closed-loop system and, thus, to analyze the stability of the system. Zhang and Shan [95] extended the work of Ram et al. [76] to solve the partial pole–zero placement problem in high-order systems using MoR.

Santos et al. [96] generalized the single-input, single-output, first-order small-gain theorem using the system receptances. Specifically, the small-gain theorem was extended to second-order systems with multiple inputs and time-varying delays with output feedback. Santos et al. also proposed a detuning strategy to address the trade-off between performance and robustness with respect to variation in delay. Because the closed-loop poles are not computed in this method, their proposed approach can be used only to analyze delay uncertainty. Araújo [97] demonstrated use of system margins and Nyquist plots to determine the closed-loop stability of TDS. It was also shown that the Padé approximation for time delay in the frequency domain is as accurate as the corresponding truncated Taylor exponential expansion.

Experimental validation of stabilization techniques for TDS have not been widely explored in the literature. Previous studies have reported experimental validation for only a small number of control strategies, including semi-discretization [98], high-order control design [98], and cluster treatment of characteristic roots [99]. However, none of these studies have explored experimental validation of the pole-placement problem using real-time experiments.

1.2.4 Reduced-order modelling of TDS

The mathematical process of approximating an infinite-dimensional system with a finite-dimensional system without losing the essence of the original system is usually referred to in the literature as reduced-order modelling. Thomson [100] carried out some of the first work in the domain of reduced-order modelling for TDS. Thomson investigated the approximation of time-delay networks obtained from infinite ladder networks (Cauer canonical form) with a maximally flat frequency response. Later, Storch [101] used Bessel polynomials to synthesize constant-time-delay networks. The motive was to achieve a stable low-pass network with constraints on realizability and circuit-loss in signal filtering, circuits, and networks. Rational-approximation problems associated with the Hankel norm were studied by Glader et al. [102]. A Fourier-series-based model-reduction technique was studied by Gu et al. [103]. Lam studied the Padé-approximated reduced-order modelling of delay systems [104, 105]. Lam calculated the L_2 and L_∞ error bounds for reduced-order models (ROM) using different classes of Padé approximants for various cases of the degrees of the numerator and denominator. As the order of the Padé approximation increases, Lam experimentally determined that Padé approximants in which the degree of the numerator is greater than that of the denominator by either 1 or 2 provided a better approximation of the time delay. Initial works that used Laguerre methods for the approximation of TDS were investigated by Mäkilä [106, 107], who explored the use of Laguerre filters to approximate infinite-dimensional systems. Fourier-Laguerre series for the approximation of TDS was studied by Partington [108]. Lam [109] analyzed the use of the Laguerre formula in the context of approximating TDS and showed that the L_2 and L_∞ norms converged. Yoon and Lee [110] studied a new method for approximating time delay ($e^{-\tau s}$) using the Frostman theorem and Blaschke product, and obtained the error bounds for the L_2 and L_∞ norms. The approximant formulated by this method has a design parameter that can be adjusted to alter the real part locations of pole-zeros of the approximant. Shift operators in terms of H_∞ and H_2/L_2 norms were analyzed by Mäkilä and Partington [111, 112]. Mäkilä and Partington [111, 112]

showed that the simple Laguerre-shift formula gives good approximations for TDS. Mäkilä and Partington also provide a generalized analysis of shift-operator-based approximations.

Harkort and Deutscher [113] developed a moment-matching approach, based on the Krylov subspace method, to obtain ROMs for linear, time-invariant (LTI) TDS. The reduced-order modelling method developed by Michiels et al. [114, 115] using spectral discretization, and the Krylov subspace method, exhibited good spectral approximations of the original model with well-approximated rightmost roots. The reduction approach resulted in the formation of a standard LTI system enabling a wide range of controller design techniques. An application of this methodology to design a fixed-order H_2 optimal controller can be found in [116]. Model reduction by the dominant pole algorithm (DPA) for first-order, second-order, and multi-input multi-output (MIMO) systems was studied by Rommes and Martins [117–119] and Rommes and Sleijpen [120]. Using the balanced truncation method based on coordinate transformation and delayed Lyapunov equation, Saadvandi et al. [121] proposed an advanced version of the DPA whose main advantage was that it did not allow the algorithm to converge to the same pole more than once. Zhang and Su [122] proposed a memory-efficient method for reduced-order modelling of TDS. The method is similar to the works proposed by Michiels et al. [114, 115]. However, a memory-efficient construction of the orthonormal basis of the projection subspace was proposed using the two-sided Arnoldi process [123]. Two techniques were studied using the proposed methodology: one that preserves the delay structure of a TDS and one that transforms a TDS into a set of linear ODEs.

Wang et al. [124] used a Padé and a truncated Taylor series expansion to approximate the exponential functions associated with time delays, and then the large-scale LTI systems were reduced using the principle of moment matching. Scarciotti and Astolfi proposed a moment-matching-based reduced-order modelling method for neutral linear and non-linear TDS [125]. The notion of moments was derived in terms of the solution of the Sylvester equations for linear TDS and by employing the center manifold theory for non-linear TDS. A family of ROMs with several free design parameters was obtained. The free design parameters can be adjusted to obtain delay-free and delay-bound models. It was mentioned that a delay-bound ROM is better at preserving the essence of the original system, but numerical results showed that the degree of error in the frequency response of the two models was identical.

Spectral and Galerkin approximations were successfully used to obtain ODE representations, characteristic roots, and stability charts for DDEs. However, its

application to reduced-order modelling of DDEs has not been explored. Wahi and Chatterjee [47] were the first to develop Galerkin approximations for DDEs, which were later extended in [48, 62, 126]. In [47, 48, 62], the DDE was converted into a partial differential equation (PDE) using a suitable transformation. The obtained PDE was then transformed into a set of ODEs using spectral methods. With a user-specified tolerance, a finite number of eigenvalues of the system of ODEs converge to the rightmost characteristic roots of the DDE. An important observation from [47, 48, 62] was that as the number of approximation terms (N) increases, the number of converged roots (N_c) also increases. N-dimensional approximated systems developed in [47, 48, 62] also include the information of the unconverged roots that do not accurately represent the dynamics of the DDE.

1.3 Motivation and outline of the thesis

Various methodologies to determine the stability of DDEs and apply the pole placement technique are highlighted in Section 1.2. Some of the existing methods to study the stability of DDEs that have gained traction over the years are cluster treatment of characteristic roots (CTCR), QPmR, pseudo-spectral collocation, and Galerkin approximations. An important drawback of the CTCR method is that the stability region is obtained using the nature of root-crossing and not the rightmost root. This essentially limits the application of the CTCR method to the pole placement technique of DDEs. To use the QPmR algorithm, one must specify the region of the complex plane in which the poles exist. This inherent need to specify the region many not always result in obtaining the rightmost root. Also, the roots so obtained may not be directly used to apply optimization-based pole placement technique. Some of the methods that explicitly give us the rightmost root, which can then be directly used to apply the pole placement technique are Galerkin approximations and pseudo-spectral collocation. With the many pole placement techniques for DDEs that exist in the literature, only the MoR is an analytical method. However, it also suffers from drawbacks as mentioned in Section 1.2.3.

Galerkin approximations have been highly successful for studying the stability characteristics of second-order DDEs [47–49, 62]. Galerkin approximations are applied to TDS by first converting the governing DDE into a PDE, then converting the PDE into a system of ODEs. Sadath and Vyasarayani [49] performed stability studies of second-order DDEs using Galerkin approximations, converting the second-order DDE into a second-order PDE and then into a system of second-order ODEs. Later, the

system of second-order ODEs were rewritten as a system of first-order ODEs. It was observed that using the second-order Galerkin method formulation, hereby referred to as the "second-order Galerkin" method, some eigenvalues of the approximating ODE system lie at the origin of the complex plane. These roots are not among the characteristic roots of the original DDE and are hereby referred to as *spurious* roots. Though the spurious roots do not affect the stability studies of the DDEs [49], they do but have an undesirable effect for pole placement and reduced-order modelling of DDEs. If the spurious roots happen to be the rightmost roots, then additional computation needs to be performed to identify them, which adds to the complexity of a pole-placement or reduced-order modelling algorithm.

In Chapter 2, to avoid spurious roots, a refined mathematical model to obtain the rightmost roots of the DDEs using Galerkin approximations is developed. This method can be directly applied to the pole placement and reduced-order modelling of DDEs.

In [47–49, 62], the authors have handled the boundary conditions within the Galerkin framework using the spectral-tau and Lagrange multiplier methods. The Galerkin approximation method using a new pseudoinverse-based technique for embedding the boundary conditions is developed in Chapter 3. Then, the pole-placement technique is used to design closed-loop feedback gains that stabilize TDS. The results are verified by a thorough comparison with those reported in the literature. Next, experimental validation is performed using a rotary inverted pendulum system (see Fig. 1.4(a)) with inherent sensing delays as well as additional time-delays that are introduced deliberately.

(a) (b)

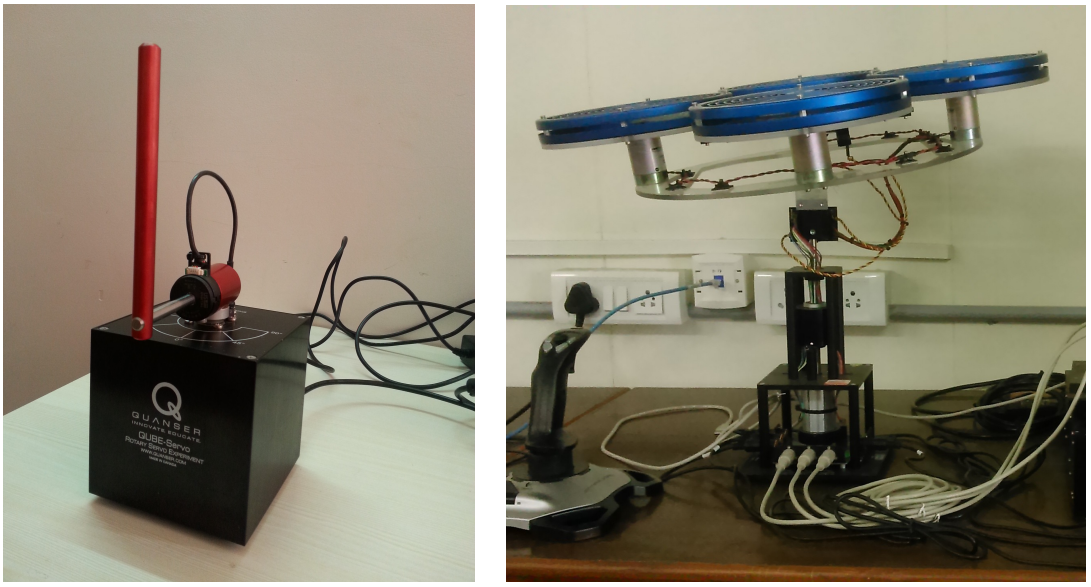

FIGURE 1.4: (a) Rotary inverted pendulum apparatus and (b) 3D hovercraft apparatus, both manufactured by Quanser Inc.

The strengths and limitations of the MoR approach for the pole placement of second-order DDEs is explored in detail in Chapter 4. In this chapter, a framework combining the strengths of the MoR approach with a Galerkin-approximation-method-based optimization technique is developed for the pole placement of second-order TDS, hereby referred to as the hybrid pole-placement technique. The optimization-based technique is applied when the analytical approach fails to achieve the desired results for second-order TDS. The results obtained were experimentally validated using a 3D hovercraft appaatus (see Fig. 1.4(b)).

The finite-dimensional models obtained using Galerkin approximations include the information of both the converged and unconverged roots of the DDE [47, 48, 62]. It was observed that the unconverged roots do not accurately represent the dynamics of the DDEs and also add to the computation cost towards analyzing their dynamics. For illustration, the roots (both converged and unconverged) obtained using the Galerkin approximations for the spring-mass-damper system (see Fig. 1.1) are shown in Fig. 1.5. In Fig. 1.5, roots represented by blue circles are the converged roots and the rest of the spectrum obtained using the Galerkin approximations are the unconverged roots.

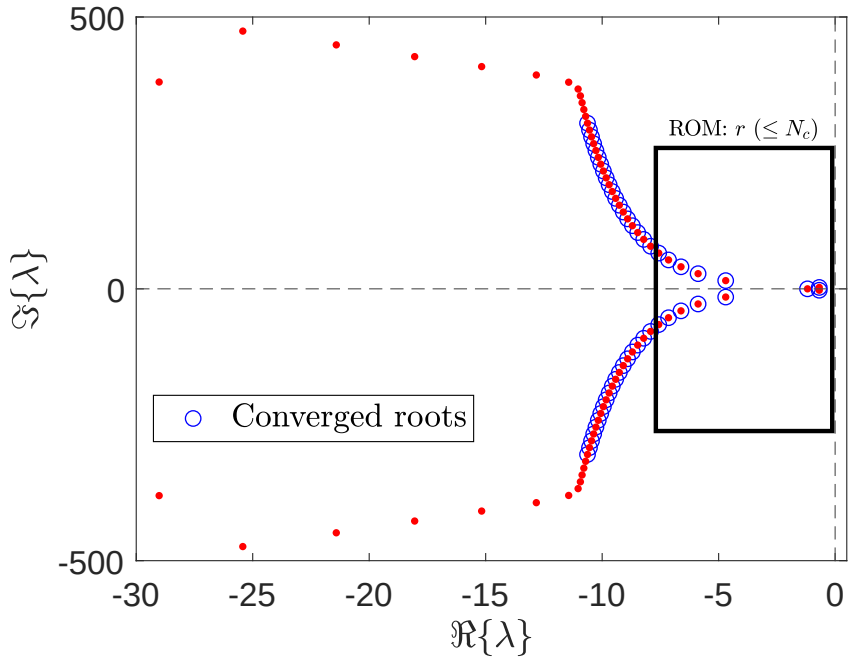

FIGURE 1.5: Converged and unconverged roots obtained using Galerkin approximations for the spring-mass-damper system.

Defining N_c as the number of converged roots obtained from the Galerkin approximations and using only their information, in Chapter 5, a further ROM (with a user-specified dimension r ($\leq N_c$)) of the DDEs is obtained by applying the eigenvalue decomposition (EVD). The proposed approach is first validated using various examples of different order from the literature. Then, ROMs are developed for a 3D hovercraft apparatus (see Fig. 1.4(b)) and the results are experimentally validated.

Chapter 6 summarizes the contribution of this thesis. This chapter also discusses the possible directions for future research.

Chapter 2

Spurious roots of DDEs using Galerkin approximations

The dynamics of time-delayed systems are governed by DDEs, which are infinite dimensional and can pose computational challenges. Several methods have been proposed for studying the stability characteristics of DDEs. One such method employs Galerkin approximations to convert DDEs into PDEs with boundary conditions; the PDEs are then converted into systems of ODEs, whereupon standard ODE methods can be applied. The Galerkin approximation method can be applied to a second-order DDE in two ways: either by converting into a second-order PDE and then into a system of second-order ODEs (the "second-order Galerkin" method), or by first expressing as two first-order DDEs and converting into a system of first-order PDEs and then into a first-order ODE system (the "first-order Galerkin" method). In this chapter, we demonstrate that these subtly different formulation procedures lead to different roots of the characteristic polynomial. In particular, the second-order Galerkin method produces spurious roots near the origin, which must then be identified through substitution into the characteristic polynomial of the original DDE. However, spurious roots do not arise if the first-order Galerkin method is used, which can reduce computation time and simplify stability analyses. These two formulation strategies are described and numerical examples to highlight their important differences are presented.

The remainder of this chapter is organized as follows. In Section 2.1, a brief outline of the second-order and first-order Galerkin formulations is given. Numerical examples are presented in Section 2.2 to demonstrate their differences, and the chapter is summarized in Section 2.3.

2.1 Mathematical modeling

Consider the following second-order DDE:

$$\ddot{x}(t) + a_1\dot{x}(t) + a_2x(t) + \sum_{r=1}^{n} b_r\dot{x}(t-\tau_r) + \sum_{q=1}^{m} c_qx(t-\tau_{n+q}) = 0, \tag{2.1}$$

where $x(t)$ is the system state vector, $\dot{x}(t)$ and $\ddot{x}(t)$ are its time derivatives, $a \in \mathbb{R}^2$, $b \in \mathbb{R}^n$, $c \in \mathbb{R}^m$, delays $\tau_i \geq 0$ for $i = 1, 2, \ldots, n+m$. Equation (2.1) is a DDE if any $\tau_i > 0$; otherwise, it is simply an ODE. History function, which describe the past stated, are given as follows:

$$x(t) = \alpha(t), \tag{2.2a}$$

$$\dot{x}(t) = \beta(t), \qquad -\bar{\tau} \leq t \leq 0, \tag{2.2b}$$

where $\bar{\tau} = \max(\tau)$. The Galerkin approximation method [47, 48, 62] can be used to convert the infinite-dimensional DDE (Eq. (2.1)) into a finite-dimensional system of ODEs. The characteristic equation of the DDE is obtained by substituting $x(t) = x_0e^{\lambda t}$ into Eq. (2.1) and equating to zero:

$$D(\lambda) \triangleq \lambda^2 + a_1\lambda + a_2 + \sum_{r=1}^{n} b_r\lambda e^{-\lambda\tau_r} + \sum_{q=1}^{m} c_qe^{-\lambda\tau_{n+q}} = 0. \tag{2.3}$$

In the following, second-order and first-order Galerkin formulations are outlined.

2.1.1 Second-order Galerkin method

In this formulation, the governing second-order DDE is first converted into a second-order PDE; the PDE is then converted into a system of second-order ODEs which are finally written in first-order form. A brief outline of the formulation is presented (further detail can be found in Sadath and Vyasarayani [49]). First, the transformation given by $y(s,t) = x(t+s)$ is applied. Differentiating this transformation with respect to t and, separately, with respect to s reveals the following relation:

$$\frac{\partial y(s,t)}{\partial t} = \frac{\partial y(s,t)}{\partial s}, \qquad -\bar{\tau} \leq s \leq 0, \qquad t \geq 0. \tag{2.4}$$

Differentiating Eq. (2.4) with respect to t results in a second-order PDE:

$$\frac{\partial^2 y(s,t)}{\partial t^2} = \frac{\partial^2 y(s,t)}{\partial t\partial s}, \qquad -\bar{\tau} \leq s \leq 0, \qquad t \geq 0. \tag{2.5}$$

Thus, the initial value problem (Eqs. (2.1) and (2.2)) is re-cast as an initial-boundary value problem. Boundary conditions for Eq. (2.5) are obtained by substituting $s = 0$ and $s = -\bar{\tau}$ into $y(s,t) = x(t+s)$:

$$y(0,t) = x(t) \quad \Rightarrow \quad \left.\frac{\partial y(s,t)}{\partial t}\right|_{s=0} = \dot{x}(t) \quad \Rightarrow \quad \left.\frac{\partial^2 y(s,t)}{\partial t^2}\right|_{s=0} = \ddot{x}(t), \tag{2.6a}$$

$$y(-\bar{\tau},t) = x(t-\bar{\tau}), \tag{2.6b}$$

and the initial conditions are obtained from the history functions (Eq. (2.2)):

$$y(s,0) = x(s)\alpha(s), \tag{2.7a}$$

$$\dot{y}(s,0) = \dot{x}(s) = \beta(s), \quad -\bar{\tau} \leq s \leq 0. \tag{2.7b}$$

Notice that, by construction, history functions $\alpha(t)$ and $\beta(t)$ are now related through differentiation: from Eq. (2.7), we have $\beta(t) = \dot{\alpha}(t)$. This constraint was not present in the original problem statement and, as it will be shown below, is not present in the first-order Galerkin formulation. It is this artificial constraint that produces the spurious roots.

Briefly, the formulation concludes as follows. A series solution is assumed and the first N terms are retained:

$$y(s,t) = \sum_{i=1}^{\infty} \phi_i(s)\eta_i(t) \approx \sum_{i=1}^{N} \phi_i(s)\eta_i(t) = \boldsymbol{\phi}^{\mathrm{T}}(s)\boldsymbol{\eta}(t), \tag{2.8}$$

where $\boldsymbol{\phi}(s) \triangleq [\phi_1(s), \phi_2(s), \ldots, \phi_N(s)]^{\mathrm{T}}$ and $\boldsymbol{\eta}(t) = [\eta_1(t), \eta_2(t), \ldots, \eta_N(t)]^{\mathrm{T}}$ are the vectors of basis functions and coordinates, respectively. We substitute the truncated series solution into Eq. (2.5), pre-multiply by $\boldsymbol{\phi}(s)$, and integrate over the domain $s \in [-\bar{\tau}, 0]$ to obtain the following second-order ODEs:

$$\mathbf{M}\ddot{\boldsymbol{\eta}}(t) = \mathbf{C}\dot{\boldsymbol{\eta}}(t), \tag{2.9}$$

where $\mathbf{M} \triangleq \int_{-\bar{\tau}}^{0} \boldsymbol{\phi}(s)\boldsymbol{\phi}^{\mathrm{T}}(s)\mathrm{d}s$, $\mathbf{C} \triangleq \int_{-\bar{\tau}}^{0} \boldsymbol{\phi}(s)\boldsymbol{\phi}'(s)\mathrm{d}s$, and $\boldsymbol{\phi}'(s)$ denotes the derivative of $\boldsymbol{\phi}(s)$ with respect to s. The boundary conditions for the original DDE (Eq. 2.1) are given as follows:

$$\mathbf{m}\ddot{\boldsymbol{\eta}}(t) = \mathbf{c}\dot{\boldsymbol{\eta}}(t) + \mathbf{k}\boldsymbol{\eta}(t), \tag{2.10}$$

where $\mathbf{m}$, $\mathbf{c}$, and $\mathbf{k}$ are computed as follows:

$$\mathbf{m} = \boldsymbol{\phi}^{\mathrm{T}}(0), \tag{2.11}$$

$$\mathbf{c} = -a_1\boldsymbol{\phi}^{\mathrm{T}}(0) - \sum_{r=1}^{n} b_r\boldsymbol{\phi}^{\mathrm{T}}(-\tau_r), \tag{2.12}$$

$$\mathbf{k} = -a_2\boldsymbol{\phi}^{\mathrm{T}}(0) - \sum_{q=1}^{m} c_q\boldsymbol{\phi}^{\mathrm{T}}(-\tau_{n+q}). \tag{2.13}$$

The boundary conditions can be incorporated into Eq. 2.9 using the spectral-tau method [62], ultimately resulting in a system of first-order ODEs:

$$\dot{\mathbf{r}}(t) = \begin{bmatrix} \mathbf{0} & \mathbf{I} \\ \widetilde{\mathbf{M}}^{-1}\widetilde{\mathbf{K}} & \widetilde{\mathbf{M}}^{-1}\widetilde{\mathbf{C}} \end{bmatrix} \mathbf{r}(t) = \mathbf{G}_{\mathrm{so}}\mathbf{r}(t), \tag{2.14}$$

where $\mathbf{r}(t) \triangleq \left[\boldsymbol{\eta}^{\mathrm{T}}(t), \dot{\boldsymbol{\eta}}^{\mathrm{T}}(t)\right]^{\mathrm{T}} \in \mathbb{R}^{2N}$ is the state vector, and matrices $\widetilde{\mathbf{M}}$, $\widetilde{\mathbf{C}}$ and $\widetilde{\mathbf{K}}$ are defined as follows:

$$\widetilde{\mathbf{M}} = \begin{bmatrix} \bar{\mathbf{M}} \\ \mathbf{m} \end{bmatrix}, \quad \widetilde{\mathbf{C}} = \begin{bmatrix} \bar{\mathbf{C}} \\ \mathbf{c} \end{bmatrix}, \quad \widetilde{\mathbf{K}} = \begin{bmatrix} \mathbf{0} \\ \mathbf{k} \end{bmatrix}. \tag{2.15}$$

The solution of Eq. (2.14) approximates that of the original DDE (Eq. (2.1)), and the eigenvalues $(\hat{\lambda}_i, i = 1, 2, \ldots, 2N)$ of $\mathbf{G}_{so}$ converge to the characteristic roots of Eq. (2.3) as N increases [47, 62]. Error E_i is defined as the absolute value of $D(\hat{\lambda}_i)$, obtained by substituting $(\hat{\lambda}_i)$ into Eq. (2.3). In this chapter, root i is considered to have converged if error $E_i < 10^{-6}$.

2.1.2 First-order Galerkin method

In this formulation, the governing second-order DDE is first converted into a system of first-order DDEs; we then obtain a system of first-order PDEs and, finally, arrive at a system of first-order ODEs [74, 127]. We begin by defining state vector $\mathbf{w}(t) = [w(t),\ \dot{w}(t)]^{\mathrm{T}}$ and rewriting Eq. (2.1) as follows:

$$\dot{\mathbf{w}}(t) = \mathbf{A}\mathbf{w}(t) + \sum_{r=1}^{n} \mathbf{B}_r\dot{\mathbf{w}}(t-\tau_r) + \sum_{q=1}^{m} \mathbf{Q}_q\mathbf{w}(t-\tau_{n+q}), \tag{2.16}$$

where, $\mathbf{A}$, $\mathbf{B}_r$ and $\mathbf{Q}_q$ are given as follows:

$$\mathbf{A} = \begin{bmatrix} 0 & 1 \\ -a_2 & -a_1 \end{bmatrix}, \quad \mathbf{B}_r = \begin{bmatrix} 0 & 0 \\ 0 & -b_r \end{bmatrix}, \quad \mathbf{Q}_q = \begin{bmatrix} 0 & 0 \\ -c_q & 0 \end{bmatrix}. \tag{2.17}$$

We apply the transformation $\mathbf{y}(s,t) = \mathbf{w}(t+s)$ and differentiate with respect to t and, separately, with respect to s to obtain the following relation (analogous to Eq. (2.4)):

$$\frac{\partial \mathbf{y}(s,t)}{\partial t} = \frac{\partial \mathbf{y}(s,t)}{\partial s}, \quad -\bar{\tau} \leq s \leq 0 \qquad t \geq 0. \tag{2.18}$$

The boundary conditions for this first-order PDE (Eq. (2.18)) are obtained by substituting $s = 0$ and $s = -\bar{\tau}$ into the transformation $\mathbf{y}(s,t) = \mathbf{w}(t+s)$:

$$\mathbf{y}(0,t) = \mathbf{w}(t) \quad \Rightarrow \quad \left.\frac{\partial \mathbf{y}(s,t)}{\partial t}\right|_{s=0} = \dot{\mathbf{w}}(t), \tag{2.19a}$$

$$\mathbf{y}(-\bar{\tau},t) = \mathbf{w}(t-\bar{\tau}). \tag{2.19b}$$

Combining Eq. (2.19) with Eq. (2.16), we obtain the following:

$$\left.\frac{\partial \mathbf{y}(s,t)}{\partial t}\right|_{s=0} = \mathbf{A}\mathbf{y}(0,t) + \sum_{r=1}^{n} \mathbf{B}_r \mathbf{y}(-\tau_r,t) + \sum_{q=1}^{m} \mathbf{Q}_q \mathbf{y}(-\tau_{n+q},t). \tag{2.20}$$

Thus, we have converted the original first-order DDE (Eq. (2.1)) into an equivalent system of first-order PDEs (Eq. (2.18)) with boundary conditions given by Eq. (2.20).

We arrive at a system of first-order ODEs by assuming a series solution and retaining the first N terms:

$$y_i(s,t) = \sum_{j=1}^{\infty} \phi_j(s) z_{ij}(t) = \sum_{j=1}^{N} \phi_j(s) z_{ij}(t) = \boldsymbol{\phi}^{\mathrm{T}}(s) \boldsymbol{z}_i(t), \quad i = 1,2, \tag{2.21}$$

where $\boldsymbol{\phi}(s) \triangleq [\phi_1(s),\ \phi_2(s), \ldots,\ \phi_N(s)]^{\mathrm{T}}$ and $\boldsymbol{z}_i(t) \triangleq [z_{i1}(t),\ z_{i2}(t), ...,\ z_{iN}(t)]^{\mathrm{T}}$ are the vectors of basis functions and coordinates, respectively. We define $\boldsymbol{\Psi}(s) \in \mathbb{R}^{2N \times 2}$ and $\boldsymbol{\beta}(t) \in \mathbb{R}^{2N \times 1}$ as follows:

$$\boldsymbol{\Psi}(s) = \begin{bmatrix} \boldsymbol{\phi}(s) & \mathbf{0} \\ \mathbf{0} & \boldsymbol{\phi}(s) \end{bmatrix}, \quad \boldsymbol{\beta}(t) = \begin{Bmatrix} \boldsymbol{z}_1(t) \\ \boldsymbol{z}_2(t) \end{Bmatrix}. \tag{2.22}$$

Equation (2.21) can then be rewritten as $\mathbf{y}(s,t) = \boldsymbol{\Psi}^{\mathrm{T}}(s)\boldsymbol{\beta}(t)$ and substituted into Eq. (2.18) to arrive at the following:

$$\boldsymbol{\Psi}^{\mathrm{T}}(s)\dot{\boldsymbol{\beta}}(t) = \boldsymbol{\Psi}'(s)^{\mathrm{T}}\boldsymbol{\beta}(t), \tag{2.23}$$

Pre-multiplying Eq. (2.23) by $\mathbf{\Psi}(s)$ and integrating over the domain $s \in [-\bar{\tau}, 0]$ produces a system of first-order ODEs:

$$\mathbf{P}\dot{\boldsymbol{\beta}}(t) = \mathbf{R}\boldsymbol{\beta}(t), \tag{2.24}$$

Matrices $\mathbf{P}$ and $\mathbf{R}$ are square, block-diagonal matrices, and of dimension $2N$:

$$\mathbf{P} = \begin{bmatrix} \mathbf{P}^{(1)} & \mathbf{0} \\ \mathbf{0} & \mathbf{P}^{(2)} \end{bmatrix}^{\mathrm{T}}, \quad \mathbf{R} = \begin{bmatrix} \mathbf{R}^{(1)} & \mathbf{0} \\ \mathbf{0} & \mathbf{R}^{(2)} \end{bmatrix}^{\mathrm{T}}, \tag{2.25}$$

where submatrices $\mathbf{P}^{(i)}$ and $\mathbf{R}^{(i)}$ are defined as follows:

$$\mathbf{P}^{(i)} \triangleq \int_{-\bar{\tau}}^{0} \boldsymbol{\phi}_i(s)\boldsymbol{\phi}_i^{\mathrm{T}}(s)\mathrm{ds}, \quad \mathbf{R}^{(i)} \triangleq \int_{-\bar{\tau}}^{0} \boldsymbol{\phi}_i(s)\boldsymbol{\phi}_i'(s)^{\mathrm{T}}\mathrm{ds}, \quad i = 1, 2. \tag{2.26}$$

The matrix of boundary conditions is obtained by substituting the series solution (Eq. (2.21)) into Eq. (2.20):

$$\mathbf{\Psi}^{\mathrm{T}}(0)\dot{\boldsymbol{\beta}}(t) = \left[\mathbf{A}\mathbf{\Psi}^{\mathrm{T}}(0) + \sum_{r=1}^{n} \mathbf{B}_r\mathbf{\Psi}^{\mathrm{T}}(-\tau_r) + \sum_{q=1}^{m} \mathbf{Q}_q\mathbf{\Psi}^{\mathrm{T}}(-\tau_{n+q})\right]\boldsymbol{\beta}(t). \tag{2.27}$$

Equations (2.24) and (2.27) can be combined as follows:

$$\mathbf{U}\dot{\boldsymbol{\beta}}(t) = \mathbf{V}\boldsymbol{\beta}(t) \tag{2.28a}$$

$$\Rightarrow \quad \dot{\boldsymbol{\beta}}(t) = \mathbf{U}^{-1}\mathbf{V}\boldsymbol{\beta}(t) \triangleq \mathbf{G}_{fo}\boldsymbol{\beta}(t), \tag{2.28b}$$

where $\mathbf{U}$ and $\mathbf{V}$ are square matrices of dimension $2N$ and are obtained by replacing N^{th} and $2N^{\mathrm{th}}$ rows of Eq. (2.24) with the first and second rows of Eq. (2.27), respectively. The solution of Eq. (2.28) approximates that of the original DDE (Eq. (2.1)), and the eigenvalues $(\hat{\lambda}_i, i = 1, 2, \ldots, 2N)$ of $\mathbf{G}_{fo}$ converge to the characteristic roots of Eq. (2.3) as N increases [47, 62]. We define error E_i and the criterion for determining convergence as described above.

In spectral methods, one must select an appropriate set of basis functions $\boldsymbol{\phi}(s)$ for obtaining the solution of the approximating ODE system. We use shifted Legendre polynomials, as they have been shown to have good convergence properties [62]:

$$\phi_1(s) = 1 \tag{2.29a}$$

$$\phi_2(s) = 1 + \tfrac{2s}{\bar{\tau}} \tag{2.29b}$$

$$\phi_k(s) = \frac{(2k-3)\phi_2(s)\phi_{k-1}(s) - (k-2)\phi_{k-2}(s)}{k-1}, \quad k = 3, 4, \ldots, N. \tag{2.29c}$$

With these basis functions, matrices $\mathbf{M}$ and $\mathbf{C}$ in the second-order formulation (Eq. (2.9)) and matrices $\mathbf{P}$ and $\mathbf{R}$ in the first-order formulation (Eq. (2.25)) can be expressed in closed form, as reported previously [49]. For both second-order and first-order formulations, considering N terms in the series solution (Eqs. (2.8) and (2.21)) results in approximately $N/2$ converged eigenvalues.

2.2 Results and discussion

In this section, two examples are presented that compare the results obtained using the second-order and first-order Galerkin formulations.

2.2.1 Example 1

Consider the following second-order DDE with delay $\tau = 1$:

$$\ddot{x}(t) + \dot{x}(t) + x(t) + x(t-\tau) = 0. \tag{2.30}$$

We use $N = 50$ terms in the series solution (i.e., $\mathbf{G}_{so}$ and $\mathbf{G}_{fo}$ are each of dimension $2N = 100$). Figure 2.1 shows the rightmost eigenvalues of $\mathbf{G}_{\text{so}}$ (Eq. (2.14)) and $\mathbf{G}_{fo}$ (Eq. (2.28)). In each case, we obtain 22 converged roots—that is, $\mathbf{G}_{so}$ and $\mathbf{G}_{fo}$ each have 22 eigenvalues $\hat{\lambda}_i$. When substituted into the characteristic equation of the original DDE (Eq. (2.3)), we obtain an error of $E_i < 10^{-6}$. However, as shown in Fig. 2.1(a), the second-order formulation produces spurious roots—in fact, there are 49 spurious roots very close to the origin. Note that, in this example, the spurious roots happen to be the rightmost eigenvalues of $\mathbf{G}_{so}$ and could be misinterpreted as the rightmost eigenvalues of the original DDE. Since the second-order formulation is known to produce spurious roots, each root must therefore be substituted into the characteristic equation (Eq. (2.3)) to ensure its authenticity. The absence of spurious roots in the first-order formulation (see Fig. 2.1(b)) guarantees that the roots converge starting with the rightmost characteristic root of the DDE, which avoids the additional step of computing E_i [127] and makes this formulation particularly useful for solving pole-placement problems [74].

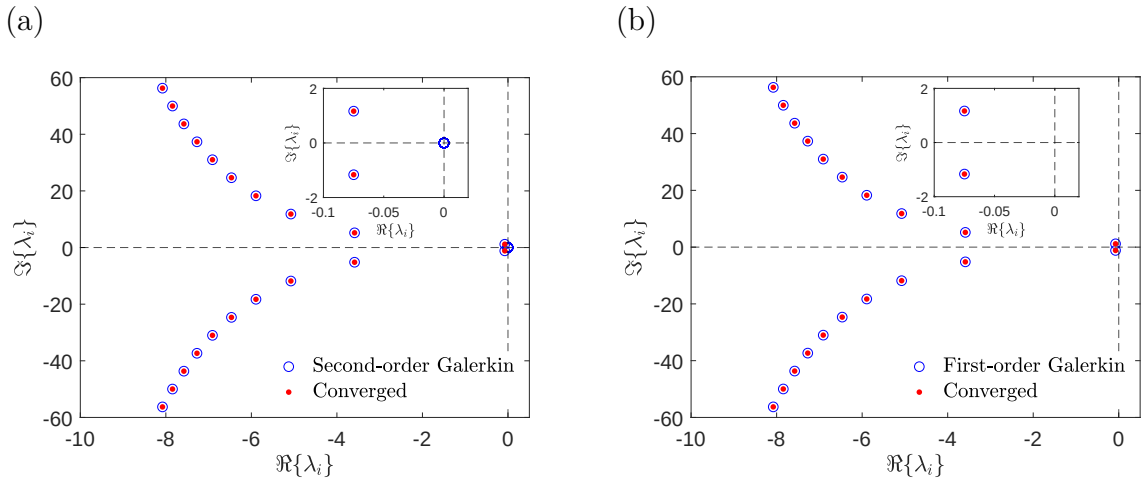

FIGURE 2.1: Characteristic roots of Eq. (2.30) obtained using the (a) second-order and (b) first-order Galerkin formulations

2.2.2 Example 2

Consider the following second-order DDE with delays $\tau_1 > 0$ and $\tau_2 > 0$:

$$\ddot{x}(t) + \dot{x}(t) + x(t) + \dot{x}(t - \tau_1) + x(t - \tau_2) = 0. \tag{2.31}$$

We again use $N = 50$ terms in the series solution. Figure 2.2 shows the rightmost eigenvalues of $\mathbf{G}_{so}$ and $\mathbf{G}_{fo}$ for $\tau_1 = \tau_1 = 1$. In this example, we obtain 23 converged roots using each formulation. As shown in Fig. 2.2(a), the second-order formulation again produces spurious roots: there are 49 spurious roots very close to the origin, and these are once again the rightmost roots of $\mathbf{G}_{so}$. These spurious roots lie at the origin and hence do they do not affect the stability chart (Fig. 2.3). In fact, as shown in Fig. 2.4(a) for $\tau_1 = \tau_1 = 3$, the spurious roots lie at the origin even if the closed-loop system is unstable, but the same do not appear when using the first-order formulation (see Fig. 2.4(b)). Nevertheless, as mentioned previously, it is generally favorable to avoid spurious roots.

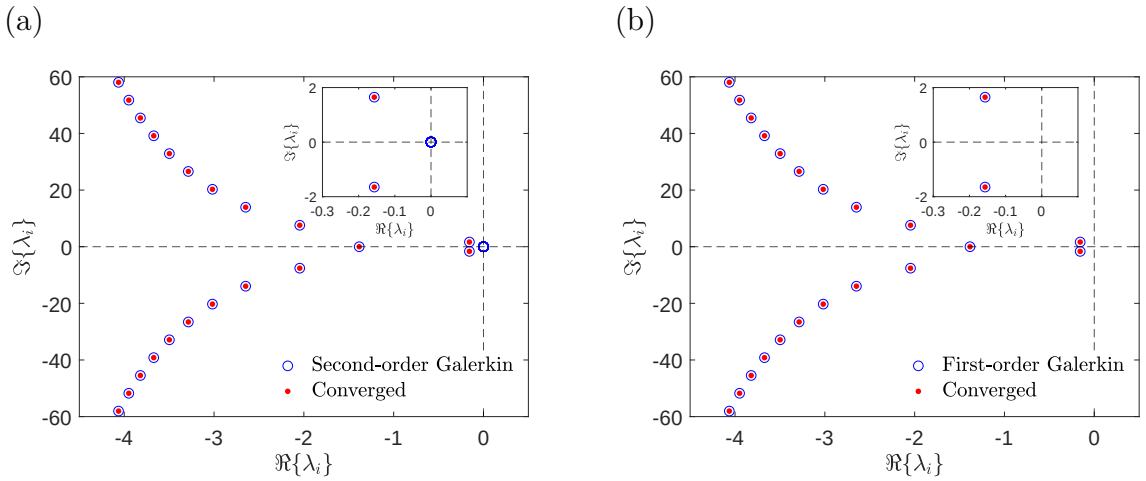

FIGURE 2.2: Characteristic roots of Eq. (2.31) with $\tau_1 = \tau_1 = 1$ obtained using the (a) second-order and (b) first-order Galerkin formulations.

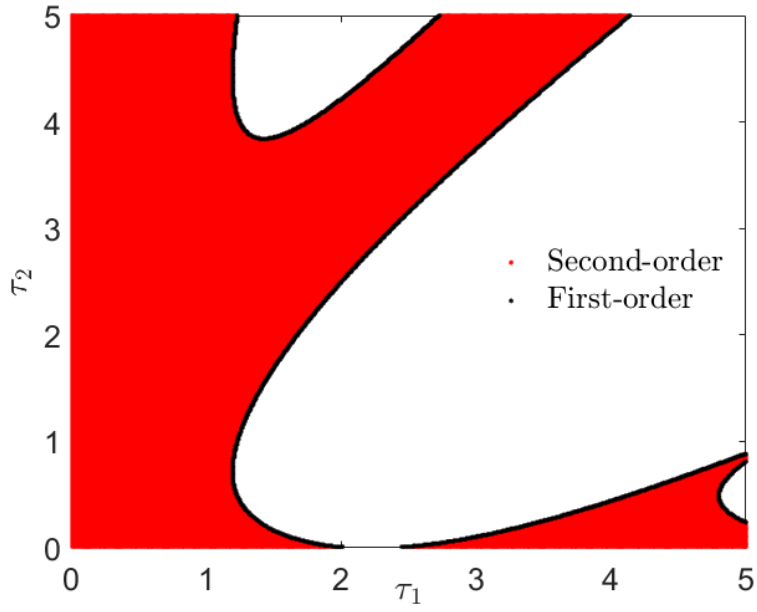

FIGURE 2.3: Stability chart of Eq. (2.31) obtained using the first-order (black line) and second-order (red region) Galerkin formulations.

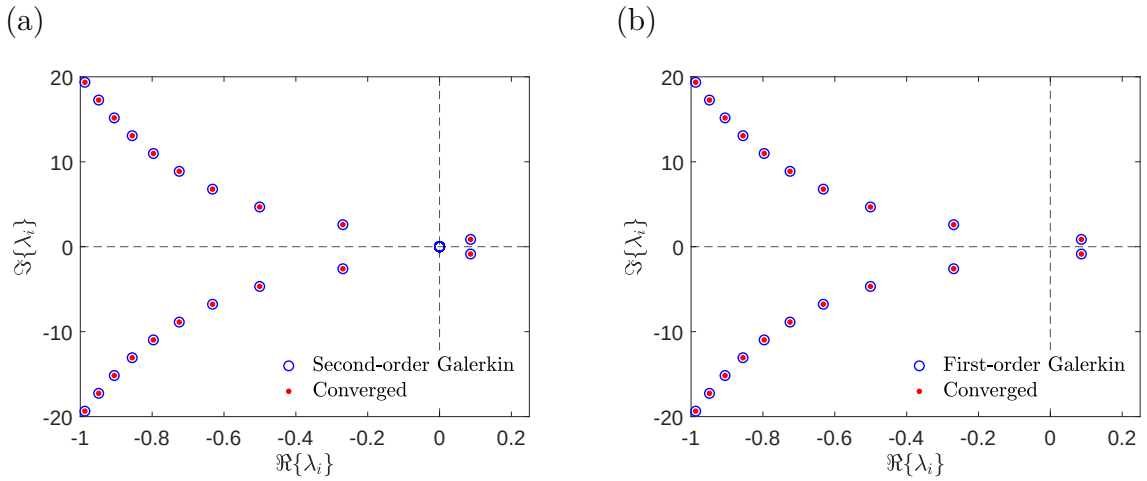

FIGURE 2.4: Characteristic roots of Eq. (2.31) with $\tau_1 = \tau_1 = 3$ obtained using the (a) second-order and (b) first-order Galerkin formulations.

2.2.3 Source of spurious roots

We revisit Eq. (2.14):

$$\dot{\mathbf{r}}(t) = \begin{bmatrix} \mathbf{0} & \mathbf{I} \\ \widetilde{\mathbf{M}}^{-1}\widetilde{\mathbf{K}} & \widetilde{\mathbf{M}}^{-1}\widetilde{\mathbf{C}} \end{bmatrix} \mathbf{r}(t) = \mathbf{G}_{\text{so}}\mathbf{r}(t), \tag{2.32}$$

where matrices $\widetilde{\mathbf{M}}$, $\widetilde{\mathbf{C}}$ and $\widetilde{\mathbf{K}}$ are defined in Section 2.1.1. Close inspection of $\widetilde{\mathbf{M}}^{-1}\widetilde{\mathbf{K}}$ reveals that its entries are as follows:

$$\left[\widetilde{\mathbf{M}}^{-1}\widetilde{\mathbf{K}}\right]_{ij} \begin{cases} = 0, & \text{if } 1 \leq i \leq N-1 \text{ and } 1 \leq j \leq N, \\ = 0, & \text{if } i = N \text{ and } j \text{ is even}, \\ \neq 0, & \text{if } i = N \text{ and } j \text{ is odd}, \end{cases} \tag{2.33}$$

where $i \in [1, N]$ and $j \in [1, N]$ are the row and column indices, respectively. It should be noted that, in matrix $\mathbf{G}_{\text{so}}$, the entries in rows 1 to $2N-1$ and columns 1 to N are zeros. This means that $\mathbf{G}_{\text{so}}$ has N linearly dependent columns and the system has $N-1$ eigenvalues at zero. However, matrix $\mathbf{G}_{\text{fo}}$ has full rank (i.e., $2N$ linearly independent columns) and, consequently, none of the system's eigenvalues are zero. These observations can be confirmed using Example 2. Considering $N = 4$ and

$\tau_1 = \tau_2 = 1$, we compute matrices $\mathbf{G}_{\text{so}}$ and $\mathbf{G}_{\text{fo}}$ as follows:

$$\mathbf{G}_{\text{so}} = \begin{bmatrix} 0 & 0 & 0 & 0 & 1 & 0 & 0 & 0 \\ 0 & 0 & 0 & 0 & 0 & 1 & 0 & 0 \\ 0 & 0 & 0 & 0 & 0 & 0 & 1 & 0 \\ 0 & 0 & 0 & 0 & 0 & 0 & 0 & 1 \\ 0 & 0 & 0 & 0 & 0 & 2 & 0 & 2 \\ 0 & 0 & 0 & 0 & 0 & 0 & 6 & 0 \\ 0 & 0 & 0 & 0 & 0 & 0 & 0 & 10 \\ -2 & 0 & -2 & 0 & -2 & -2 & -8 & -12 \end{bmatrix} \tag{2.34a}$$

$$\mathbf{G}_{\text{fo}} = \begin{bmatrix} 0 & 2 & 0 & 2 & 0 & 0 & 0 & 0 \\ 0 & 0 & 6 & 0 & 0 & 0 & 0 & 0 \\ 0 & 0 & 0 & 10 & 0 & 0 & 0 & 0 \\ 0 & -2 & -6 & -12 & 1 & 1 & 1 & 1 \\ 0 & 0 & 0 & 0 & 0 & 2 & 0 & 2 \\ 0 & 0 & 0 & 0 & 0 & 0 & 6 & 0 \\ 0 & 0 & 0 & 0 & 0 & 0 & 0 & 10 \\ -2 & 0 & -2 & 0 & -2 & -2 & -8 & -12 \end{bmatrix} \tag{2.34b}$$

The eigenvalues of $\mathbf{G}_{\text{so}}$ that are zeros appear as $N-1$ spurious roots at the origin, as can be seen in Figs. 2.1(a), 2.2(a), and 2.4(a).

2.3 Chapter summary

In this chapter, two approaches for applying the Galerkin approximation method to second-order DDEs are compared. The "second-order Galerkin" formulation involves converting the DDE into a second-order PDE, then into a system of second-order ODEs, and finally rewriting the ODEs in first-order form. The "first-order Galerkin" formulation involves converting the second-order DDE into two first-order DDEs, then into a system of first-order PDEs, and finally into a system of first-order ODEs. The limitations of the second-order formulation have been demonstrated both analytically and numerically with two examples. In particular, the second-order formulation imposes an artificial constraint between the two history functions, which ultimately precipitates into spurious roots in the approximating ODE system. The spurious roots lie at the origin and, thus, do not affect stability charts; however, in reduced-order modeling and pole-placement problems, additional analysis must be performed to determine whether a root is spurious. The spurious roots that arise in the second-order

formulation can be avoided by using the first-order formulation. This issue has not been reported previously, and one should be mindful of it when using this technique. The rank-deficient matrix that arises in the second-order formulation can be avoided by using the first-order formulation. As we demonstrate, the first-order formulation produces the same stability chart but no spurious roots. A substantial benefit is that the rightmost roots are true characteristic roots, which are the first to converge.

Chapter 3

Pole placement for TDS using Galerkin approximations

Many dynamic systems of practical interest have inherent time delays and thus are governed by DDEs. As explained in Chapter 1, DDEs are infinite dimensional and TDS may be difficult to stabilize using traditional controller design strategies. The Galerkin approximation method is applied using a new pseudoinverse-based technique for embedding the boundary conditions, which results in a simpler mathematical derivation than has been presented previously. Then, the pole-placement technique is used to design closed-loop feedback gains that stabilize TDS, and verify the results through comparison to those reported in the literature. Finally, experimental validation is performed by applying the proposed method to stabilize a rotary inverted pendulum system with inherent sensing delays as well as additional time delays that are introduced deliberately. The proposed approach is easily implemented and performs at least as well as existing methods.

This chapter is organized as follows. In Section 3.1, the optimization problem and mathematical modeling are described. In Section 3.2, the proposed approach is verified through comparison to results reported in the literature using existing methods. Then, the proposed approach is further validated in Section 3.3 by stabilizing DDEs obtained from the literature [66, 69]. In Section 3.4, the proposed approach is used to stabilize an experimental apparatus with inherent sensing delays as well as additional time delays that are introduced deliberately. Finally, conclusions are provided in Section 3.5.

3.1 Pole placement for DDEs

A system's closed-loop pole locations determine its stability characteristics as well as the characteristics of its time response, such as its rise time and settling time. The *pole-placement* technique can be used to adjust the closed-loop pole locations for stabilizing both single-input single-output (SISO) and MIMO systems.

3.1.1 Problem definition

Consider the following system of DDEs, expressed here in state-space form:

$$\dot{\mathbf{x}}(t) + \mathbf{A}\mathbf{x}(t) + \sum_{q=1}^{m} \mathbf{B}_q u_q(t-\tau_q) = \mathbf{0} \tag{3.1a}$$

$$u_q(t-\tau_q) = \mathbf{K}_q^{\mathrm{T}} \mathbf{x}(t-\tau_q), \quad q = 1, 2, \ldots, m, \tag{3.1b}$$

where $\mathbf{x}(t) \triangleq [x_1(t), x_2(t), \ldots, x_P(t)]^{\mathrm{T}}$ is the state vector, $\mathbf{u}(t) \triangleq [u_1(t), u_2(t), \ldots, u_m(t)]^{\mathrm{T}}$ is the control vector, $\mathbf{A} \in \mathbb{R}^{P\times P}$, $\mathbf{B}_q \in \mathbb{R}^{P\times 1}$, $\mathbf{K}_q \in \mathbb{R}^{P\times 1}$, and delays $\tau_q > 0$. Given $\mathbf{A}$, $\mathbf{B}_q$, and delays τ_q, the objective is to determine the feedback gains $\mathbf{K}_q$ that are necessary to stabilize the system (i.e., to move all poles into the left half of the complex plane). We optimize gains $\mathbf{K}_q$ by minimizing the following objective function:

$$J = \Big(\mathrm{Re}\ (\lambda_{\max}(\mathbf{K}_q)) + \alpha\Big)^2, \tag{3.2}$$

where Re $(\lambda_{\max})$ is the real part of the rightmost eigenvalue, which is a function of feedback gains $\mathbf{K}_q$, and $\alpha > 0$ is a parameter specifying the desired distance between $\lambda_{\max}$ and the imaginary axis. In this work, Eq. 3.2 is first solved with $\alpha = \alpha_0$ where $\alpha_0 > 0$ (i.e., all poles are placed in the left half of the complex plane). We then increase α by $\delta\alpha$ and solve Eq. 3.2 again, repeating this process until the optimal objective function value $J > 0$ (i.e., until $\mathbf{K}_q$ cannot be found to move $\lambda_{\max}$ to the location specified by α). We use $\alpha_0 = \delta\alpha = 1$ in the examples below. This simple algorithm was sufficient for our purposes; however, a more complex optimization problem could be designed to include other considerations, such as hardware limitations (e.g., by introducing constraints) or a desired time-delay stability margin.

3.1.2 Mathematical modeling

In this section, we extend the work of Vyasarayani, Sadath, and colleagues [48, 49, 62] and develop a new pseudoinverse-based Galerkin approximation method for finding the characteristic roots of DDEs. We begin by considering the following system of DDEs:

$$\dot{\mathbf{x}}(t) + \mathbf{A}\mathbf{x}(t) + \sum_{q=1}^{m} \mathbf{B}_q \mathbf{K}_q^{\mathrm{T}} \mathbf{x}(t - \tau_q) = \mathbf{0}, \tag{3.3}$$

where $\mathbf{x}(t)$, $\mathbf{A}$, $\mathbf{B}_q$, $\mathbf{K}_q$, and τ_q are as defined above. The characteristic equation of Eq. 3.3 is obtained by substituting $\mathbf{x}(t) = \mathbf{x}_0 e^{st}$, the determinant of which we equate to zero:

$$\det\left(s\mathbf{I} + \mathbf{A} + \sum_{q=1}^{m} \mathbf{B}_q \mathbf{K}_q^{\mathrm{T}} e^{-s\tau_q}\right) = 0. \tag{3.4}$$

Equation 3.4 is a quasi-polynomial due to the presence of transcendental terms $e^{-s\tau_q}$ and, hence, has infinitely many roots. The roots of Eq. 3.4 can be computed by formulating an abstract Cauchy problem, whereupon we obtain and solve a large linear eigenvalue problem.

We begin by converting the system of DDEs (Eq. 3.3) into a system of PDEs with time-dependent boundary conditions. We introduce the following transformation:

$$\mathbf{y}(s,t) = \mathbf{x}(t+s), \tag{3.5}$$

where $\mathbf{y}$ is a function of $s \in [-\tau, 0]$ and t, with $\tau \triangleq \max(\tau_1, \tau_2, \ldots, \tau_m)$. An abstract Cauchy problem is obtained by differentiating Eq. 3.5 with respect to s and t:

$$\frac{\partial \mathbf{y}(s,t)}{\partial t} = \frac{\partial \mathbf{x}(t+s)}{\partial (t+s)} \frac{\partial (t+s)}{\partial t} \quad \Rightarrow \quad \frac{\partial \mathbf{y}(s,t)}{\partial t} = \frac{\partial \mathbf{x}(t+s)}{\partial (t+s)}, \tag{3.6a}$$

$$\frac{\partial \mathbf{y}(s,t)}{\partial s} = \frac{\partial \mathbf{x}(t+s)}{\partial (t+s)} \frac{\partial (t+s)}{\partial s} \quad \Rightarrow \quad \frac{\partial \mathbf{y}(s,t)}{\partial s} = \frac{\partial \mathbf{x}(t+s)}{\partial (t+s)}. \tag{3.6b}$$

Upon equating Eqs. 3.6a and 3.6b, we obtain the following PDE:

$$\frac{\partial \mathbf{y}(s,t)}{\partial t} = \frac{\partial \mathbf{y}(s,t)}{\partial s}, \quad s \in [-\tau, 0]. \tag{3.7}$$

The boundary conditions for Eq. 3.7 are computed by substituting $s = 0$ and $s = -\tau$ into Eq. 3.5:

$$\mathbf{y}(0,t) = \mathbf{x}(t) \quad \Rightarrow \quad \left.\frac{\partial \mathbf{y}(s,t)}{\partial t}\right|_{s=0} = \dot{\mathbf{x}}(t), \tag{3.8a}$$

$$\mathbf{y}(-\tau, t) = \mathbf{x}(t-\tau). \tag{3.8b}$$

and then combining these relations with Eq. 3.3:

$$\frac{\partial \mathbf{y}(s,t)}{\partial t}\Big|_{s=0} + \mathbf{A}\mathbf{y}(0,t) + \sum_{q=1}^{m} \mathbf{B}_q \mathbf{K}_q^{\mathrm{T}} \mathbf{y}(-\tau_q, t) = \mathbf{0}. \tag{3.9}$$

We now assume a series solution for the PDE (Eq. 3.7):

$$y_i(s,t) = \sum_{j=1}^{\infty} \phi_{ij}(s)\eta_{ij}(t), \quad i = 1, 2, \ldots, P, \tag{3.10}$$

where $\phi_{ij}(s)$ are the basis functions, $\eta_{ij}(t)$ are the time-dependent coordinates, i represents the index into the state vector $\mathbf{x}(t)$, and j represents the corresponding term in each basis function. Because it is impossible to consider the entire infinite series, we truncate the series at N terms:

$$y_i(s,t) \approx \boldsymbol{\phi}_i^{\mathrm{T}}(s)\boldsymbol{\eta}_i(t), \quad i = 1, 2, \ldots, P, \tag{3.11}$$

where $\boldsymbol{\phi}_i(s) \triangleq [\phi_{i1}(s), \phi_{i2}(s), \ldots, \phi_{iN}(s)]^{\mathrm{T}}$ and $\boldsymbol{\eta}_i(t) = [\eta_{i1}(t), \eta_{i2}(t), \ldots, \eta_{iN}(t)]^{\mathrm{T}}$. We define matrix $\boldsymbol{\Psi}(s) \in \mathbb{R}^{NP \times P}$ and vector $\boldsymbol{\beta}(t) \in \mathbb{R}^{NP \times 1}$ as follows:

$$\boldsymbol{\Psi}(s) = \begin{bmatrix} \boldsymbol{\phi}_1(s) & \mathbf{0} & \cdots & \mathbf{0} \\ \mathbf{0} & \boldsymbol{\phi}_2(s) & \cdots & \mathbf{0} \\ \vdots & \vdots & \ddots & \vdots \\ \mathbf{0} & \mathbf{0} & \cdots & \boldsymbol{\phi}_P(s) \end{bmatrix}, \tag{3.12a}$$

$$\boldsymbol{\beta}(t) = [\boldsymbol{\eta}_1^{\mathrm{T}}(t), \boldsymbol{\eta}_2^{\mathrm{T}}(t), \ldots, \boldsymbol{\eta}_P^{\mathrm{T}}(t)]^{\mathrm{T}}, \tag{3.12b}$$

whereupon we can express Eq. 3.11 in vector form:

$$\mathbf{y}(s,t) = [\boldsymbol{\phi}_1^{\mathrm{T}}(s)\boldsymbol{\eta}_1(t), \boldsymbol{\phi}_2^{\mathrm{T}}(s)\boldsymbol{\eta}_2(t), \ldots, \boldsymbol{\phi}_P^{\mathrm{T}}(s)\boldsymbol{\eta}_P(t)]^{\mathrm{T}}, \tag{3.13}$$

$$= \boldsymbol{\Psi}^{\mathrm{T}}(s)\boldsymbol{\beta}(t). \tag{3.14}$$

Next, we substitute the series solution (Eq. 3.14) into the original PDE (Eq. 3.7):

$$\boldsymbol{\Psi}^{\mathrm{T}}(s)\dot{\boldsymbol{\beta}}(t) = \boldsymbol{\Psi}'(s)^{\mathrm{T}}\boldsymbol{\beta}(t), \tag{3.15}$$

where $\boldsymbol{\Psi}'(s)$ denotes the derivative of $\boldsymbol{\Psi}(s)$ with respect to s. Pre-multiplying Eq. 3.15 by $\boldsymbol{\Psi}(s)$ and integrating over the domain $s \in [-\tau, 0]$, we obtain the following:

$$\left(\int_{-\tau}^{0} \boldsymbol{\Psi}(s)\boldsymbol{\Psi}^{\mathrm{T}}(s)\mathrm{d}s \right) \dot{\boldsymbol{\beta}}(t) = \left(\int_{-\tau}^{0} \boldsymbol{\Psi}(s)\boldsymbol{\Psi}'(s)^{\mathrm{T}}\mathrm{d}s \right) \boldsymbol{\beta}(t). \tag{3.16}$$

Equation 3.16 can be rewritten as

$$\mathbf{C}\dot{\boldsymbol{\beta}}(t) = \mathbf{D}\boldsymbol{\beta}(t), \tag{3.17}$$

where $\mathbf{C}$ and $\mathbf{D}$ are square, block-diagonal matrices of dimension NP:

$$\mathbf{C} = \begin{bmatrix} \mathbf{C}^{(1)} & \mathbf{0} & \cdots & \mathbf{0} \\ \mathbf{0} & \mathbf{C}^{(2)} & \cdots & \mathbf{0} \\ \vdots & \vdots & \ddots & \vdots \\ \mathbf{0} & \mathbf{0} & \cdots & \mathbf{C}^{(P)} \end{bmatrix}^{\mathrm{T}}, \qquad \mathbf{D} = \begin{bmatrix} \mathbf{D}^{(1)} & \mathbf{0} & \cdots & \mathbf{0} \\ \mathbf{0} & \mathbf{D}^{(2)} & \cdots & \mathbf{0} \\ \vdots & \vdots & \ddots & \vdots \\ \mathbf{0} & \mathbf{0} & \cdots & \mathbf{D}^{(P)} \end{bmatrix}^{\mathrm{T}}. \tag{3.18}$$

Submatrices $\mathbf{C}^{(i)}$ and $\mathbf{D}^{(i)}$ are defined as follows:

$$\mathbf{C}^{(i)} \triangleq \int_{-\tau}^{0} \phi_i(s)\phi_i^{\mathrm{T}}(s)\mathrm{d}s, \qquad \mathbf{D}^{(i)} \triangleq \int_{-\tau}^{0} \phi_i(s)\phi_i'(s)^{\mathrm{T}}\mathrm{d}s. \tag{3.19}$$

Boundary conditions can be derived by substituting Eq. 3.14 into Eq. 3.9:

$$\boldsymbol{\Psi}^{\mathrm{T}}(0)\dot{\boldsymbol{\beta}}(t) = \left[-\mathbf{A}\boldsymbol{\Psi}^{\mathrm{T}}(0) - \sum_{q=1}^{m} \mathbf{B}_q\mathbf{K}_q^{\mathrm{T}}\boldsymbol{\Psi}^{\mathrm{T}}(-\tau_q)\right]\boldsymbol{\beta}(t). \tag{3.20}$$

Equations 3.17 and 3.20 can be combined as follows:

$$\mathbf{M}\dot{\boldsymbol{\beta}}(t) = \mathbf{K}\boldsymbol{\beta}(t). \tag{3.21}$$

Matrices $\mathbf{M}$ and $\mathbf{K}$ are of dimension $(NP + P) \times NP$ and are given by

$$\mathbf{M} \triangleq \begin{Bmatrix} \mathbf{C} \\ \bar{\mathbf{c}} \end{Bmatrix}, \qquad \mathbf{K} \triangleq \begin{Bmatrix} \mathbf{D} \\ \bar{\mathbf{d}} \end{Bmatrix}, \tag{3.22}$$

where $\bar{\mathbf{c}}$ and $\bar{\mathbf{d}}$ are matrices of size $P \times NP$ containing the boundary conditions:

$$\bar{\mathbf{c}} \triangleq \boldsymbol{\Psi}^{\mathrm{T}}(0), \tag{3.23a}$$

$$\bar{\mathbf{d}} \triangleq \left[-\mathbf{A}\boldsymbol{\Psi}^{\mathrm{T}}(0) - \sum_{q=1}^{m} \mathbf{B}_q\mathbf{K}_q^{\mathrm{T}}\boldsymbol{\Psi}^{\mathrm{T}}(-\tau_q)\right]. \tag{3.23b}$$

Equation 3.21 is an over-determined system of $NP + P$ equations in NP unknowns; the least-squares solution can be computed as follows:

$$\dot{\boldsymbol{\beta}}(t) = (\mathbf{M}^{+}\mathbf{K})\boldsymbol{\beta}(t), \tag{3.24}$$

where $\mathbf{M}^+$ is the Moore–Penrose inverse of $\mathbf{M}$. Finally, we define $\mathbf{G} \triangleq \mathbf{M}^+\mathbf{K}$ and write Eq. 3.24 as follows:

$$\dot{\boldsymbol{\beta}}(t) = \mathbf{G}\boldsymbol{\beta}(t). \tag{3.25}$$

Equation 3.25 is a system of ODEs that approximates the original system of DDEs (Eq. 3.3). Consequently, the eigenvalues of $\mathbf{G}$ converge to the characteristic roots of Eq. 3.3 as the number of terms in the Galerkin approximation (N) increases [62]. Convergence can be monitored by substituting the computed eigenvalues of $\mathbf{G}$ into Eq. 3.4 (the characteristic equation of Eq. 3.3) and calculating the absolute error (E). In this work, we consider eigenvalues to have converged when $E < 10^{-4}$. Also note that we use shifted Legendre polynomials as the basis functions:

$$\phi_1(s) = 1 \tag{3.26a}$$

$$\phi_2(s) = 1 + \tfrac{2s}{\tau} \tag{3.26b}$$

$$\phi_k(s) = \frac{(2k-3)\phi_2(s)\phi_{k-1}(s) - (k-2)\phi_{k-2}(s)}{k-1}, \quad k = 3, 4, \ldots, N. \tag{3.26c}$$

Shifted Legendre polynomials have shown good convergence properties [62] and facilitate expressing the entries of matrices $\mathbf{C}^{(p)}$ and $\mathbf{D}^{(p)}$, as defined in Eq. 3.19, in closed form:

$$\mathbf{C}_{ij}^{(p)} = \begin{cases} \dfrac{\tau}{2i-1}, & \text{if } i = j \\ 0, & \text{otherwise} \end{cases}, \qquad \mathbf{D}_{ij}^{(p)} = \begin{cases} 2, & \text{if } i < j \text{ and } i + j \text{ is odd} \\ 0, & \text{otherwise} \end{cases}, \tag{3.27}$$

where $i = 1, 2, \ldots, N$; $j = 1, 2, \ldots, N$; and $\tau = \max(\tau_1, \tau_2, \ldots, \tau_m)$.

3.2 Verification of pseudoinverse method

In this section, we verify the pseudoinverse-based Galerkin approximation method by applying the procedure described in Section 3.1.2 to two test problems. We compare our results to those obtained using the QPmR algorithm [91] and the pseudospectral differencing (PSD) method [53, 128].

3.2.1 First-order DDE with two delays

Consider the following first-order DDE with delays τ and $\tau + b$:

$$\dot{x}(t) = ax(t) + \frac{x(t-\tau) - x(t-\tau-b)}{b}. \tag{3.28}$$

The characteristic equation is obtained by substituting $x(t) = e^{st}$:

$$s - a - \frac{1}{b}e^{-s\tau} + \frac{1}{b}e^{-s(\tau+b)} = 0. \tag{3.29}$$

To test the robustness of the proposed approach, we find the rightmost roots of Eq. 3.29 using parameters $\tau = 1$ and $a = b = 10^r$ for $r = -1, -2, \ldots, -6$. As shown in Figs. 3.1 and 3.2, the roots obtained using the pseudoinverse-based Galerkin approach compare favorably with those obtained using the existing QPmR [91] and PSD [53, 128] methods.

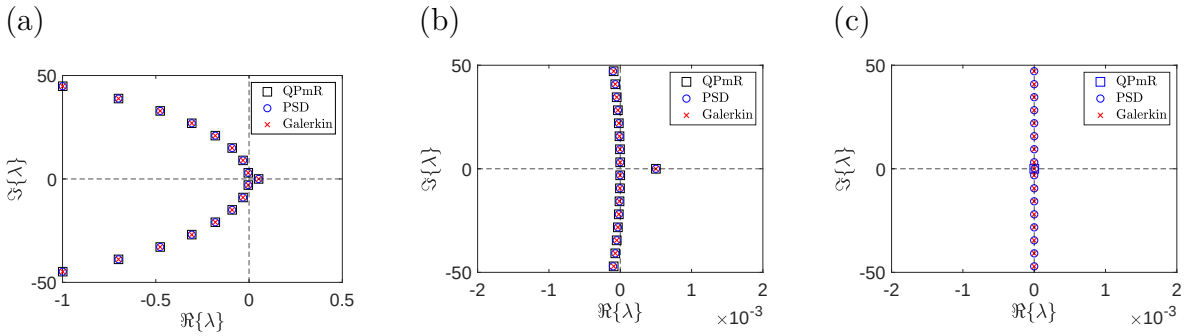

FIGURE 3.1: Characteristic roots of Eq. 3.28 using the QPmR algorithm, the PSD method, and the proposed pseudoinverse-based Galerkin approximation method: (a) $a = b = 10^{-1}$, (b) $a = b = 10^{-3}$, and (c) $a = b = 10^{-6}$.

As expected from inspection of Eq. 3.29, the rightmost root approaches zero as r decreases. The three methods have very similar precision; for example, when $a = b = 10^{-6}$, the errors are $E_{\text{Galerkin}} = 1.000124 \times 10^{-6}$, $E_{\text{PSD}} = 1.000008 \times 10^{-6}$, and $E_{\text{QPmR}} = 0.999891 \times 10^{-6}$. However, note in Fig. 3.1c that the QPmR method identified only one root when $a = b = 10^{-6}$. Another disadvantage of the QPmR method is the requirement to specify the region of the complex plane into which the poles should be placed.

Based on the results of Figs. 3.1a, 3.1a and 3.1c the pseudospectral differencing method appears to perform well. The proposed pseudoinverse-based Galerkin approximation method was further compared with the PSD method using a Monte Carlo

simulation. We computed the roots of Eq. 3.29 using $N = 25k$ for $k = 1, 2, \ldots, 5$, where N is the size of the linear eigenvalue problem being solved. In the Galerkin method, N corresponds to the number of terms in the series solution (Eq. 3.11); in the PSD method, N is the number of collocation points. We selected parameters uniformly from the ranges $a \in [1, 10]$, $b \in [1, 5]$, and $\tau \in [0.1, 5.1]$, repeating 10,000 times for each value of N. On average, more roots converged using the proposed Galerkin method than the PSD method, as shown in Table 3.1.

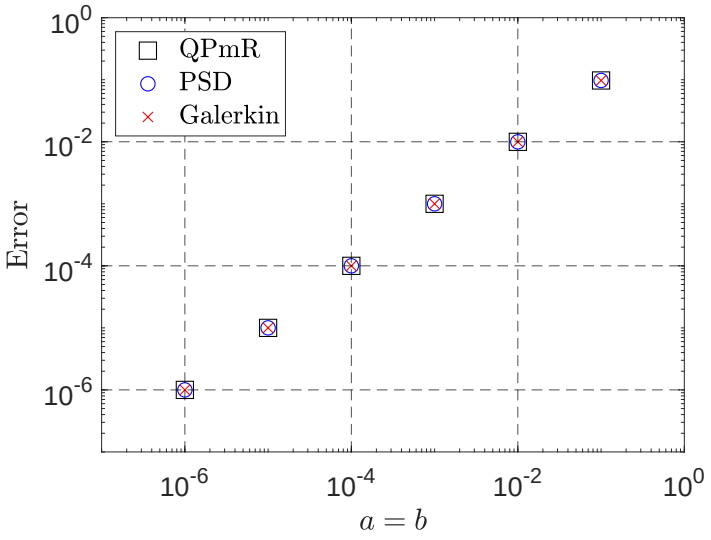

FIGURE 3.2: Errors obtained upon substituting into the characteristic equation (Eq. 3.29) the rightmost eigenvalue computed using the QPmR algorithm, the PSD method, and the proposed pseudoinverse-based Galerkin approximation method.

TABLE 3.1: Number of converged roots of Eq. 3.29, averaged over 10,000 trials.

N	Galerkin method	PSD method
25	8.0	6.0
50	21.5	15.4
75	34.4	25.8
100	48.5	36.3
125	63.2	48.0

3.2.2 Second-order DDE with three delays

Consider the following second-order DDE with delays τ_1, τ_2, and $\tau_1 + \tau_2$:

$$\ddot{x}(t)+a_1\dot{x}(t)+a_2x(t)+a_3\dot{x}(t-\tau_1)+a_4x(t-\tau_1)+ a_5\dot{x}(t-\tau_2)+a_6\dot{x}(t-\tau_1-\tau_2) = 0, \quad (3.30)$$

where $a_1 = 7.1$, $a_2 = 21.1425$, $a_3 = 6$, $a_4 = 14.8$, $a_5 = 2$, and $a_6 = 8$. As demonstrated by the stability chart shown in Fig. 3.3, the results obtained using the proposed Galerkin method are in agreement with those obtained using the spectral tau method [49, 62].

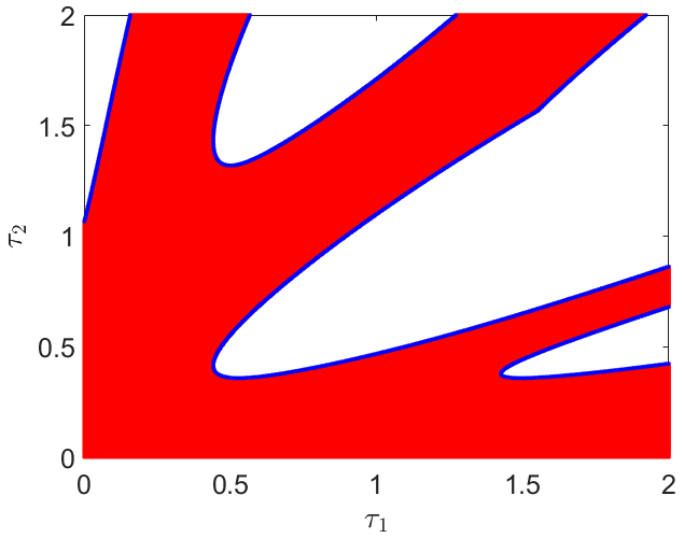

FIGURE 3.3: Stability diagram for the second-order DDE given by Eq. 3.30 obtained using the spectral tau method (red region) and the proposed pseudoinverse-based Galerkin approximation method (blue lines).

3.3 Results and discussion

In this section, we apply the methods described in Section 3.1 to two example problems taken from the literature [66, 69]. We obtain the characteristic roots of DDEs using the pseudoinverse-based Galerkin approximation method and improve closed-loop stability using the proposed optimization strategy.

3.3.1 Example from Niu et al.

Consider the following first-order system [69]:

$$\dot{x}(t) = ax(t) + a_d x(t-\tau) + u(t) \tag{3.31a}$$

$$u(t) = kx(t), \tag{3.31b}$$

where $a = \tau = 1$ and $a_d = -1$. We use $N = 100$ terms in the series solution (Eq. 3.11), thereby converting Eq. 3.31 into a system of ODEs of the form given by Eq. 3.25, where $\mathbf{G} \in \mathbb{R}^{100\times100}$. We select an initial guess of $k = 0.8$, which results in the rightmost eigenvalues shown in Fig. 3.4. Note that the rightmost eigenvalue has a positive real component ($\mathrm{Re}\,(\lambda_{\max}) = 1.5976$). Thus, the system is unstable for $k = 0.8$.

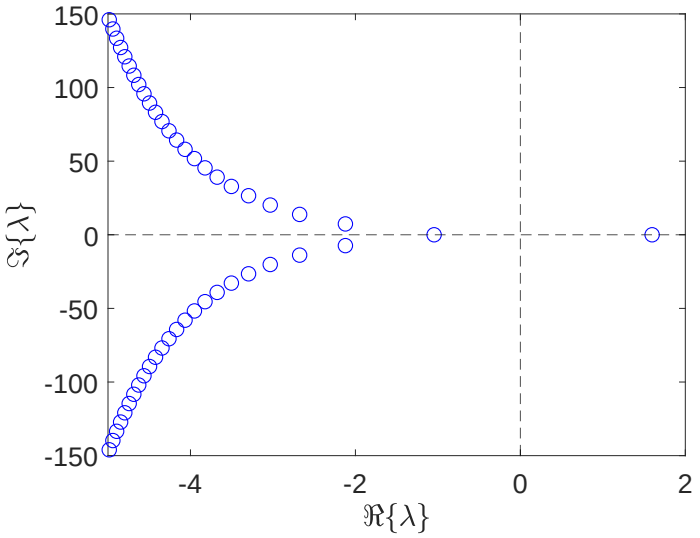

FIGURE 3.4: Rightmost characteristic roots of Eq. 3.31 using initial feedback gain $k = 0.8$.

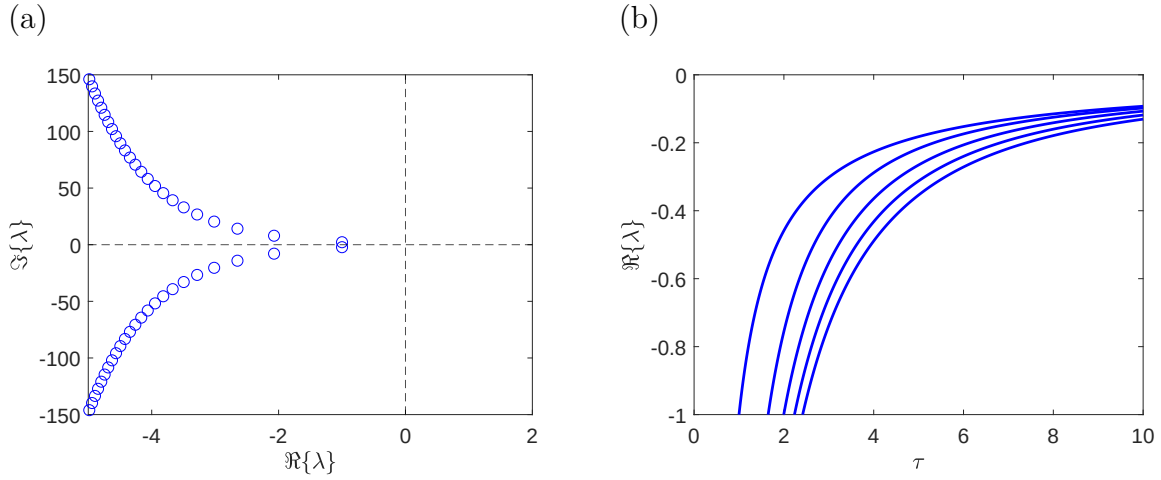

FIGURE 3.5: Rightmost characteristic roots of Eq. 3.31 with delay $\tau = 1$ (a) and the variation of the five rightmost roots with respect to delay τ (b) using optimal feedback gain $k^* = -3.5978$.

To stabilize this system, we set $\alpha = 1$ in the objective function (Eq. 3.2) and solve the minimization problem using the Nelder–Mead algorithm in MATLAB via the `fminsearch` function. The optimal gain was found to be $k^* = -3.5978$, resulting in the rightmost eigenvalues shown in Fig. 3.5(a).

Note that the rightmost eigenvalue has a real component of -1, indicating that stability has been achieved. As shown in Fig. 3.5(b), the system will remain stable for delays substantially greater than $\tau = 1$ when using feedback gain k^*. Note that the optimal objective function value of $J^* = 0$ is obtained when $\alpha = 1$ in the objective function (Eq. 3.2), indicating that α could be increased to achieve an even larger stability margin.

3.3.2 Example from Michiels et al.

We now consider the following third-order system [66]:

$$\dot{\mathbf{x}}(t) = \mathbf{A}\mathbf{x}(t) + \mathbf{B}\mathbf{u}(t-\tau) \tag{3.32a}$$

$$\mathbf{u}(t) = \mathbf{K}^{\mathrm{T}}\mathbf{x}(t), \tag{3.32b}$$

where delay $\tau = 5$, and $\mathbf{A}$ and $\mathbf{B}$ are defined as follows:

$$\mathbf{A} = \begin{bmatrix} -0.08 & -0.03 & 0.2 \\ 0.2 & -0.04 & -0.005 \\ -0.06 & 0.2 & -0.07 \end{bmatrix}, \qquad \mathbf{B} = \begin{Bmatrix} -0.1 \\ -0.2 \\ 0.1 \end{Bmatrix}. \tag{3.33}$$

We again use $N = 100$ terms in the series solution (Eq. 3.11), now obtaining a system of ODEs (Eq. 3.25) in which $\mathbf{G} \in \mathbb{R}^{300\times 300}$. We use as an initial guess the gains reported in Michiels et al. [66]: $\mathbf{K} = [0.719, 1.04, 1.29]^{\mathrm{T}}$. As shown in Fig. 3.6, the rightmost eigenvalues have a positive real component when the delay is $\tau = 5$ ($\mathrm{Re}\,(\lambda_{\max}) = 0.0232$) and the system is stable only for delays $\tau < 3.9466$.

The system can be stabilized using the same procedure as before. We set $\alpha = 1$ in the objective function (Eq. 3.2) and minimize using the Nelder–Mead algorithm. The optimal gains were found to be $\mathbf{K}^* = [0.5473, 0.8681, 0.5998]^{\mathrm{T}}$; as shown in Fig. 3.7(a), the rightmost eigenvalue was moved to $\mathrm{Re}\,(\lambda_{\max}) = -0.0931$. Once again, the rightmost eigenvalue has a negative real component and, thus, the closed-loop system is stable. As shown in Fig. 3.7(b), the system will remain stable for delays up to

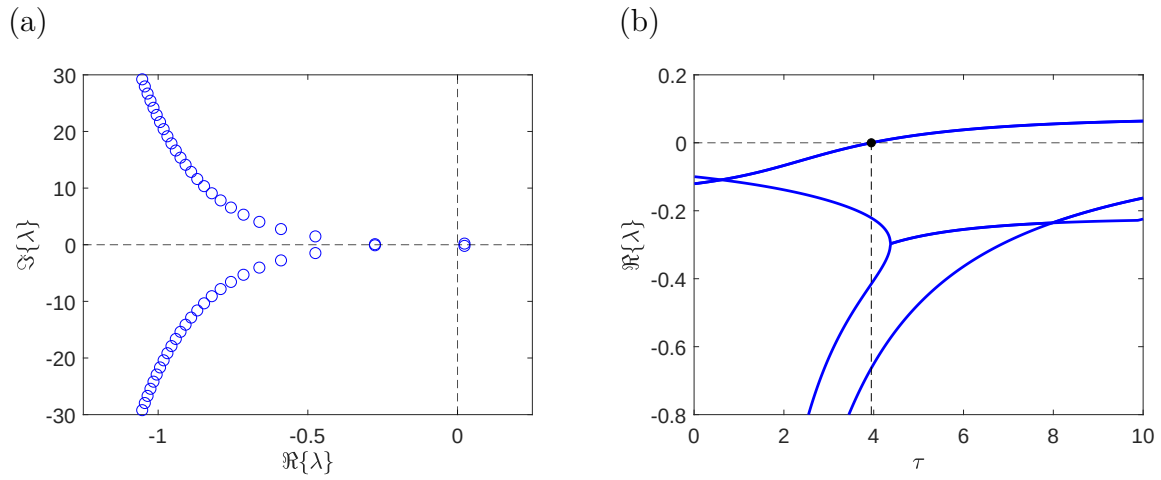

FIGURE 3.6: Rightmost characteristic roots of Eq. 3.32 with delay $\tau = 5$ (a) and the variation of the rightmost roots with respect to delay τ (b) using initial feedback gains $\mathbf{K} = [0.719, 1.04, 1.29]^{\mathrm{T}}$.

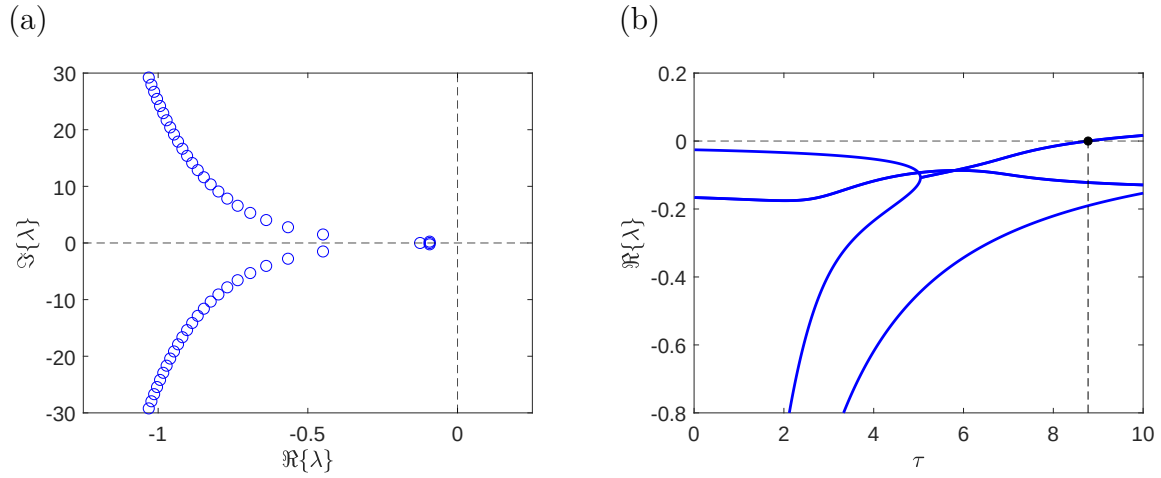

FIGURE 3.7: Rightmost characteristic roots of Eq. 3.32 with delay $\tau = 5$ (a) and the variation of the rightmost roots with respect to delay τ (b) using optimal feedback gains $\mathbf{K}^* = [0.5473, 0.8681, 0.5998]^{\mathrm{T}}$.

$\tau = 8.7739$ using optimal feedback gains $\mathbf{K}^*$. In contrast to the example of Section 3.3.1, the optimal objective function value is greater than zero ($J^* = 0.8223$) in this case, indicating that the stability margin cannot be increased by increasing α.

3.4 Experimental validation

In this section, we validate the proposed Galerkin method using the rotary inverted pendulum apparatus (QUBE-Servo Rotary Servo Experiment, Quanser Inc., Markham, Ontario, Canada) shown in Fig. 3.8. The apparatus consists of a free-swinging rigid pendulum mounted to the end of a servo-driven rotary arm. The position of the arm is given by θ as it rotates about the vertical axis; the position of the pendulum is $\gamma = 0^{\circ}$ when hanging at rest and $\gamma = 180^{\circ}$ when inverted.

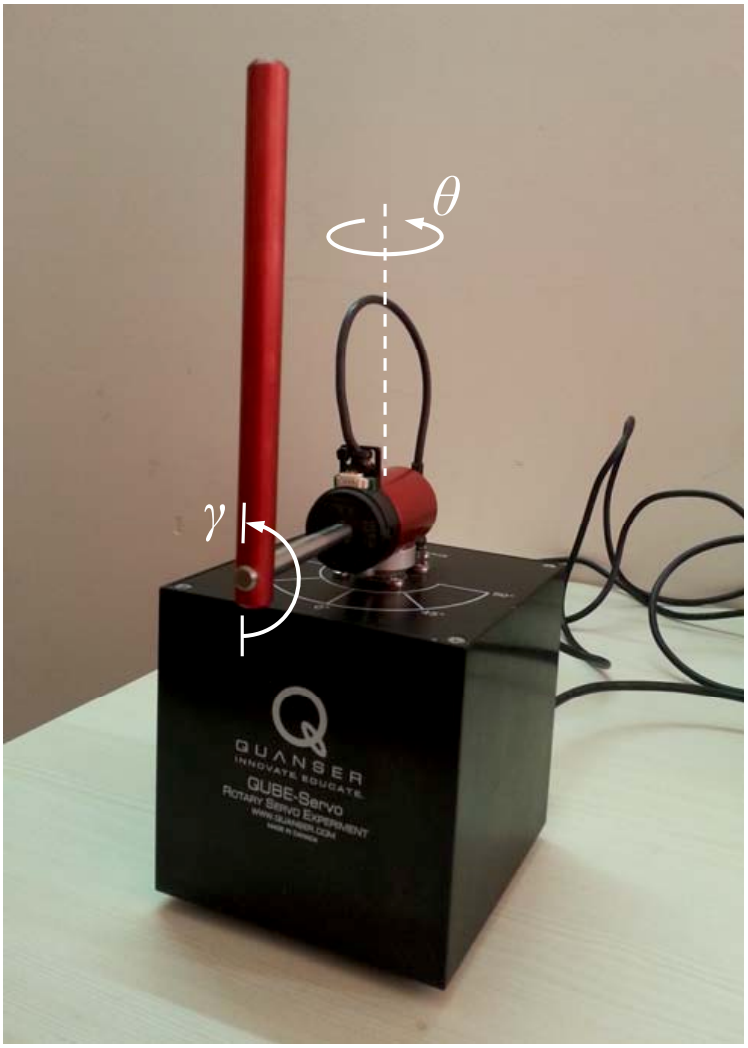

FIGURE 3.8: Rotary inverted pendulum apparatus, shown here with $\theta \approx 0^{\circ}$ and $\gamma \approx 180^{\circ}$.

The linearized equations of motion for the rotary inverted pendulum system are as follows:

$$(J_r + m_p\ell_r^2)\ddot{\theta}(t) - \frac{1}{2}m_p\ell_p\ell_r\ddot{\gamma}(t) = T(t) - B_r\dot{\theta}(t) \tag{3.34a}$$

$$\left(J_p + \frac{1}{4}m_p\ell_p^2\right)\ddot{\gamma}(t) - \frac{1}{2}m_p\ell_p\ell_r\ddot{\theta}(t) - \frac{1}{2}m_p\ell_p g\gamma(t) = -B_p\dot{\gamma}(t), \tag{3.34b}$$

where ℓ_p, m_p, and J_p are the pendulum's length, mass, and moment of inertia with respect to its pivot; ℓ_r is the length of the rotary arm; J_r is the equivalent moment of inertia acting on the servo shaft; B_p and B_r represent the viscous damping about the pendulum's pivot and the servo shaft, respectively; g is the gravitational acceleration; and $T(t)$ is the torque applied to the rotary arm by the servo. The torque $T(t)$ can be computed as follows:

$$T(t) = \frac{k_m}{R_m}\left(V_m(t) - \frac{k_m^2}{R_m}\dot{\theta}(t)\right), \tag{3.35}$$

where k_m is the DC motor back-emf constant, R_m is the electrical resistance of the DC motor armature, and $V_m(t)$ is the control input (voltage). The numerical values of these parameters are provided by Quanser [2] and are listed in Table 3.2. The linearized equations of motion for the rotary inverted pendulum system (Eq. 3.34) can be expressed in state-space form:

$$\dot{\mathbf{x}}(t) = \mathbf{A}\mathbf{x}(t) + \mathbf{B}u(t) \tag{3.36a}$$

$$u(t) = -\mathbf{K}^{\mathrm{T}}\mathbf{x}(t), \tag{3.36b}$$

TABLE 3.2: Parameter values for the rotary inverted pendulum apparatus [2].

Parameter	Value	Units
ℓ_p	0.129	m
ℓ_r	0.085	m
m_p	0.024	kg
J_p	3.32820×10^{-5}	kg m^2
J_r	5.71979×10^{-5}	kg m^2
B_p	0	N m s/rad
B_r	0	N m s/rad
R_m	8.4	Ω
k_m	0.042	V s/rad
g	9.81	m/s^2

where $\mathbf{x} \triangleq \left[\theta(t), \gamma(t), \dot{\theta}(t), \dot{\gamma}(t)\right]^{\mathrm{T}}$, $u(t) \triangleq V(t)$, and $\mathbf{A}$ and $\mathbf{B}$ are given as follows:

$$\mathbf{A} = \begin{bmatrix} 0 & 0 & 1 & 0 \\ 0 & 0 & 0 & 1 \\ 0 & 149.2751 & -0.0104 & 0 \\ 0 & 261.6091 & -0.0103 & 0 \end{bmatrix}, \qquad \mathbf{B} = \begin{Bmatrix} 0 \\ 0 \\ 49.7275 \\ 49.1493 \end{Bmatrix}. \tag{3.37}$$

The controller samples at a rate of 500 Hz; thus, the system has an inherent delay of 2 ms. We begin by controlling the rotary inverted pendulum system without introducing any additional delays. We use feedback gains $\mathbf{K} = [-2, 30, -2, 2.5]^{\mathrm{T}}$, which are provided by Quanser for the balance control exercise [129]. The steady-state response of the physical system is shown in Fig. 3.9. The system is stable about its vertical equilibrium ($\gamma = 180^{\circ}$) and recovers from an external disturbance.

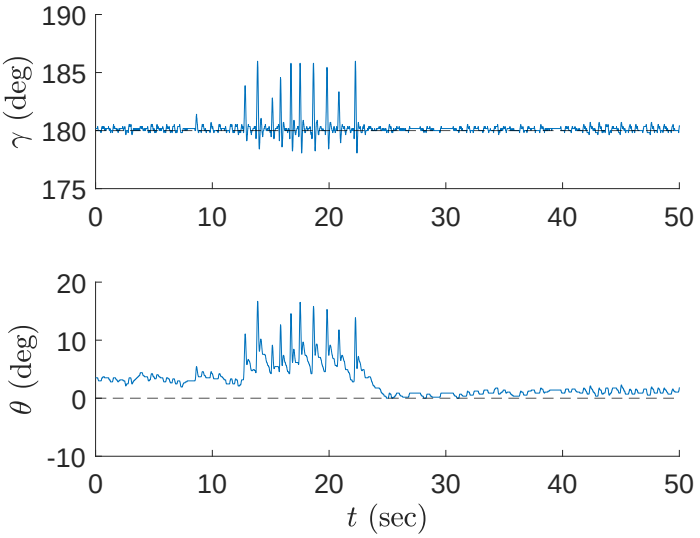

FIGURE 3.9: Stable response of the inverted pendulum (γ) and rotary arm (θ) with inherent delay of 2 ms and feedback gains $\mathbf{K} = [-2, 30, -2, 2.5]^{\mathrm{T}}$. An external disturbance is applied between 13 and 23 seconds.

We now introduce an additional sensing delay τ, resulting in the following state-space representation of the rotary inverted pendulum system:

$$\dot{\mathbf{x}}(t) = \mathbf{A}\mathbf{x}(t) + \mathbf{B}u(t - \tau), \tag{3.38}$$

where $\mathbf{A}$ and $\mathbf{B}$ are given by Eq. 3.37. We first assess the stability of the system using the proposed pseudoinverse-based Galerkin method, then verify our predictions

experimentally. The real component of the rightmost roots of the system are shown in Fig. 3.10 as functions of delay τ, using the same feedback gains $\mathbf{K}$ as above.

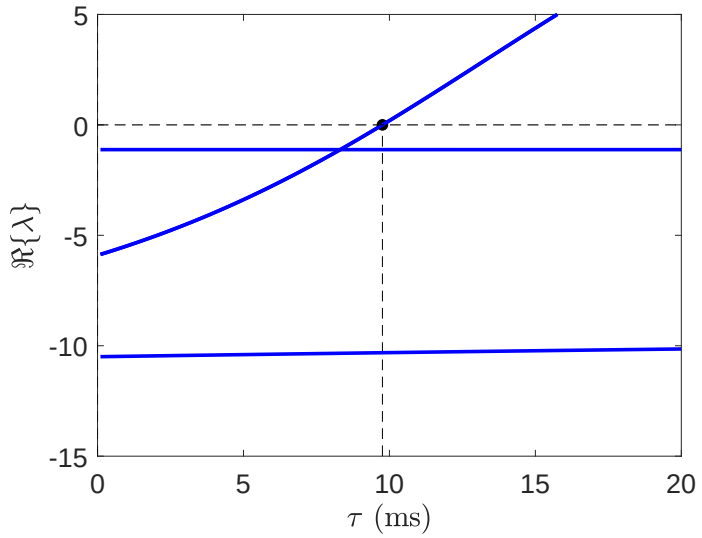

FIGURE 3.10: Variation of the rightmost roots of Eq. 3.38 with respect to delay τ using feedback gains $\mathbf{K} = [-2, 30, -2, 2.5]^{\mathrm{T}}$. The critical delay is $\tau = 9.76$ ms.

The *critical delay* is the delay at which the system will become unstable; as shown, the simulations indicate a critical delay of $\tau = 9.76$ ms. As shown in Fig. 3.11, the four rightmost characteristic roots of Eq. 3.38 lie in the left half of the complex plane when $\tau = 5$ ms, indicating that the system is stable; when $\tau = 10$ ms, two roots are in the right half of the complex plane and the system is unstable.

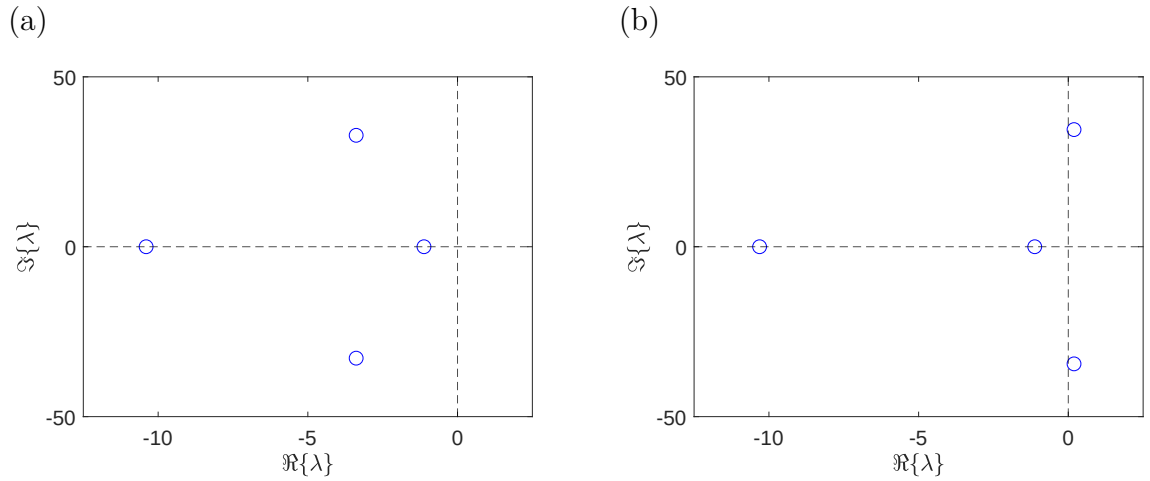

FIGURE 3.11: Rightmost characteristic roots of Eq. 3.38 with delay (a) $\tau = 5$ ms and (b) $\tau = 10$ ms, using feedback gains $\mathbf{K} = [-2, 30, -2, 2.5]^{\mathrm{T}}$.

We validate experimentally by deliberately introducing additional delay into the feedback controller, in increments of 0.5 ms. The physical system remained stable when delays of up to 7.5 ms were introduced (Fig. 3.12(a)) and was unstable with an additional delay of 8 ms (Fig. 3.12(b)).

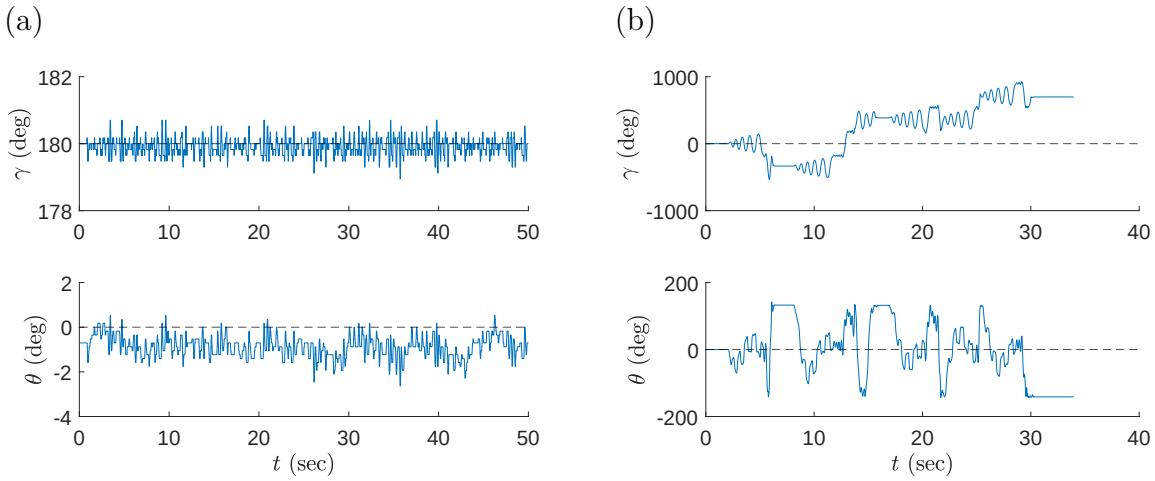

FIGURE 3.12: System response of the inverted pendulum (γ) and rotary arm (θ) using feedback gains $\mathbf{K}^* = [-2, 30, -2, 2.5]^{\mathrm{T}}$, with total delay of (a) $\tau = 2 + 7.5 = 9.5$ ms–stable response and (b) $\tau = 2 + 8 = 10$ ms–unstable response.

Thus, when added to the inherent delay of 2 ms, the physical system exhibited a critical delay of between 9.5 and 10 ms, which is in agreement with the predicted critical delay of $\tau = 9.76$ ms.

We now stabilize Eq. 3.38 with delay $\tau = 10$ ms using the pseudoinverse-based Galerkin method and the procedure described in Section 3.1. We set $\alpha = \alpha_0 = 1$ in the objective function (Eq. 3.2) and solve the minimization problem using the Nelder–Mead algorithm in MATLAB via the `fminsearch` function. We repeat the optimization procedure, increasing α by $\delta\alpha = 1$ each iteration, until the real component of the rightmost pole is unable to reach $-\alpha$. In this case, the algorithm terminates at $\alpha = 6$, where the objective function value is $J^* = 0.000222$, the optimal feedback gains are $\mathbf{K}^* = [-2.3443, 31.3406, -1.1797, 2.7717]^{\mathrm{T}}$, and the rightmost pole location is $\mathrm{Re}(\lambda_{\max}) = -5.9851$. As shown in Fig. 3.13, the physical system is stable when a delay of 10 ms is introduced deliberately (producing a total delay of $\tau = 12$ ms) and recovers from an external disturbance. As shown, the system is robust to external disturbances even without controlling the frequency of oscillations induced by the optimal feedback gains.

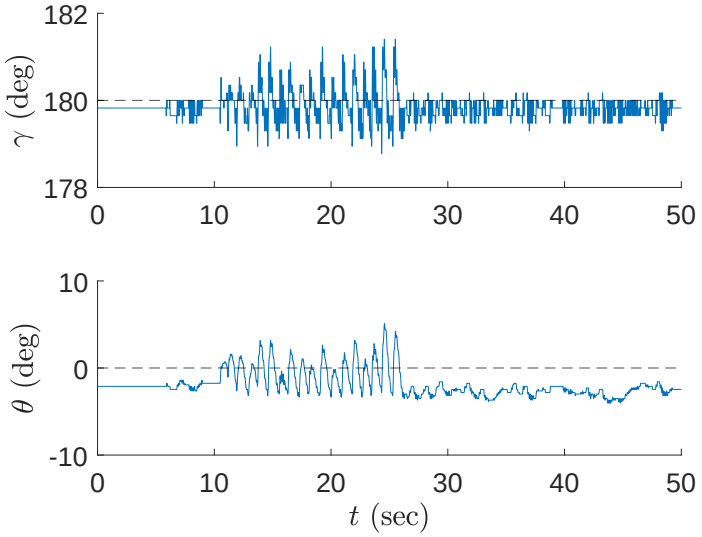

FIGURE 3.13: Stable response of the inverted pendulum (γ) and rotary arm (θ) with total delay of $\tau = 2 + 10 = 12$ ms and optimal feedback gains $\mathbf{K}^* = [-2.3443, 31.3406, -1.1797, 2.7717]^{\mathrm{T}}$. An external disturbance is applied between 12 and 27 seconds.

The pseudoinverse-based Galerkin method predicts a critical delay of $\tau = 17.7$ ms when using the optimal feedback gains $\mathbf{K}^*$ computed above (Fig. 3.14).

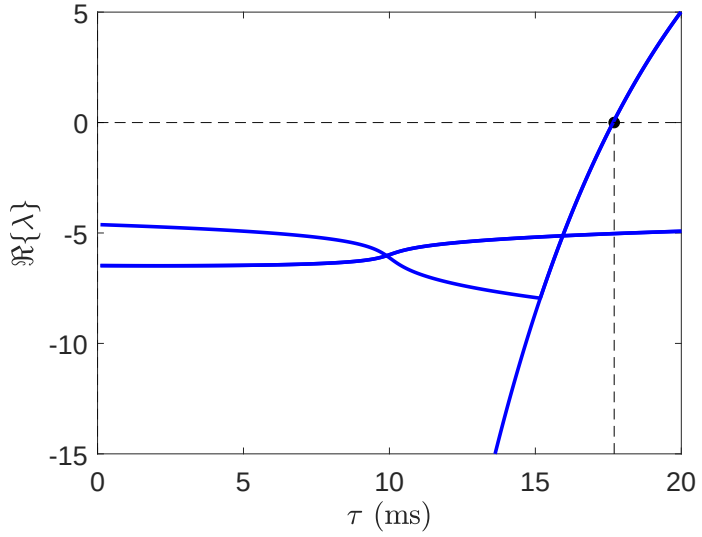

FIGURE 3.14: Variation of the rightmost roots of Eq. 3.38 with respect to delay τ using optimal feedback gains $\mathbf{K}^* = [-2.3443, 31.3406, -1.1797, 2.7717]^{\mathrm{T}}$. The critical delay is $\tau = 17.7$ ms.

We again validate this result experimentally by deliberately introducing additional delay into the feedback controller, in increments of 0.5 ms. The physical system remained stable when delays of up to 15 ms were introduced (Fig. 3.15(a)) and was unstable when this delay was increased to 15.5 ms (Fig. 3.15(b)).

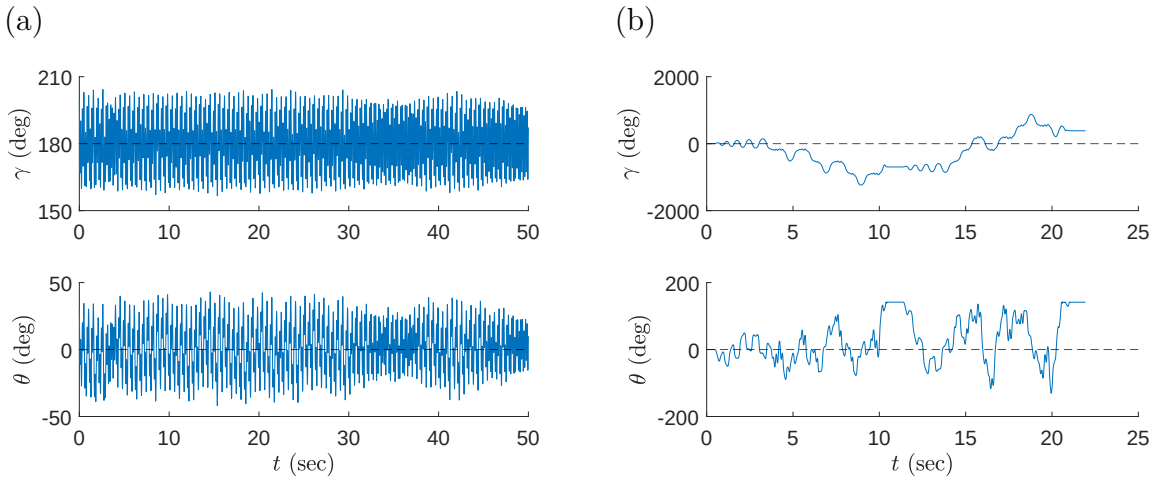

FIGURE 3.15: System response of the inverted pendulum (γ) and rotary arm (θ) using optimal feedback gains $\mathbf{K}^* = [-2.3443, 31.3406, -1.1797, 2.7717]^{\mathrm{T}}$, with total delay of (a) $\tau = 2 + 15 = 17$ ms–stable response and (b) $\tau = 2 + 15.5 = 17.5$ ms–unstable response.

Thus, when added to the inherent delay of 2 ms, the physical system exhibited a critical delay of between 17 and 17.5 ms, which is within 1–4% of the predicted critical delay of $\tau = 17.7$ ms. The pseudoinverse-based Galerkin method provided a simple and reliable means of predicting and optimizing the stability of the rotary inverted pendulum system.

3.5 Chapter summary

In this chapter, the pole placement problem for TDS with constant delays is explored. A Galerkin approximation method using a new pseudoinverse-based strategy for embedding the boundary conditions was developed, and the results were verified through comparison to those obtained using the QPmR algorithm, the PSD method, and the spectral tau method. The proposed Galerkin method results in a simpler mathematical derivation than was presented previously in the works of Vyasarayani, Sadath, and colleagues [48, 49, 62]. The proposed method was validated experimentally by

stabilizing a rotary inverted pendulum system with inherent and deliberate state feedback delays. A simple optimization strategy was employed to increase the time-delay stability margin.

Chapter 4

Hybrid method-of-receptances and optimization-based technique for pole placement in TDS

Consider the following second-order system with feedback control:

$$\mathbf{M}\ddot{\mathbf{x}}(t) + \mathbf{C}\dot{\mathbf{x}}(t) + \mathbf{K}\mathbf{x}(t) = \mathbf{b}u(t-\tau) \tag{4.1a}$$

$$u(t-\tau) = \mathbf{f}^{\mathrm{T}}\dot{\mathbf{x}}(t-\tau) + \mathbf{g}^{\mathrm{T}}\mathbf{x}(t-\tau), \tag{4.1b}$$

where $\mathbf{x}$ is the state vector; $\mathbf{M}$, $\mathbf{C}$, and $\mathbf{K}$ are the mass, damping, and stiffness matrices; u is the control effort, which is mapped onto the states by $\mathbf{b}$; $\mathbf{f}$ and $\mathbf{g}$ contain the control gains; and τ is a time delay.

As demonstrated in the previous chapter, pole placement is a classical problem in the control theory domain. The objective is to design a controller that places the closed-loop poles at specific locations, thereby resulting in the desired system behaviour. In this chapter, the pole-placement problem for systems governed by second-order DDEs is considered. Time delays in Eq. (4.1) turn a finite-dimensional system of ODEs into an infinite-dimensional system due to the transcendental nature of the characteristic equation. This infinite dimensionality makes the pole-placement problem challenging for TDS [5–7]. Because tuning an infinite number of parameters is impossible, our objective is to tune finitely many parameters to control an infinite-dimensional system.

In this chapter, a pole-placement technique for TDS that combines the strengths of the method of receptances and an optimization-based strategy is presented. The method of receptances is simple and efficient, but may fail for certain systems and time

delays. On the other hand, the optimization-based strategy guarantees the location of the rightmost pole but is more computationally demanding. Other established methods to design controllers for TDS include the Smith predictor, the modified Smith predictor, and finite spectrum assignment [130]; however, the performance of these methods depends on the accuracy of an internal model. For example, these techniques will stabilize an otherwise unstable TDS only if the internal model is predicted accurately and if the effects of initial conditions and disturbances are known. These techniques are also sensitive to inaccuracies in the implementation of the control law, and require computing integrals of past control inputs which, when approximated using numerical quadrature, can affect system stability. By contrast, an internal model is not required in our proposed hybrid method, so it does not suffer from these limitations. Finally, it should be noted that the Smith predictor, the modified Smith predictor, and finite spectrum assignment are sensitive to small perturbations in time delay around an assumed operating point; as it will be shown, the proposed approach exhibits robustness to perturbations in time delay.

In this chapter, an optimization-based strategy is proposed to address the limitations of the method of receptances. The pole-placement method of Michiels et al. [66] also employs optimization; however, the proposed approach in this chapter differs in two substantial respects. First, Michiels et al. obtain the characteristic roots using subspace iteration [131] whereas Galerkin approximations are in this chapter. Second, Michiels et al. use a gradient descent algorithm for pole placement, which may fail to find the globally optimal solution; particle swarm optimization (PSO) is proposed to avoid converging to a local optimum.

The remainder of this chapter is organized as follows. Section 4.1 briefly describes the method of receptances for completeness. In Section 4.2, a detailed mathematical derivation of the Galerkin approximations to find the characteristic roots of quadratic TDS with a single delay is provided. The optimization problem is defined in Section 4.3. In Section 4.4, the proposed method is applied to stabilize examples given by Ram et al. [75]. Finally, experimental validation using a 3D hovercraft apparatus is presented in Section 4.5.

4.1 Method of Receptances

In this section, the MoR is briefly described for completeness. Consider the following system, which is obtained upon substituting $\mathbf{x}(t) = \mathbf{x}_0 e^{rt}$ into Eq. (4.1):

$$\Big(r^2\mathbf{M} + r\mathbf{C} + \mathbf{K}\Big)\mathbf{x}_0 e^{rt} = \Big(r\mathbf{b}\mathbf{f}^{\mathrm{T}} + \mathbf{b}\mathbf{g}^{\mathrm{T}}\Big)\mathbf{x}_0 e^{r(t-\tau)}. \tag{4.2}$$

Equation (4.2) can be rewritten as follows:

$$\Big[r^2\mathbf{M} + r(\mathbf{C} - \mathbf{b}\mathbf{f}^{\mathrm{T}}e^{-r\tau}) + (\mathbf{K} - \mathbf{b}\mathbf{g}^{\mathrm{T}}e^{-r\tau})\Big]\mathbf{x}_0 = 0. \tag{4.3}$$

The receptance matrices associated with the open-loop system ($\mathbf{H}_o(r)$) and closed-loop system ($\mathbf{H}_c(r)$) are the following:

$$\mathbf{H}_o(r) = \Big[r^2\mathbf{M} + r\mathbf{C} + \mathbf{K}\Big]^{-1} \tag{4.4a}$$

$$\mathbf{H}_c(r) = \Big[r^2\mathbf{M} + r(\mathbf{C} - \mathbf{b}\mathbf{f}^{\mathrm{T}}e^{-r\tau}) + (\mathbf{K} - \mathbf{b}\mathbf{g}^{\mathrm{T}}e^{-r\tau})\Big]^{-1} \tag{4.4b}$$

Matrix $\mathbf{H}_c(r)$ can be computed using the Sherman–Morrison formula [132]:

$$\mathbf{H}_c(r) = \mathbf{H}_o(r) + \frac{\mathbf{H}_o(r)\mathbf{b}(\mathbf{g} + r\mathbf{f})^{\mathrm{T}}\mathbf{H}_o(r)e^{-r\tau}}{1 - (\mathbf{g} + r\mathbf{f})^{\mathrm{T}}\mathbf{H}_o(r)\mathbf{b}e^{-r\tau}}. \tag{4.5}$$

Note that the values of r that render $\mathbf{H}_c(r)$ unbounded are the eigenvalues of the closed-loop system. Thus, the characteristic equation of Eq. (4.5) is the following:

$$(\mathbf{g} + r\mathbf{f})^{\mathrm{T}}\mathbf{H}_o(r)\mathbf{b} = e^{r\tau}, \tag{4.6}$$

where the control vectors $\mathbf{f}$ and $\mathbf{g}$ can be computed given the system matrices ($\mathbf{M}$, $\mathbf{C}$, and $\mathbf{K}$), the vector that maps the control effort onto the states ($\mathbf{b}$), the delay (τ), and eigenvalues r_k, $k = 1, 2, \ldots, 2n$:

$$\begin{bmatrix} r_1\mathbf{r}_1^{\mathrm{T}} & \mathbf{r}_1^{\mathrm{T}} \\ r_2\mathbf{r}_2^{\mathrm{T}} & \mathbf{r}_2^{\mathrm{T}} \\ \vdots & \vdots \\ r_{2n}\mathbf{r}_{2n}^{\mathrm{T}} & \mathbf{r}_{2n}^{\mathrm{T}} \end{bmatrix} \begin{Bmatrix} \mathbf{f} \\ \mathbf{g} \end{Bmatrix} = \begin{Bmatrix} e^{r_1\tau} \\ e^{r_2\tau} \\ \vdots \\ e^{r_{2n}\tau} \end{Bmatrix} \tag{4.7}$$

where $\mathbf{r}_k \triangleq \mathbf{H}_o(r_k)\mathbf{b}$. Thus, the control vectors $\mathbf{f}$ and $\mathbf{g}$ can be obtained simply by solving a linear system of $2n$ equations (Eq. (4.7)) for $2n$ unknowns.

As stated in Chapter 1, the MoR approach is computationally straightforward

but can suffer from spillover—that is, the poles placed at the specified locations may not be the dominant poles. A separate analysis must be performed to compute the characteristic roots and, thus, to determine whether the resulting closed-loop system is stable. The roots of the TDS are computed explicitly using Galerkin approximations with the spectral-tau method (described below). In situations where spillover is detected in the solution provided by the MoR approach, a new optimization-based pole-placement strategy is proposed. The proposed optimization strategy makes use of the information about the characteristic roots that is provided by the Galerkin approximations.

A TDS has a transcendental characteristic equation. Several methods have been proposed in the literature to compute the characteristic roots of a TDS, including the Lambert W function [5], Galerkin approximations [48, 49], semi-discretization [51], pseudospectral collocation [53], continuous-time approximation [57], and homotopy continuation [45]. In this work, Galerkin approximations are used to compute the characteristic roots. First, the equation governing the dynamics of the TDS (which is a DDE) is first converted into a PDE with boundary conditions. The PDE is then approximated by a system of ODEs, the eigenvalues of which are the approximate roots of the characteristic equation of the TDS. The efficacy of Galerkin approximations in studying the stability of DDEs has been demonstrated previously [49, 62, 133, 134]. These studies have also shown that the eigenvalues of the approximate ODE system converge to the eigenvalues of the original DDE system starting from the rightmost root.

The boundary conditions in previous work using Galerkin approximations have been handled using the spectral-tau and Lagrange multiplier methods [49, 62, 133, 134]. In this chapter, the spectral-tau method for embedding the boundary conditions is used because, with this method, the formulation can be generalized such that only the boundary conditions differ for different problems. Several options also exist for selecting the basis functions. In this chapter, shifted Legendre polynomials are used as the basis functions because of their superior convergence properties compared to other basis functions, such as mixed Fourier and Chebyshev polynomials [62].

4.2 Mathematical modelling

In this section, the mathematical model for finding the characteristic roots of a DDE using Galerkin approximations is presented. We consider systems of DDEs of the form

given in Eq. (4.1) higher-order systems have also been considered in the literature [74]. We begin by expressing Eq. (4.1) in first-order form:

$$\dot{\bar{\mathbf{x}}}(t) + \bar{\mathbf{A}}\bar{\mathbf{x}}(t) + \bar{\mathbf{b}}u(t-\tau) = 0 \tag{4.8a}$$

$$u(t-\tau) = \bar{\mathbf{k}}^{\mathrm{T}}\bar{\mathbf{x}}(t-\tau) \tag{4.8b}$$

where $\bar{\mathbf{x}}(t) \triangleq [\dot{\mathbf{x}}^{\mathrm{T}}(t), \mathbf{x}^{\mathrm{T}}(t)]^{\mathrm{T}} \in \mathbb{R}^{P\times 1}$ is the state vector, u is the control effort, and $\tau > 0$ is the time delay. Matrix $\bar{\mathbf{A}} \in \mathbb{R}^{P\times P}$ and vectors $\bar{\mathbf{b}} \in \mathbb{R}^{P\times 1}$ and $\bar{\mathbf{k}} \in \mathbb{R}^{P\times 1}$ are given as follows:

$$\bar{\mathbf{A}} \triangleq \begin{bmatrix} \mathbf{M}^{-1}\mathbf{C} & \mathbf{M}^{-1}\mathbf{K} \\ -\mathbf{I} & 0 \end{bmatrix}, \qquad \bar{\mathbf{b}} \triangleq \begin{Bmatrix} -\mathbf{M}^{-1}\mathbf{b} \\ 0 \end{Bmatrix}, \qquad \bar{\mathbf{k}} \triangleq \begin{Bmatrix} \mathbf{f} \\ \mathbf{g} \end{Bmatrix}, \tag{4.9}$$

where $\mathbf{I}$ is the identity matrix. The characteristic equation of Eq. (4.8) can be obtained by substituting $\bar{\mathbf{x}}(t) = \bar{\mathbf{x}}_0 e^{st}$ and equating the determinant to zero:

$$\det(s\mathbf{I} + \bar{\mathbf{A}} + \bar{\mathbf{b}}\bar{\mathbf{k}}^{\mathrm{T}}e^{-s\tau}) = 0. \tag{4.10}$$

Equation (4.10) is a quasi-polynomial due to the transcendental terms $e^{-s\tau}$ and therefore has infinitely many roots. These roots can be computed by formulating an abstract Cauchy problem, ultimately resulting in a large linear eigenvalue problem.

We first convert the system of DDEs (Eq. (4.8)) into a system of PDEs with time-dependent boundary conditions. We perform the following transformation:

$$\mathbf{y}(s,t) = \bar{\mathbf{x}}(t+s), \tag{4.11}$$

where $\mathbf{y}$ is a function of $s \in [-\tau, 0]$ and t. We obtain an abstract Cauchy problem by differentiating Eq. (4.11) with respect to s and t:

$$\frac{\partial \mathbf{y}(s,t)}{\partial t} = \frac{\partial \bar{\mathbf{x}}(t+s)}{\partial (t+s)}\frac{\partial (t+s)}{\partial t} = \frac{\partial \bar{\mathbf{x}}(t+s)}{\partial (t+s)}, \tag{4.12a}$$

$$\frac{\partial \mathbf{y}(s,t)}{\partial s} = \frac{\partial \bar{\mathbf{x}}(t+s)}{\partial (t+s)}\frac{\partial (t+s)}{\partial s} = \frac{\partial \bar{\mathbf{x}}(t+s)}{\partial (t+s)}. \tag{4.12b}$$

Equating Eqs. (4.12a) and (4.12b) results in the following PDE:

$$\frac{\partial \mathbf{y}(s,t)}{\partial t} = \frac{\partial \mathbf{y}(s,t)}{\partial s}, \quad s \in [-\tau, 0]. \tag{4.13}$$

The boundary conditions for Eq. (4.13) can be computed from Eq. (4.11) upon substituting $s = 0$ and $s = -\tau$:

$$\mathbf{y}(0,t) = \bar{\mathbf{x}}(t), \tag{4.14a}$$

$$\mathbf{y}(-\tau,t) = \bar{\mathbf{x}}(t-\tau). \tag{4.14b}$$

Differentiating Eq. (4.14a) with respect to t provides the following relationship between $\mathbf{y}(s,t)$ and the state derivatives $\dot{\bar{\mathbf{x}}}(t)$:

$$\left.\frac{\partial \mathbf{y}(s,t)}{\partial t}\right|_{s=0} = \dot{\bar{\mathbf{x}}}(t). \tag{4.15}$$

Finally, we combine Eq. (4.14) with Eq. (4.8):

$$\left.\frac{\partial \mathbf{y}(s,t)}{\partial t}\right|_{s=0} + \bar{\mathbf{A}}\mathbf{y}(0,t) + \bar{\mathbf{b}}\bar{\mathbf{k}}^{\mathrm{T}}\mathbf{y}(-\tau,t) = 0. \tag{4.16}$$

We now approximate the solution of the PDE given in Eq. (4.13) with the following series:

$$y_i(s,t) = \sum_{j=1}^{\infty} \phi_{ij}(s)\eta_{ij}(t), \quad i = 1,2,\ldots,P, \tag{4.17}$$

where $\phi_{ij}(s)$ are the basis functions, $\eta_{ij}(t)$ are the coordinates (which are time dependent), i is the index into the state vector $\bar{\mathbf{x}}(t)$, and j is the corresponding term in each basis function. In this work, we use shifted Lagrange polynomials as the basis functions:

$$\phi_1(s) = 1 \tag{4.18a}$$

$$\phi_2(s) = 1 + \frac{2s}{\tau} \tag{4.18b}$$

$$\phi_k(s) = \frac{(2k-3)\phi_2(s)\phi_{k-1}(s) - (k-2)\phi_{k-2}(s)}{k-1}, \qquad k = 3,4,\ldots,N. \tag{4.18c}$$

Shifted Lagrange polynomials are selected for their superior convergence properties, as shown in previous studies (e.g., [62]). We truncate the infinite series (Eq. (4.17)) at N terms:

$$y_i(s,t) \approx \boldsymbol{\phi}_i^{\mathrm{T}}(s)\boldsymbol{\eta}_i(t), \quad i = 1,2,\ldots,P, \tag{4.19}$$

where $\boldsymbol{\phi}_i(s) \triangleq [\phi_{i1}(s), \phi_{i2}(s), \ldots, \phi_{iN}(s)]^{\mathrm{T}}$ and $\boldsymbol{\eta}_i(t) \triangleq [\eta_{i1}(t), \eta_{i2}(t), \ldots, \eta_{iN}(t)]^{\mathrm{T}}$. For simplicity of notation, we define the following:

$$\boldsymbol{\Phi}(s) \triangleq \begin{bmatrix} \boldsymbol{\phi}_1(s) & 0 & \cdots & 0 \\ 0 & \boldsymbol{\phi}_2(s) & \cdots & 0 \\ \vdots & \vdots & \ddots & \vdots \\ 0 & 0 & \cdots & \boldsymbol{\phi}_P(s) \end{bmatrix} \in \mathbb{R}^{NP \times P} \tag{4.20a}$$

$$\boldsymbol{\beta}(t) \triangleq [\boldsymbol{\eta}_1^{\mathrm{T}}(t), \boldsymbol{\eta}_2^{\mathrm{T}}(t), \ldots, \boldsymbol{\eta}_P^{\mathrm{T}}(t)]^{\mathrm{T}} \in \mathbb{R}^{NP \times 1}, \tag{4.20b}$$

and express Eq. (4.19) in vector form:

$$\mathbf{y}(s,t) = [\boldsymbol{\phi}_1^{\mathrm{T}}(s)\boldsymbol{\eta}_1(t), \boldsymbol{\phi}_2^{\mathrm{T}}(s)\boldsymbol{\eta}_2(t), \ldots, \boldsymbol{\phi}_P^{\mathrm{T}}(s)\boldsymbol{\eta}_P(t)]^{\mathrm{T}} \tag{4.21}$$

$$= \boldsymbol{\Phi}^{\mathrm{T}}(s)\boldsymbol{\beta}(t). \tag{4.22}$$

We now obtain a system of ODEs by substituting the series solution (Eq. (4.21)) into the PDE (Eq. (4.13)), pre-multiplying the result by $\boldsymbol{\Phi}(s)$, and integrating over the domain $s \in [-\tau, 0]$:

$$\mathbf{G}\ddot{\boldsymbol{\beta}}(t) = \mathbf{H}\dot{\boldsymbol{\beta}}(t), \tag{4.23}$$

where $\mathbf{G}$ and $\mathbf{H}$ are square, block-diagonal matrices of dimension NP:

$$\mathbf{G} \triangleq \begin{bmatrix} \mathbf{G}^{(1)} & 0 & \cdots & 0 \\ 0 & \mathbf{G}^{(2)} & \cdots & 0 \\ \vdots & \vdots & \ddots & \vdots \\ 0 & 0 & \cdots & \mathbf{G}^{(P)} \end{bmatrix}^{\mathrm{T}}, \qquad \mathbf{H} \triangleq \begin{bmatrix} \mathbf{H}^{(1)} & 0 & \cdots & 0 \\ 0 & \mathbf{H}^{(2)} & \cdots & 0 \\ \vdots & \vdots & \ddots & \vdots \\ 0 & 0 & \cdots & \mathbf{H}^{(P)} \end{bmatrix}^{\mathrm{T}}. \tag{4.24}$$

Submatrices $\mathbf{G}^{(i)}$ and $\mathbf{H}^{(i)}$ are defined as follows:

$$\mathbf{G}^{(i)} \triangleq \int_{-\tau}^{0} \phi_i(s)\phi_i^{\mathrm{T}}(s)\mathrm{d}s, \qquad \mathbf{H}^{(i)} \triangleq \int_{-\tau}^{0} \phi_i(s)\phi_i'(s)^{\mathrm{T}}\mathrm{d}s, \tag{4.25}$$

where $\phi_i'(s)$ denotes the derivative of $\phi_i(s)$ with respect to s. Note that the use of shifted Lagrange polynomials as basis functions allows us to express submatrices $\mathbf{G}^{(i)}$ and $\mathbf{H}^{(i)}$ in closed form [62].

The boundary conditions that transform the initial value problem into an initial–boundary value problem are obtained by substituting Eq. (4.11) into Eq. (4.8), where $\mathbf{y}(s,t)$ is given by Eq. (4.21):

$$\boldsymbol{\Phi}^{\mathrm{T}}(0)\dot{\boldsymbol{\beta}}(t) + \left[\bar{\mathbf{A}}\boldsymbol{\Phi}^{\mathrm{T}}(0) + \bar{\mathbf{b}}\bar{\mathbf{k}}^{\mathrm{T}}\boldsymbol{\Phi}^{\mathrm{T}}(-\tau)\right]\boldsymbol{\beta}(t) = 0. \tag{4.26}$$

We embed the boundary conditions (Eq. (4.26)) into the ODE system (Eq. (4.23)) using the spectral-tau method:

$$\tilde{\mathbf{G}}\ddot{\boldsymbol{\beta}}(t) = \tilde{\mathbf{H}}\dot{\boldsymbol{\beta}}(t) + \tilde{\mathbf{K}}\boldsymbol{\beta}(t), \tag{4.27}$$

where $\tilde{\mathbf{G}}$, $\tilde{\mathbf{H}}$, and $\tilde{\mathbf{K}}$ are the matrices obtained upon replacing every iN-th row of Eq. (4.23) with the i-th row of Eq. (4.26) for $i = 1, 2, \ldots, P$. Finally, we define state vector $\boldsymbol{\zeta}(t) \triangleq \left[\dot{\boldsymbol{\beta}}(t)^{\mathrm{T}}, \boldsymbol{\beta}(t)^{\mathrm{T}}\right]^{\mathrm{T}}$ and rewrite Eq. (4.27) as follows:

$$\dot{\boldsymbol{\zeta}}(t) = \mathbf{Z}\boldsymbol{\zeta}(t), \tag{4.28}$$

where the eigenvalues of $\mathbf{Z}$ can be used to study the stability of the system.

Equation (4.28) is a system of ODEs whose response approximates that of the original system of DDEs (Eq. (4.8)). As N (the number of terms retained in the series solution, Eq. (4.19)) increases, the eigenvalues of $\mathbf{Z}$ converge to the characteristic roots of Eq. (4.8) [62]. We define the absolute error ϵ as the value of the characteristic equation (Eq. (4.10)) upon substitution of the eigenvalues of $\mathbf{Z}$. In this work, we define the convergence criterion to be $\epsilon < 10^{-4}$ and, thus, obtain the spectrum of the original DDE system (Eq. (4.8)) from the ODE system (Eq. (4.28)).

4.3 Problem definition

Consider the second-order system given by Eq. (4.1). Given $\mathbf{M}$, $\mathbf{C}$, $\mathbf{K}$, and τ, we wish to determine the feedback gains $\mathbf{f}$ and $\mathbf{g}$ that place all roots in the left half of the complex plane and create a specified spectral gap between the rightmost root and the imaginary axis. We find the gains $\mathbf{f}$ and $\mathbf{g}$ by minimizing the following objective function:

$$J = \Big(\mathrm{Re}\{\lambda_{\max}(\mathbf{f}, \mathbf{g})\} + \alpha\Big)^2, \tag{4.29}$$

where $\mathrm{Re}\{\lambda_{\max}\}$ is the real part of the rightmost eigenvalue, which is a function of feedback gains $\mathbf{f}$ and $\mathbf{g}$, and $\alpha > 0$ is the desired spectral gap. If a solution $(\mathbf{f}^*, \mathbf{g}^*)$ is obtained where $J(\mathbf{f}^*, \mathbf{g}^*) = 0$, then the rightmost root is placed at the desired location—that is, $\mathrm{Re}\{\lambda_{\max}\} = -\alpha$. However, if $J(\mathbf{f}^*, \mathbf{g}^*) > 0$, then the rightmost root is not placed at the desired location (i.e., the spectral gap is less than α), but the precise location of the rightmost root is still obtained and, thus, the stability of the system can be determined. In practice, it may be necessary to accompany the objective function (Eq. (4.29)) with constraints on the feedback gains $\mathbf{f}$ and $\mathbf{g}$. In Section 4.5, we

solve a constrained optimization problem whose constraints ensure the gains are within a physically realizable range. In this work, the objective function given by Eq. (4.29) is minimized using the PSO technique. PSO is a widely used swarm-intelligence-based algorithm due to its simplicity, flexibility, and ease of implementation [135].

4.4 Results and discussion

In this section, we demonstrate the strengths and limitations of the MoR approach, and we employ Galerkin approximations to obtain the characteristic roots corresponding to the solutions obtained using MoR. When the MoR approach does not achieve the desired spectral gap, we use the proposed optimization-based technique to improve the solution.

4.4.1 Example 1

Consider the system obtained upon substituting the following matrices into Eq. (4.1) (from [75]):

$$\mathbf{M} = \begin{bmatrix} 1 & 0 \\ 0 & 1 \end{bmatrix}, \quad \mathbf{C} = \begin{bmatrix} 0.1 & -0.1 \\ -0.1 & 0.1 \end{bmatrix}, \quad \mathbf{K} = \begin{bmatrix} 2 & -1 \\ -1 & 1 \end{bmatrix}. \tag{4.30}$$

We use MoR to place the eigenvalues of this system at two location sets: $S_1 \triangleq [-1, -1 \pm i, -2]$ (from [75]) and $S_2 \triangleq [-0.5, -1 \pm i, -2]$. It was observed that, for some delays $\tau \in [0.001, 1.5]$, the system becomes unstable when the desired location of the rightmost roots is S_1. Using location set S_2, spillover of the dominant roots still occurs but the system remains stable for the entire range of τ. Galerkin approximations are used to obtain the characteristic roots for this system, where feedback gains $\mathbf{f}$ and $\mathbf{g}$ are obtained using MoR. Figure 4.1 illustrates the locations of the three rightmost roots as delay τ varies, using target pole locations S_1 and S_2. As shown, spillover is evident in both cases—that is, for some values of delay τ, the real part of the rightmost root is not in the desired location. Specifically, for location set S_1 (Fig. 4.1(a)), there is always a pole at -1 as desired but, for some delays τ, there is also a pole to the right of -1; in the case of location set S_2 (Fig. 4.1(b)), there is a pole at -0.5 as desired but there is also a pole to the right of -0.5 for some values of delay τ. It is important to note that, in some situations, spillover of the dominant roots will result in an unstable closed-loop system.

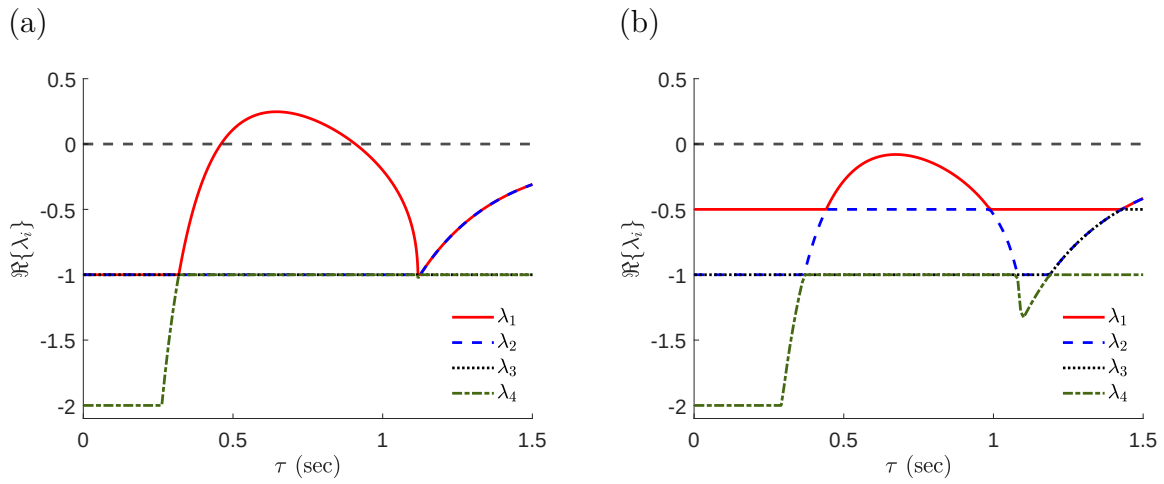

FIGURE 4.1: Locations of the four roots of Eq. (4.1) as delay τ varies, using MoR with location sets (a) S_1 and (b) S_2. Matrices $\mathbf{M}$, $\mathbf{C}$, and $\mathbf{K}$ are given by Eq. (4.30).

We now solve the pole-placement problem for the same system using the proposed optimization-based strategy. Figure 4.2 illustrates the location of the rightmost root as delay τ varies, using $\alpha = 1$ and $\alpha = 0.5$ in the objective function (Eq. (4.29)). These values of α correspond to the spectral gaps described by location sets S_1 and S_2. When $\alpha = 0.5$ (Fig. 4.2(b)), $\mathrm{Re}\{\lambda_{\max}\} \approx -0.5$ for all delays τ—a substantial improvement over the performance of the MoR approach. An improvement is also observed when $\alpha = 1$ (Fig. 4.2(a)): although spillover still occurs over a similar range of τ, the deviation from the desired pole location is reduced significantly. Similar results are observed when using different optimization parameters, such as the relative tolerance and the number of generations. Because Galerkin approximations are used in the proposed optimization-based strategy, the stability of the system can be evaluated in cases of spillover without requiring any additional analysis.

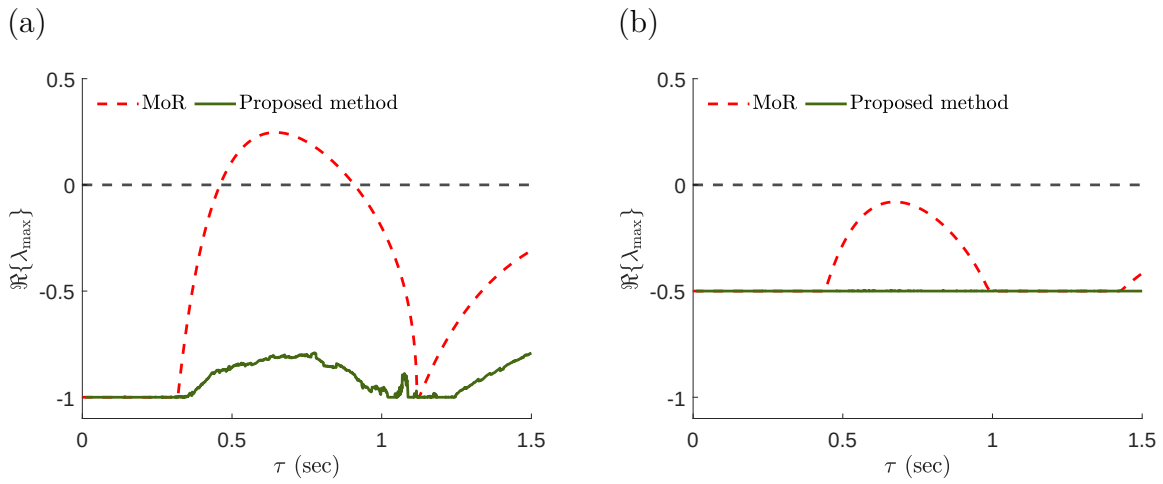

FIGURE 4.2: Location of the rightmost root of Eq. (4.1) as delay τ varies, using the proposed optimization-based strategy with (a) $\alpha = 1$ and (b) $\alpha = 0.5$. Matrices $\mathbf{M}$, $\mathbf{C}$, and $\mathbf{K}$ are given by Eq. (4.30). The rightmost roots from Fig. 4.1 are shown for comparison (dashed lines).

4.4.2 Example 2

We now consider a second-order example given in Ram et al. [75], where $\mathbf{M} = 1$, $\mathbf{C} = 0.01$, $\mathbf{K} = 5$, and $\mathbf{b} = 1$ in Eq. (4.1):

$$\ddot{x}(t) + 0.01\dot{x}(t) + 5x(t) = f\dot{x}(t-\tau) + gx(t-\tau), \tag{4.31}$$

where delay $\tau > 0$. We again compare the performance of the MoR approach with that of the optimization-based strategy, using a location set of $S \triangleq [-0.5, -47]$ for the former and $\alpha = 0.5$ for the latter. Figure 4.3 illustrates the locations of the two rightmost roots of Eq. (4.31) as delay τ varies, with feedback gains $\mathbf{f}$ and $\mathbf{g}$ determined using the MoR approach and the optimization-based strategy. We observe spillover using the MoR approach (Fig. 4.3(a)) when $\tau \in [0.093, 0.210]$ and $\tau > 0.838$, resulting in instability for delays exceeding 1.134 seconds. By contrast, there is no spillover of the rightmost root for any value of τ and the system is never unstable when the optimization-based strategy is used (Fig. 4.3(b)).

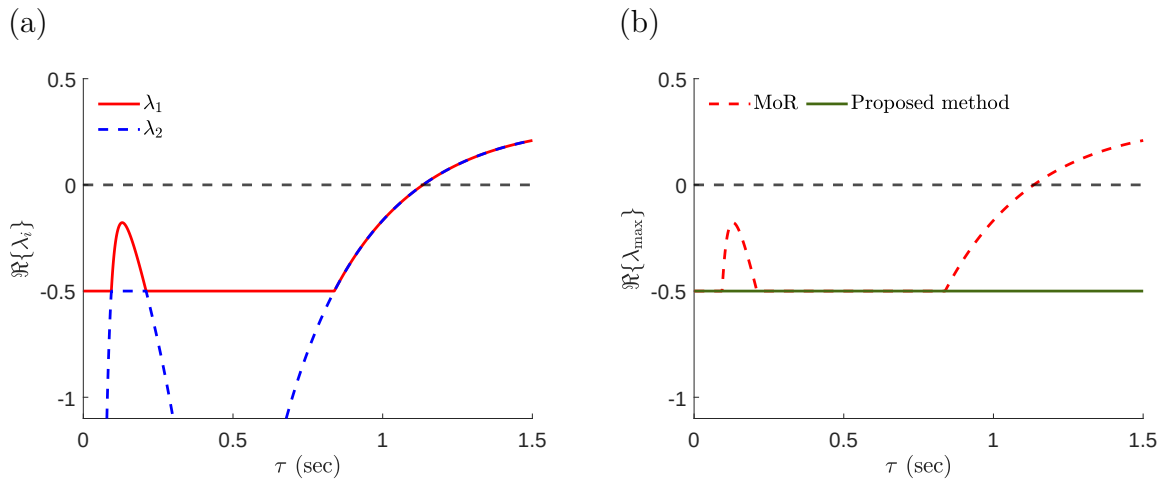

FIGURE 4.3: Locations of the rightmost roots of Eq. (4.31) as delay τ varies: (a) the two rightmost roots obtained using the MoR approach, and (b) the rightmost root obtained using the proposed optimization-based strategy with $\alpha = 0.5$. The rightmost root from panel (a) is displayed in panel (b) for comparison (dashed line).

4.5 Experimental validation

We validated the proposed approach experimentally using a 3D hovercraft apparatus (Quanser Inc., Markham, Ontario, Canada), as shown in Fig. 4.4. The hovercraft is a decoupled system—that is, its motion about the yaw, pitch, and roll axes is decoupled. Our experiments comprised motion about only the yaw axis, which nevertheless required coordination of all four motors. The experimental apparatus has an inherent time delay of 2 ms, which is well below the critical delays encountered in this study. The equation governing the motion of this system about the yaw axis is given as follows [1]:

$$\ddot{\theta}_y = -0.1304(f\dot{\theta}_y(t-\tau) + g\theta_y(t-\tau)), \tag{4.32}$$

where θ_y is the yaw angle. As shown in Fig. 4.5(a), the feedback gains f and g computed using the MoR approach result in an unstable system for delays exceeding $\tau = 131$ ms. The optimization-based strategy (with $\alpha = 6$) increased the amount of delay that can be tolerated to $\tau = 194$ ms (Fig. 4.5(b)).

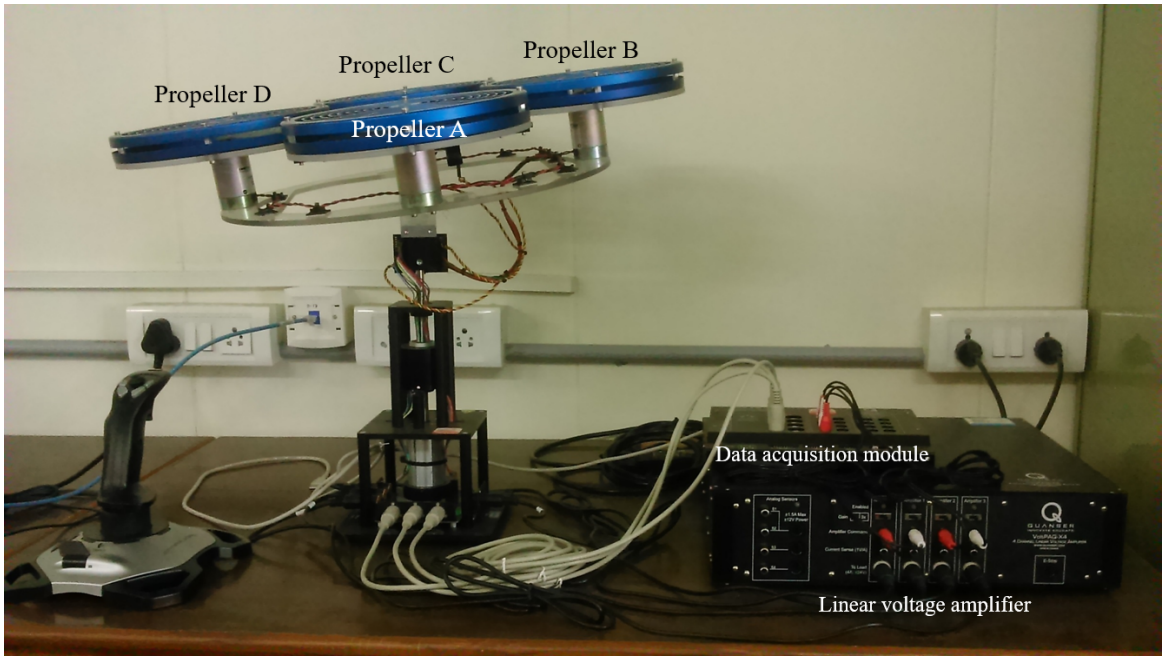

FIGURE 4.4: 3D hovercraft apparatus used for experimental validation.

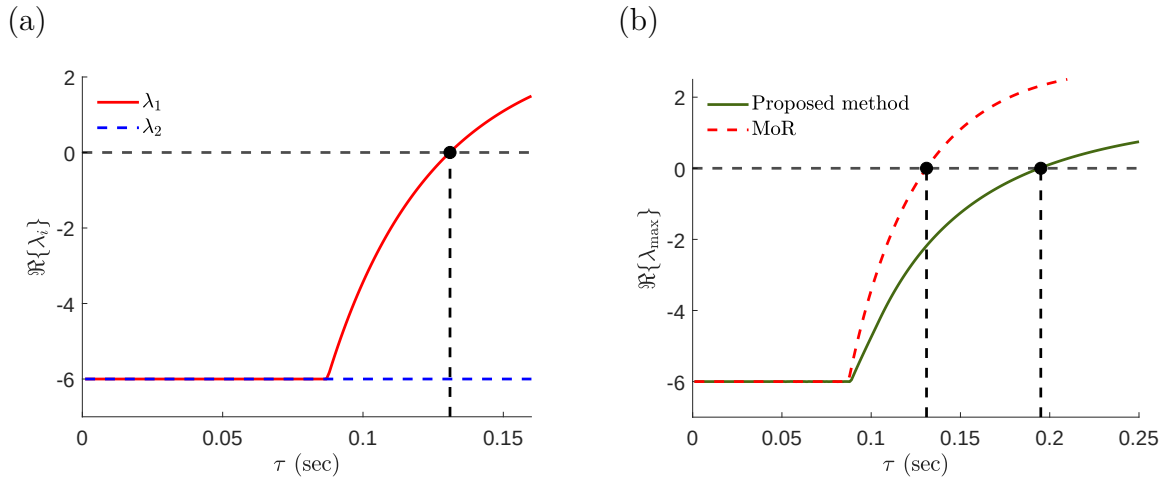

FIGURE 4.5: Locations of the rightmost roots of Eq. (4.32) as delay τ varies: (a) the two rightmost roots obtained using the MoR approach, and (b) the rightmost root obtained using the proposed optimization-based strategy with $\alpha = 6$. The rightmost root from panel (a) is displayed in panel (b) for comparison (dashed line).

To validate these results, we deliberately introduced a delay into the experimental system and computed feedback gains using the proposed optimization-based strategy for four values of τ: 131 ms, 140 ms, 150 ms, and 160 ms Table 4.1. The system response for a delay of $\tau = 131$ ms is shown in Fig. 4.6(a). A square waveform input

of magnitude $\pm 5^{\circ}$ was provided as the reference trajectory. Clearly, the feedback gains obtained using the optimization-based strategy resulted in a stable system; gains obtained using the MoR approach result in instability. Figures 4.6(b), 4.7(a) and 4.7(b) illustrate the system response for the same reference signal when the delay is increased beyond 131 ms. As shown, the system response remains stable in all cases. The motor voltages for four values of delay τ: 131 ms, 140 ms, 150 ms, and 160 ms (corresponding to the yaw angle shown in Figs. 4.6(a), 4.6(b), 4.7(a) and 4.7(b)) are shown in Figs. 4.8, 4.9, 4.10 and 4.11.

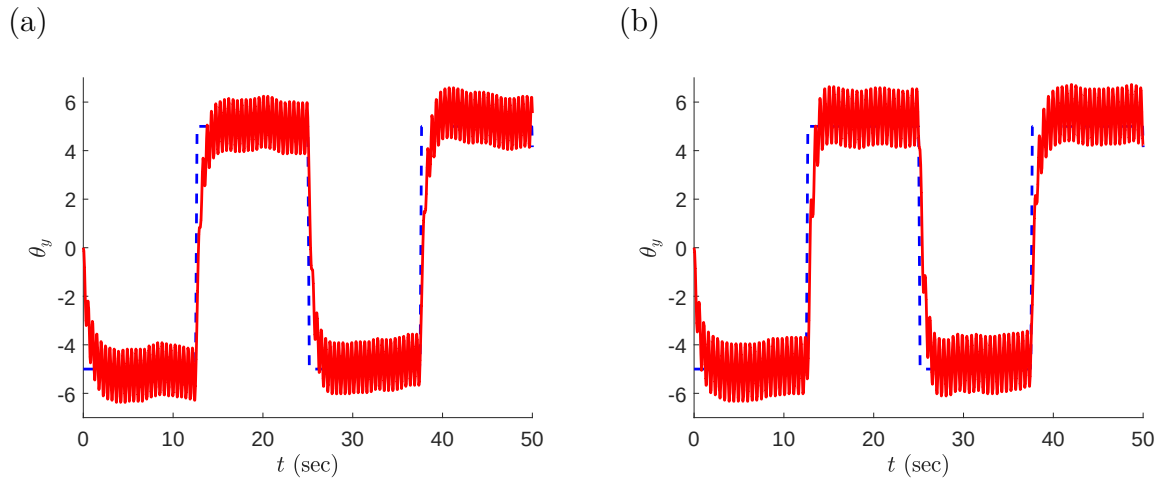

FIGURE 4.6: Yaw angle ($\theta_y(t)$) of 3D hovercraft apparatus with feedback gains obtained using the proposed optimization-based strategy and delays of (a) 131 ms and (b) 140 ms. The reference signal is also shown (dashed line).

TABLE 4.1: Feedback gains obtained using the proposed optimization-based strategy for the 3D hovercraft apparatus.

Delay τ (ms)	Feedback gains f	g
131	44.2624	111.8034
140	43.2896	111.8034
150	42.2095	111.8034
160	41.1300	111.8034

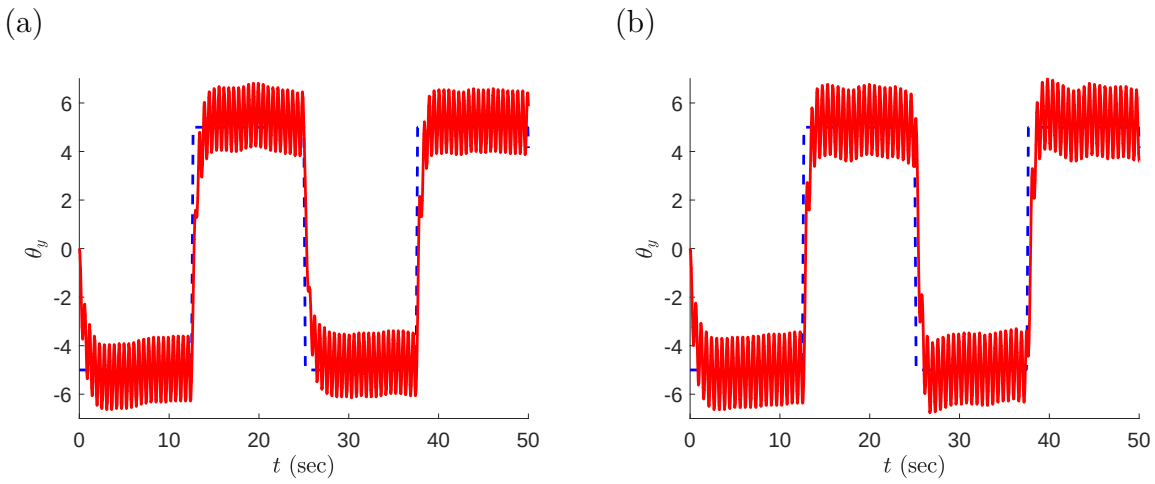

FIGURE 4.7: Yaw angle ($\theta_y(t)$) of 3D hovercraft apparatus with feedback gains obtained using the proposed optimization-based strategy and delays of (a) 150 ms and (b) 160 ms. The reference signal is also shown (dashed line).

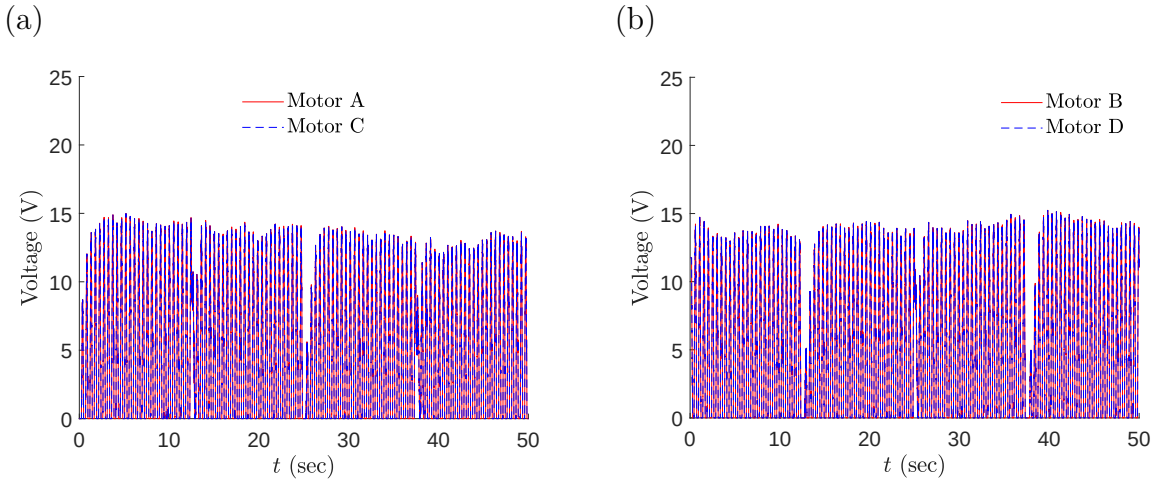

FIGURE 4.8: Voltage of (a) motors A and C, and (b) motors B and D in the 3D hovercraft apparatus with feedback gains obtained using the proposed optimization-based strategy and a delay of 131 ms.

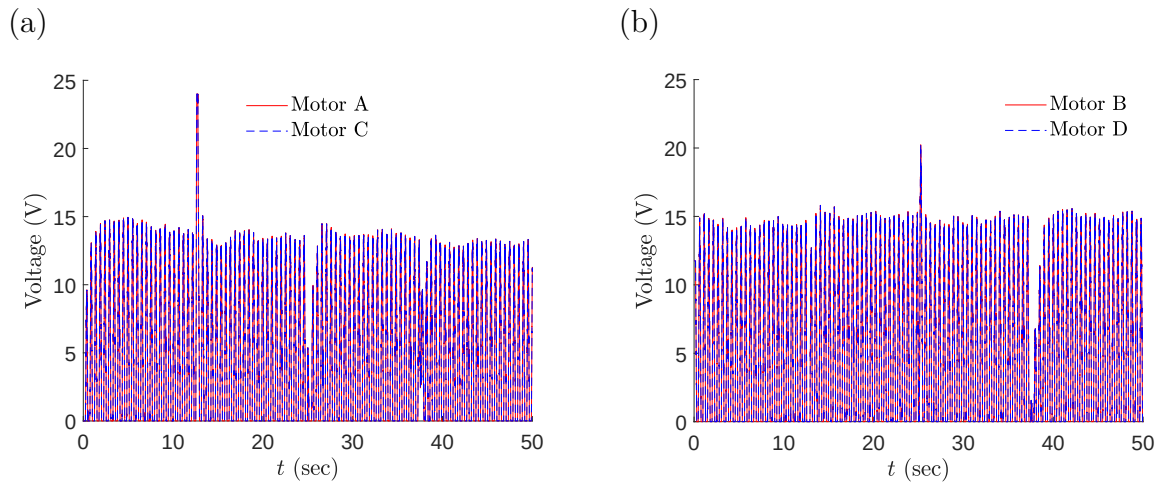

FIGURE 4.9: Voltage of (a) motors A and C, and (b) motors B and D in the 3D hovercraft apparatus with feedback gains obtained using the proposed optimization-based strategy and a delay of 140 ms.

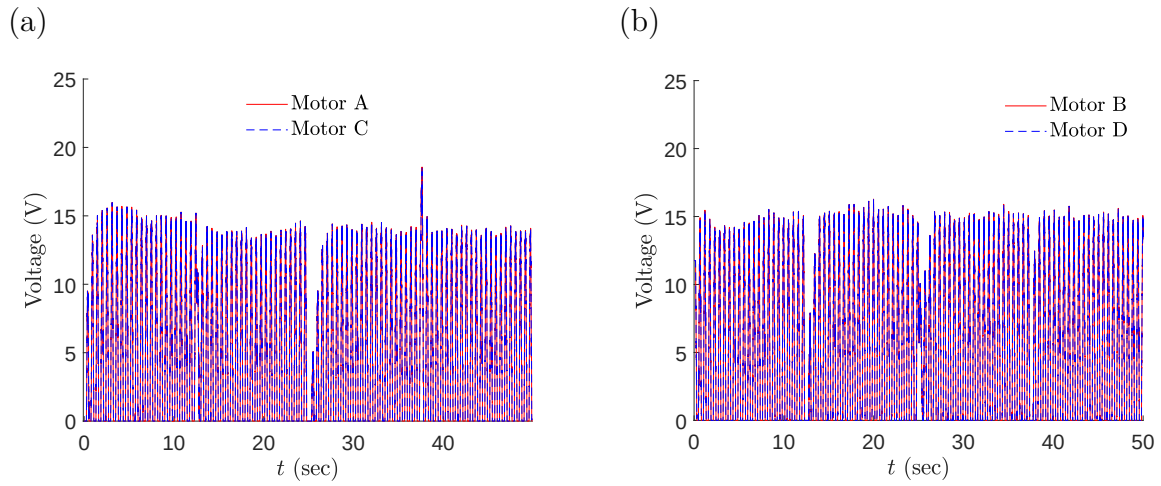

FIGURE 4.10: Voltage of (a) motors A and C, and (b) motors B and D in the 3D hovercraft apparatus with feedback gains obtained using the proposed optimization-based strategy and a delay of 150 ms.

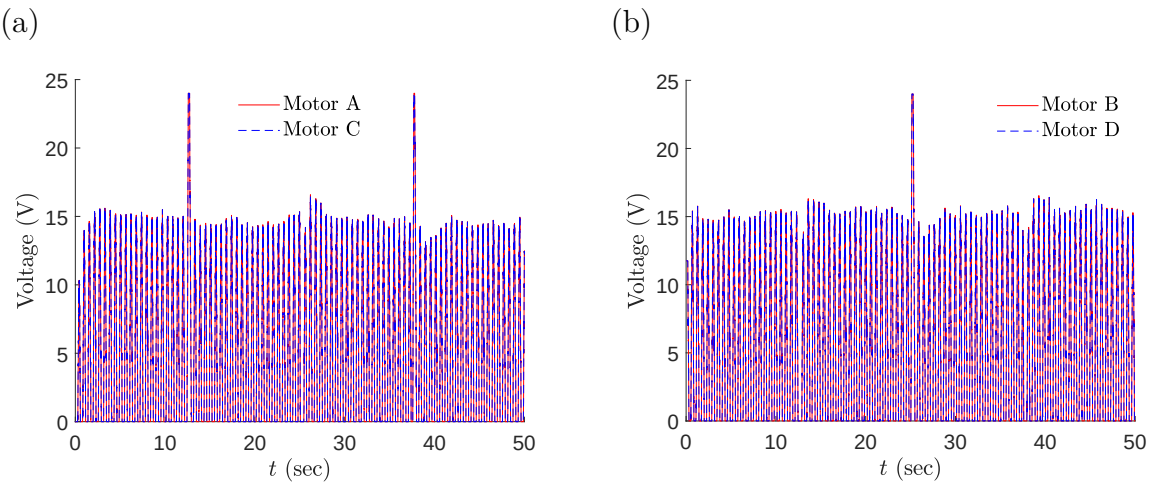

FIGURE 4.11: Voltage of (a) motors A and C, and (b) motors B and D in the 3D hovercraft apparatus with feedback gains obtained using the proposed optimization-based strategy and a delay of 160 ms.

4.6 Chapter summary

In this chapter, a hybrid method-of-receptances and optimization-based technique has been proposed to solve the pole-placement problem in TDS. Using examples from the literature, it has been demonstrated that the MoR approach can place the dominant root to the right of the specified location, resulting in a deficient spectral gap and potentially an unstable closed-loop system. An optimization-based strategy is proposed to complement the MoR approach by providing improved feedback gains for those delays where the MoR solution is unacceptable. The efficacy of this strategy was demonstrated using examples from the literature. Experimental validation was performed using a 3D hovercraft apparatus with a deliberately introduced delay. We demonstrated that the optimization-based strategy was able to stabilize the hovercraft for delays exceeding those that can be accommodated by the MoR approach. Thus, the proposed hybrid method-of-receptances and optimization-based technique expands the range of TDS to which pole placement can be applied.

Chapter 5

Reduced-order modelling of TDS using Galerkin approximations and eigenvalue decomposition

In this chapter, an r-dimensional ROM for infinite-dimensional DDEs is developed. The eigenvalues of the ROM match the r rightmost characteristic roots of the DDE with a user-specified tolerance of ϵ. Initially, the DDE is approximated by an N-dimensional set of ODEs using Galerkin approximations. However, only N_c ($< N$) eigenvalues of this N-dimensional model match (with a tolerance of ϵ) the rightmost characteristic roots of the DDEs. By performing numerical simulations, an empirical relationship for N_c is obtained as a function of N and ϵ for a scalar DDE with multiple delays. Using EVD, an r ($= N_c$)-dimensional model is constructed. First, an appropriate r is chosen, and then the minimum value of N at which at least r roots converge is selected. For each of the test cases considered, the time and frequency responses of the original DDE obtained using direct numerical simulations are compared with the corresponding r- and N-dimensional systems. By judiciously selecting r, solutions of the ROM and DDE match closely. Next, an r-dimensional model is developed for an experimental 3D hovercraft in the presence of delay. The time responses of the r-dimensional model compared favorably with the experimental results.

This chapter is organized as follows. Section 5.1 gives a detailed account of developing the ROMs using Galerkin approximations and the EVD method. In Section 5.2, first an empirical relationship between N_c, N and ϵ for a first-order DDE with multiple delays is obtained, and then ROMs are developed for first-order two-delay and a third-order single-delay test cases from the literature [66]. The test cases were subjected to different inputs, and time and frequency responses were obtained which

were compared with those of the original TDS. Experimental validation of the proposed approach is then demonstrated in Section 5.3 using a 3D hovercraft. Section 5.4 summarizes the work.

5.1 Mathematical modelling

For brevity, in this section, the development of the proposed method is shown for only a first-order single-delay system. The proposed method can be applied to higher-order DDEs with multiple delays. Consider the following first-order single-delay system:

$$\dot{x}(t) = ax(t) + bu(t), \tag{5.1a}$$
$$u(t) = k[r(t) - x(t-\tau)], \tag{5.1b}$$

where a and b are coefficients, $u(t)$ is the control signal, k is the feedback gain, $r(t)$ is the reference input, $\alpha(t)$ is the initial function and delay $\tau > 0$. The characteristic equation of Eq. (5.1) is obtained as follows:

$$s - a + bke^{-s\tau} = 0. \tag{5.2}$$

Equation (5.2) is a quasi-polynomial due to the presence of the transcendental term $e^{-s\tau}$ and therefore has infinitely many roots. We begin by converting the DDE (Eq. (5.1)) into a PDE with time-dependent boundary conditions. Following [47], we introduce the following transformation:

$$y(s,t) = x(t+s), \tag{5.3}$$

where y is a function of $s \in [-\tau, 0]$ and t. From the methodology described by Vyasarayani et al. [48, 62], the initial value problem (Eq. (5.1)) can be transformed into an initial-boundary value problem as follows:

$$\frac{\partial y(s,t)}{\partial t} = \frac{\partial y(s,t)}{\partial s}, \qquad s \in [-\tau, 0], \tag{5.4a}$$
$$\left.\frac{\partial y(s,t)}{\partial t}\right|_{s=0} = ay(0,t) - bky(-\tau,t) + bkr(t). \tag{5.4b}$$

Now, assume a series solution for the above PDE:

$$y(s,t) = \sum_{i=1}^{\infty} \phi_i(s)\eta_i(t), \tag{5.5}$$

where, $\phi_i(s)$ are the basis functions and $\eta_i(t)$ are the time-dependent coordinates. For practical and computing purposes, the infinite series is truncated at N terms and Eq. (5.5) can be rewritten as:

$$y(s,t) \approx \sum_{i=1}^{N} \phi_i(s)\eta_i(t) = \boldsymbol{\phi}^T(s)\boldsymbol{\eta}(t), \tag{5.6}$$

where $\boldsymbol{\phi}(s) \triangleq [\phi_1(s), \phi_2(s), \cdots, \phi_N(s)]^T$ and $\boldsymbol{\eta}(t) \triangleq [\eta_1(t), \eta_2(t), \cdots, \eta_N(t)]^T$.

Substituting Eq. (5.6) in Eq. (5.4a), we get

$$\boldsymbol{\phi}^T(s)\dot{\boldsymbol{\eta}}(t) = \boldsymbol{\phi}'(s)^T\boldsymbol{\eta}(t). \tag{5.7}$$

Here, $\boldsymbol{\phi}'(s)$ denotes the derivative of $\boldsymbol{\phi}(s)$ with respect to s. Premultiplying Eq. (5.7) by $\boldsymbol{\phi}(s)$ and integrating over the domain $s \in [-\tau, 0]$, we obtain the following:

$$\int_{-\tau}^{0} \boldsymbol{\phi}(s)\boldsymbol{\phi}(s)^T ds\dot{\boldsymbol{\eta}}(t) = \int_{-\tau}^{0} \boldsymbol{\phi}(s)\boldsymbol{\phi}'(s)^T ds\boldsymbol{\eta}(t). \tag{5.8}$$

Equation (5.8) can be rewritten as:

$$\mathbf{C}\dot{\boldsymbol{\eta}}(t) = \mathbf{D}\boldsymbol{\eta}(t), \tag{5.9}$$

where $\mathbf{C}$ and $\mathbf{D}$ are of dimension $N \times N$ and are given as follows:

$$\mathbf{C} \triangleq \int_{-\tau}^{0} \boldsymbol{\phi}(s)\boldsymbol{\phi}(s)^T ds, \quad \mathbf{D} \triangleq \int_{-\tau}^{0} \boldsymbol{\phi}(s)\boldsymbol{\phi}'(s)^T ds. \tag{5.10}$$

Boundary conditions are derived by substituting Eq. (5.6) in Eq. (5.4b) and is given as follows:

$$\boldsymbol{\phi}^T(0)\dot{\boldsymbol{\eta}}(t) = (a\boldsymbol{\phi}^T(0) - bk\boldsymbol{\phi}^T(-\tau))\boldsymbol{\eta}(t) + bkr(t). \tag{5.11}$$

The boundary conditions can be incorporated into Eq. (5.9) using various techniques such as spectral least-squares [48], spectral-tau [47, 62, 136] or by embedding

them directly into the PDE [137]. In the current work, the boundary conditions given by Eq. (5.11) are incorporated into Eq. (5.9) using the spectral-tau method [62] and the system of equations can be written as follows:

$$\mathbf{M}\dot{\boldsymbol{\eta}}(t) = \mathbf{K}\boldsymbol{\eta}(t) + \mathbf{U}r(t), \tag{5.12}$$

where $\mathbf{M}$, $\mathbf{K}$ and $\mathbf{U}$ are given as follows:

$$\mathbf{M} = \begin{bmatrix} \tilde{\mathbf{C}} \\ \boldsymbol{\phi}^T(0) \end{bmatrix}, \ \mathbf{K} = \begin{bmatrix} \tilde{\mathbf{D}} \\ -bk\boldsymbol{\phi}^T(-\tau), \end{bmatrix}, \ \mathbf{U} = \begin{bmatrix} \mathbf{Z} \\ 1 \end{bmatrix}. \tag{5.13}$$

The dimensions of matrices $\mathbf{M}$, $\mathbf{K}$ and $\mathbf{U}$ are $N \times N$, $N \times N$ and $N \times 1$ respectively. Here, the dimensions of $\tilde{\mathbf{C}}$ and $\tilde{\mathbf{D}}$ are $(N-1) \times N$ and these matrices are obtained by deleting the last row of $\mathbf{C}$ and $\mathbf{D}$ respectively. $\mathbf{Z} \triangleq \mathbf{0}$ with dimension $(N-1) \times 1$. Equation (5.12) is a deterministic system of N equations with N unknowns in $\boldsymbol{\eta}(t)$.

Equation (5.12) can be written as follows:

$$\dot{\boldsymbol{\eta}}(t) = \mathbf{L}\boldsymbol{\eta}(t) + \mathbf{J}r(t), \tag{5.14}$$

where $\mathbf{L} = \mathbf{M}^{-1}\mathbf{K}$ and $\mathbf{J} = \mathbf{M}^{-1}\mathbf{U}$ and the spectrum of $\mathbf{L}$ is defined as:

$$S = \{\lambda_i \mid det.(\lambda\mathbf{I} - \mathbf{L}) = 0, Re(\lambda_1) > ... > Re(\lambda_N)\}. \tag{5.15}$$

In this work, shifted Legendre polynomials are used as basis functions:

$$\phi_1(s) = 1, \ \phi_2(s) = 1 + \frac{2s}{\tau}, \tag{5.16a}$$

$$\phi_k(s) = \frac{(2k-3)\phi_2(s)\phi_{k-1}(s) - (k-2)\phi_{k-2}(s)}{k-1}, k \geq 3. \tag{5.16b}$$

Shifted Legendre polynomials have shown better convergence properties [62] and facilitate expressing the entries of matrices $\mathbf{C}$ and $\mathbf{D}$, as defined in Eq. (5.10), in closed form as follows:

$$\mathbf{C}_{ij} = \begin{cases} \frac{\tau}{2i-1}, & \text{if } i = j \\ 0, & \text{otherwise} \end{cases}, \tag{5.17a}$$

$$\mathbf{D}_{ij} = \begin{cases} 2, & \text{if } i \leq j \text{ and } i+j \text{ is odd} \\ 0, & \text{otherwise} \end{cases}, \tag{5.17b}$$

where $i = 1, 2, ..., N$ and $j = 1, 2, ..., N$. Initial conditions $\boldsymbol{\eta}(0)$ for Eq. (5.14) can be obtained as follows:

$$\boldsymbol{\eta}(0) = C^{-1} \int_{-\tau}^{0} \boldsymbol{\phi}(s)\alpha(s)ds. \tag{5.18}$$

By solving Eq. (5.14), the approximate solution of the DDE given by Eq. (5.1) can be obtained from Eq. (5.6) as follows:

$$x(t) \approx \hat{x}(t) = y(0,t) = \boldsymbol{\phi}^T(0)\boldsymbol{\eta}(t). \tag{5.19}$$

The system of ODEs given by Eq. (5.14) is the N^{th}-order Galerkin-approximated system for the original TDS given by Eq. (5.1), hereby referred to as the full-order Galerkin (FOG) system, and the time response obtained is represented by $\hat{x}(t)$. By considering $r(t) = 0$, the eigenvalues of $\mathbf{L}$ converge to the characteristic roots of Eq. (5.2). By increasing the approximating terms, N, of the FOG system, the number of converged eigenvalues N_c of $\mathbf{L}$ increases [62]. With a set error criterion, i.e., by defining the absolute error to be ϵ, those eigenvalues of $\mathbf{L}$ that result in $\epsilon < 10^{-4}$ when substituted in Eq. (5.2) are considered to be converged.

To ease the complexity of computation, a further lower-dimensional model is built using only the converged eigenvalues of $\mathbf{L}$ by applying the EVD method. $\mathbf{L}$ can be diagonalized as $\mathbf{L} = \mathbf{PDP}^{-1}$, with $\mathbf{D}$ being a diagonal matrix containing the eigenvalues and $\mathbf{P}$ containing the corresponding eigenvectors of $\mathbf{L}$, respectively. Equation (5.14) can now be rewritten as:

$$\dot{\boldsymbol{\eta}}(t) = \mathbf{PDP}^{-1}\boldsymbol{\eta}(t) + \mathbf{J}r(t). \tag{5.20}$$

Pre-multiplying Eq. (5.20) with $\mathbf{P}^{-1}$ and by defining $\boldsymbol{\zeta}(t) = \mathbf{P}^{-1}\boldsymbol{\eta}(t)$ and $\mathbf{E} = \mathbf{P}^{-1}\mathbf{J}$, we get:

$$\dot{\boldsymbol{\zeta}}(t) = \mathbf{D}\boldsymbol{\zeta}(t) + \mathbf{E}r(t). \tag{5.21}$$

Equation (5.21) is a diagonal system that consists of both converged and unconverged eigenvalues of $\mathbf{L}$. Now, we disregard the unconverged eigenvalues and consider only the r $(= N_c)$ converged eigenvalues of $\mathbf{L}$, which results in an r^{th}-order system as follows:

$$\dot{\boldsymbol{\zeta}}_r(t) = \mathbf{D}_r\boldsymbol{\zeta}_r(t) + \mathbf{E}_r r(t), \tag{5.22}$$

where $\mathbf{D}_r = \text{diag.}[\lambda_1,\ \lambda_2,\ ...,\ \lambda_r]$, $\mathbf{P}_r = [\mathbf{p}_1\ \mathbf{p}_2\ ...\ \mathbf{p}_r]$ and $\mathbf{p}_i$ are the eigenvectors corresponding to the converged eigenvalues λ_i. $\mathbf{E}_r$ is the input vector constructed from

$\mathbf{E}$ considering only the columns of $\mathbf{E}$ corresponding to the r converged eigenvalues of $\mathbf{D}$ and is given as $\mathbf{E}_r = [\mathbf{e}_1\ \mathbf{e}_2\ ...\ \mathbf{e}_r]^T$. Initial conditions for Eq. (5.22) can be specified as $\boldsymbol{\zeta}_r(0) = [\zeta_1(0),\ \zeta_2(0), ...,\ \zeta_r(0)]^T$. An interesting observation is that the FOG system given by Eq. (5.14) can be approximately reconstructed using Eq. (5.22) by using the inverse transformation $\bar{\boldsymbol{\eta}}(t) = \mathbf{P}_r\boldsymbol{\zeta}_r(t)$ and $\bar{\boldsymbol{\eta}}(t)$ is the reconstructed FOG system. At the same time, the reconstructed reduced-order solution of the TDS described by Eq. (5.1) is obtained by:

$$\bar{x}(t) = \boldsymbol{\phi}^T(0)\bar{\boldsymbol{\eta}}(t). \tag{5.23}$$

We refer to the r^{th}-order reduced system as the Galerkin eigenvalue decomposed (GEVD) system and the time response obtained is represented by $\bar{x}(t)$. Taking the Laplace transform of Eq. (5.14) and assuming the initial conditions to be zero, we get:

$$\boldsymbol{\eta}(s) = [s\mathbf{I} - \mathbf{L}]^{-1}\mathbf{J}R(s). \tag{5.24}$$

Using the relation $\hat{X}(s) = \boldsymbol{\phi}^T(0)\boldsymbol{\eta}(s)$ (Eq. (5.19)), in the Laplace domain, we obtain:

$$\hat{Y}(s) = \frac{\hat{X}(s)}{R(s)} = \boldsymbol{\Phi}(0)^T[s\mathbf{I} - \mathbf{L}]^{-1}\mathbf{J}. \tag{5.25}$$

Equation (5.25) is the N^{th}-order Galerkin-approximated LTI transfer function for the original TDS given by Eq. (5.1) and hereby referred to as the full-order transfer function (FOTF), and the frequency response obtained is represented by $\hat{Y}(s)$. Taking the Laplace transform of Eq. (5.22) and assuming the initial conditions to be zero, we get:

$$\boldsymbol{\zeta}_r(s) = [s\mathbf{I} - \mathbf{D}_r]^{-1}\mathbf{E}_r R(s). \tag{5.26}$$

Premultiplying Eq. (5.26) with $\mathbf{P}_r$ and using the inverse transformation, $\mathbf{P}_r\boldsymbol{\zeta}_r(s) = \bar{\boldsymbol{\eta}}(s)$, in the Laplace domain, we get:

$$\bar{\boldsymbol{\eta}}(s) = \mathbf{P}_r[s\mathbf{I} - \mathbf{D}_r]^{-1}\mathbf{E}_r R(s). \tag{5.27}$$

Premultiplying Eq. (5.27) with $\boldsymbol{\Phi}(0)^T$ and using the reconstruction relation, $\bar{X}(s) = \boldsymbol{\phi}^T(0)\bar{\boldsymbol{\eta}}(s)$ (Eq. (5.23)), in the Laplace domain, we get:

$$\bar{Y}(s) = \frac{\bar{X}(s)}{R(s)} = \boldsymbol{\Phi}(0)^T\mathbf{P}_r[s\mathbf{I} - \mathbf{D}_r]^{-1}\mathbf{E}_r. \tag{5.28}$$

We thus obtain an r^{th}-order LTI transfer function, which we refer to as the Galerkin eigenvalue decomposed transfer function (GETF), and the frequency response obtained is represented by $\bar{Y}(s)$. The poles of the transfer function given by Eq. (5.28) match the r $(= N_c)$ rightmost poles of the TDS with a tolerance of ϵ. However, not all N poles of the transfer function given by Eq. (5.25) converge to the poles of the TDS. It is only the N_c $(< N)$ poles of the transfer function given by Eq. (5.25) that converge to the poles of the TDS within a tolerance of ϵ.

For the examples dealt with in this chapter, it was observed that the time taken for MATLAB to compute the eigenvalues and eigenvectors of $\mathbf{L}$ took less than 1 second. Now, as the dimension of $\mathbf{L}$ increases, the computational time required to calculate the eigenvalues and eigenvectors also increases. For systems of large dimension $(N > 10^3)$, depending on the desired order of the ROM, only the r rightmost eigenvalues $\mathbf{D}_r$ and eigenvectors $\mathbf{P}_r$ of $\mathbf{L}$ must be computed. Therefore, one need not solve the full eigenvalue problem for $\mathbf{L}$; instead, one can use an implicitly restarted Arnoldi algorithm [138] and compute only the reduced eigenspectrum. For large systems, this will help in quickly developing and analyzing the ROMs. Alternatively, one can use the proper orthogonal decomposition or dynamic mode decomposition to obtain the approximate reduced basis $\mathbf{P}_r$ for the problem [139].

5.2 Numerical results

In this section, we first arrive at an empirical relationship between N_c, N and ϵ for a first-order DDE with multiple delays. Then, we compare the characteristic roots, time and frequency responses of the ROMs with those of the DDE.

5.2.1 Empirical Relationship between N_c, N and ϵ

To obtain a relationship between N_c, N and ϵ, the following scalar DDE with multiple delays is considered:

$$\dot{x}(t) = ax(t) + \sum_{q=1}^{m} b_q x(t - \tau_q). \tag{5.29}$$

TABLE 5.1: Average N_c from Monte Carlo simulations of Eq. (5.29)

N \ ϵ	10^{-6}	10^{-5}	10^{-4}	10^{-3}
25	6	7	7	8
50	19	20	21	22
75	32	33	35	36
100	46	47	49	51
125	60	61	63	65
150	74	76	78	80

For various test cases, using the procedure described in Section 5.1, the characteristic roots are obtained for the DDE given by Eq. (5.29). Average N_c is obtained by performing 10,000 Monte Carlo simulations with parameters taken from uniform distributions for Eq. (5.29) with $m = 25$ (delays), $a \in [-10, 10]$, $b_q \in [-10, 50]$ and $\tau_q \in [0.1, 10.1]$. By varying N and ϵ in the intervals $[25, 150]$ and $[10^{-6}, 10^{-3}]$ respectively, the empirical relationship for N_c is obtained. Table 5.1 shows average N_c (rounded to nearest integer) for each value of N and ϵ. Figures 5.1(a) and 5.1(b) show the variation of N_c with respect to ϵ and N respectively. It can clearly be seen from Fig. 5.1 that for a fixed N, N_c increases as ϵ increases and for a fixed ϵ, N_c increases as N increases.

(a) Variation of N_c with ϵ

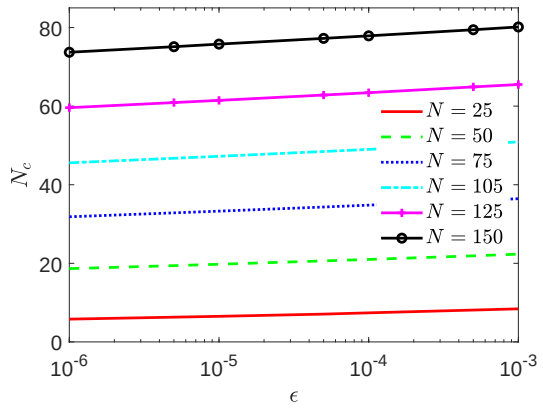

(b) Variation of N_c with N

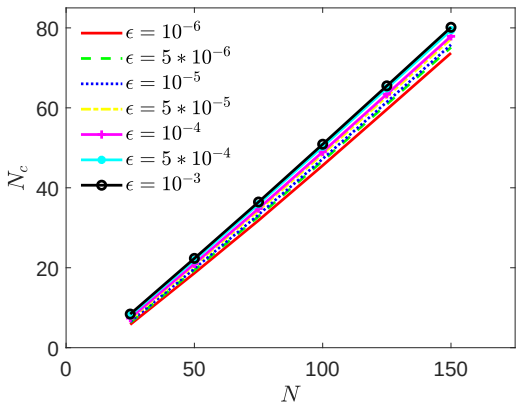

FIGURE 5.1: Variation of N_c with ϵ and N of Eq. (5.29).

From the above data, an empirical relationship is obtained for N_c given N and ϵ, and is given as follows:

$$N_c = (lN - m)\epsilon^n, \tag{5.30}$$

where $l = 0.6004$, $m = 3.1293$ and $n = 0.0017\epsilon^{(-0.231)}$.

5.2.2 Numerical Examples

Example 1: Consider the following first-order two-delay system:

$$\dot{x} + ax(t) + b_1x(t - \tau_1) + b_2x(t - \tau_2) = f(t),\ \tau > 0, \tag{5.31}$$

where $a = 1$, $b_1 = b_2 = 1$, $\tau_1 = 1$ and $\tau_2 = 2$.

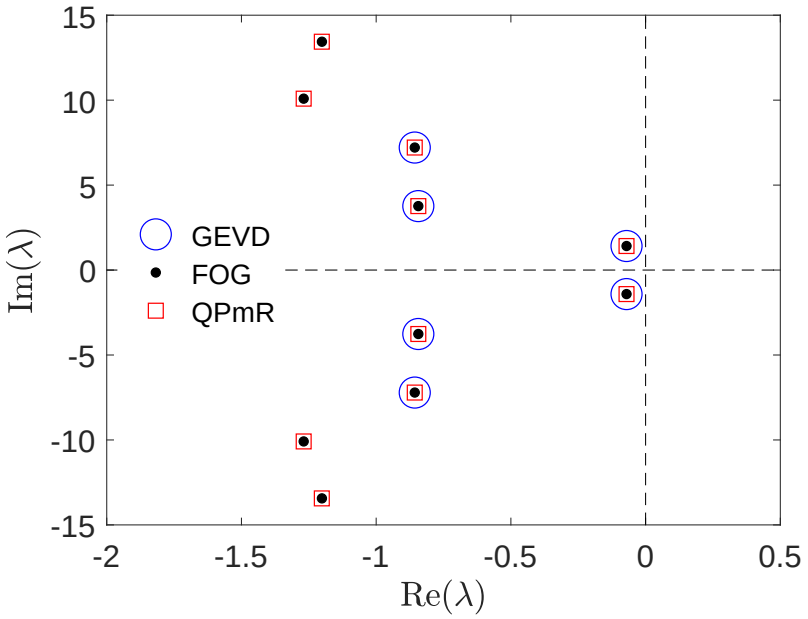

FIGURE 5.2: Roots of Eq. (5.31) using QPmR and spectral-tau methods.

As described earlier, depending on the required order r of the ROM, the minimum required N is computed. For the system described by Eq. (5.31) and for $r = 6$, we found that N must be at least 20. With $N = 20$ in the series solution (Eq. (5.6)), Eq. (5.31) is converted into a system of ODEs of the form given by Eq. (5.14), where $\mathbf{L} \in \mathbb{R}^{20\times20}$. Figure 5.2 shows the characteristic roots of Eq. (5.31) obtained using the QPmR method [91], eigenvalues of the 20^{th}-order FOG system given by Eq. (5.14), and the 6^{th}-order GEVD system given by Eq. (5.22). It is to be noted that in Fig. 5.2, only 10 rightmost roots of the TDS obtained using QPmR and 10 rightmost eigenvalues of

the FOG system are shown. For some of the roots, though, it appears from Fig. 5.2 that the roots obtained using QPmR are close to the eigenvalues of the FOG system but only the 6 rightmost roots converged with a tolerance of $\epsilon < 10^{-4}$. Due to the inherent property of the spectral methods, the convergence starts from the rightmost root and it can clearly be seen from Fig. 5.2 that for $N = 20$, $N_c = 6$ roots converged.

Next, the time response for the TDS given by Eq. (5.31) using 20^{th}-order FOG system (Eq. (5.14)) and 6^{th}-order GEVD system (Eq. (5.22)) models are obtained. The time response for the TDS is obtained using direct numerical simulation performed using the *dde*23 MATLAB solver. The GEVD system is constructed from the r $(= 6)$ converged rightmost eigenvalues of the FOG system. Figure 5.3(a) shows the system responses obtained for Eq. (5.31) and the 6^{th}-order GEVD system. It can clearly be seen in Fig. 5.3(a) that, for a forcing function of the form $f(t) = \sin(t)$, the time responses of the TDS and the 6^{th}-order GEVD system are identical.

(a) System response (b) Error plot

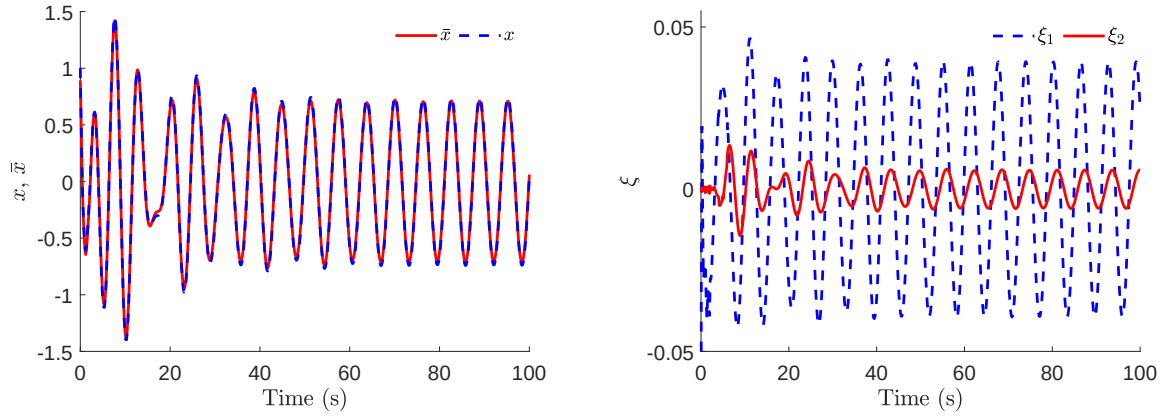

FIGURE 5.3: Time response and error plot of Eq. (5.31) for $f(t) = \sin(t)$.

For a particular state, errors are defined as $\xi_1(t) = x(t) - \bar{x}(t)$ and $\xi_2(t) = x(t) - \hat{x}(t)$. The error plot for Eq. (5.31) is shown in Fig. 5.3(b). The maximum of $|\xi_1(t)|$ and $|\xi_2(t)|$ are on the order of 10^{-2} and 10^{-3}, respectively. It can be inferred that the 20^{th}-order FOG system and 6^{th}-order GEVD system effectively capture the stability as well as the time response characteristics of the original infinite-dimensional DDE system given by Eq. (5.31).

Next, we compare the frequency responses of the ROMs with the TDS given by Eq. (5.31). The 6^{th}-order GETF of the TDS can be obtained using Eq. (5.28) as follows:

$$\bar{Y}(s) = \frac{n(s)}{d(s)}, \tag{5.32}$$

where $n(s) = 0.6821s^5 + 5.487s^4 + 52.87s^3 + 203.7s^2 + 603.2s + 625.6$ and $d(s) = 1.335s^6 + 4.729s^5 + 97.43s^4 + 175.2s^3 + 1258s^2 + 454.8s + 2101$.

(a) Frequency response (b) Error plot

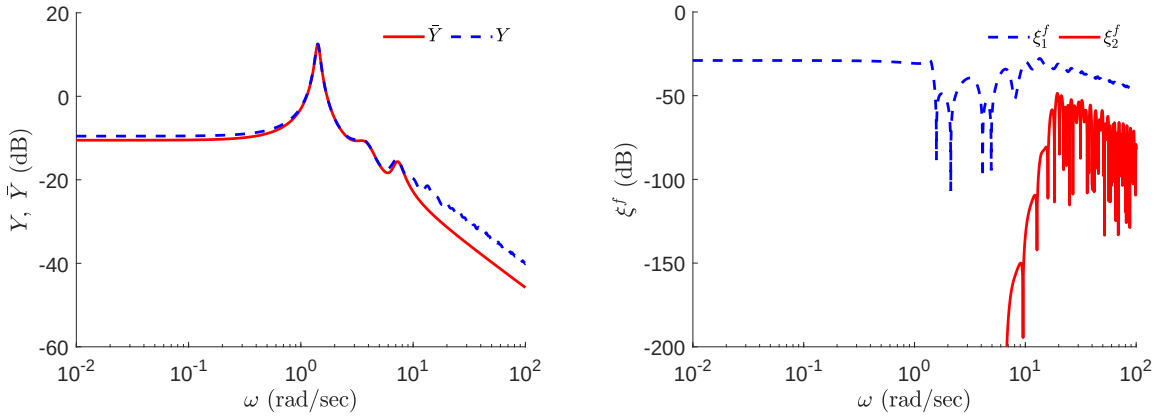

FIGURE 5.4: Frequency response and error plot of Eq. (5.31).

Figure 5.4(a) shows the frequency response of the TDS and 6^{th}-order GETF. For a particular transfer function, the errors in the frequency responses are defined as $\xi_1^f = Y(s) - \bar{Y}(s)$ and $\xi_2^f = Y(s) - \hat{Y}(s)$. The error plot is shown in Fig. 5.4(b). It can be seen that the 6^{th}-order GETF reveals an approximation error smaller than -30 dB for all frequencies, whereas the 20^{th}-order FOTF reveals an approximation error smaller than -50 dB for all frequencies.

(a) Frequency response (b) Error plot

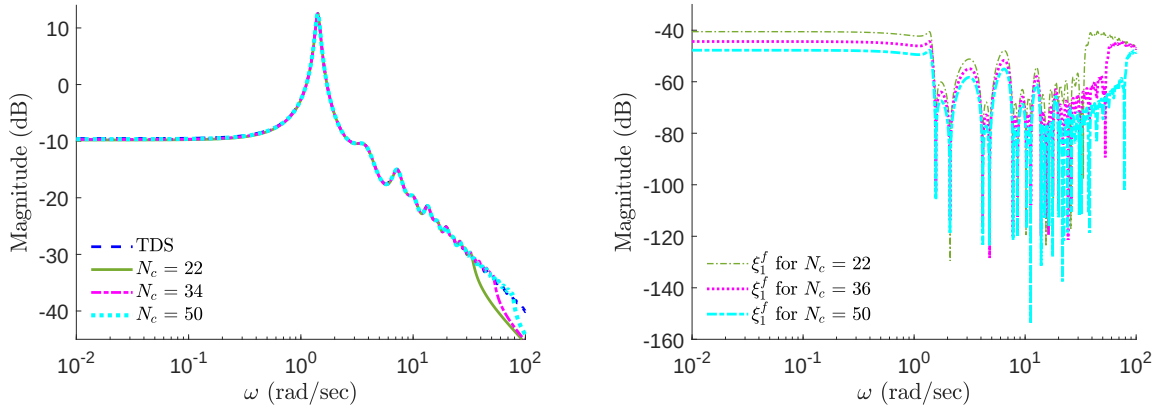

FIGURE 5.5: Frequency response and error plot of Eq. (5.31) for different degrees of GETF.

The denominator of Eq. (5.32) can be arranged as follows:

$$d(s) = (s^2+0.1417s+2.0055)\times(s^2+1.6866s+14.8857)\times(s^2+1.7140s+52.7174) \quad (5.33)$$

Due to the quadratic factors with complex roots, the frequency response of $\bar{Y}(s)$ will have three resonant peaks each near the natural/corner frequency (ω_n) of the terms in Eq. (5.33). The natural/corner frequencies can be obtained from the quadratic factors as $\omega_{n1} = 1.4161\, rad/s$, $\omega_{n2} = 3.8581\, rad/s$ and $\omega_{n3} = 7.2606\, rad/s$. Due to the desired property of dominant eigenvalue convergence of the proposed methodology, the ROM GETF captures the dominant eigenvalues and the natural frequencies of the TDS. It can be seen from Fig. 5.4 that the resonant peaks of the 6^{th}-order GETF are in close agreement with those of the TDS. Moreover, the sharpness of the peaks governed by the damping ratio ζ are also in close agreement with the response of the TDS. Another important observation that can be made from Fig. 5.4 is that the frequency response of the GETF closely matches that of the TDS up to the largest natural frequency contained in the GETF. We denote the largest natural frequency at which the divergence occurs as the critical frequency (f_c). Next, the effect of r on f_c is studied. For this, r is increased and the corresponding N is obtained for different values of r. The various values of r considered are 22, 34 and 50. Figure 5.5(a) shows the frequency response of GETF and TDS for different orders (r) of GETF. It can clearly be seen that increasing the order (r) of GETF increases f_c (Fig. 5.5(a)) and subsequently decreases the ξ_1^f (Fig. 5.5(b)). In other words, if we include more natural frequencies of the TDS in modelling the GETF, a larger frequency operating range of the GETF can be obtained. Therefore, if the operating frequency of the GETF is within f_c, the obtained GETF can be used; otherwise, the order of the GETF can be increased to contain higher natural frequencies of the TDS. The choice of the order of the GETF system is therefore a parameter to be decided depending upon the user specifications.

Modelling a system usually involves a tradeoff between accuracy and complexity. A higher-order model might reveal less error but subsequently increases the complexity of the model leading to a higher implementation cost. However, a lower-order model is attractive for controller design [140].

Example 2: Consider the following third-order system [66]:

$$\dot{\mathbf{x}} = \mathbf{A}\mathbf{x} + \mathbf{B}\mathbf{u}, \quad (5.34a)$$

$$\mathbf{u} = \mathbf{K}^T[\mathbf{r}(t) - \mathbf{x}(t-\tau)], \quad \tau > 0, \quad (5.34b)$$

where $\tau = 3$ and matrices $\mathbf{A}$, $\mathbf{B}$ and $\mathbf{K}$ are defined as follows:

$$\mathbf{A} = \begin{bmatrix} -0.08 & -0.03 & 0.2 \\ 0.2 & -0.04 & -0.005 \\ -0.06 & 0.2 & -0.07 \end{bmatrix}, \quad \mathbf{B} = \begin{bmatrix} -0.1 \\ -0.2 \\ 0.1 \end{bmatrix}, \quad \mathbf{K} = \begin{bmatrix} 0.7190 \\ 1.0400 \\ 1.2900 \end{bmatrix}. \tag{5.35}$$

With the above defined $\mathbf{A}$, $\mathbf{B}$, $\mathbf{K}$, τ and considering $r = 8$, the minimum corresponding N obtained is 18. Performing the mathematical process as described in Section 5.1, for $N = 18$, we get $\mathbf{L} \in \mathbb{R}^{54\times 54}$. Characteristic roots of Eq. (5.34) obtained using QPmR, eigenvalues of the 54^{th}-order FOG system and 8^{th}-order GEVD system are shown in Fig. 5.6. Note that, in Fig. 5.6, only the 12 rightmost roots of the TDS obtained using QPmR and the 14 rightmost eigenvalues of the FOG system are shown. For some of the roots, though, it appears from Fig. 5.6 that the roots obtained using QPmR are close to the eigenvalues of the FOG system, but only the 8 rightmost roots converged with a tolerance of $\epsilon < 10^{-4}$.

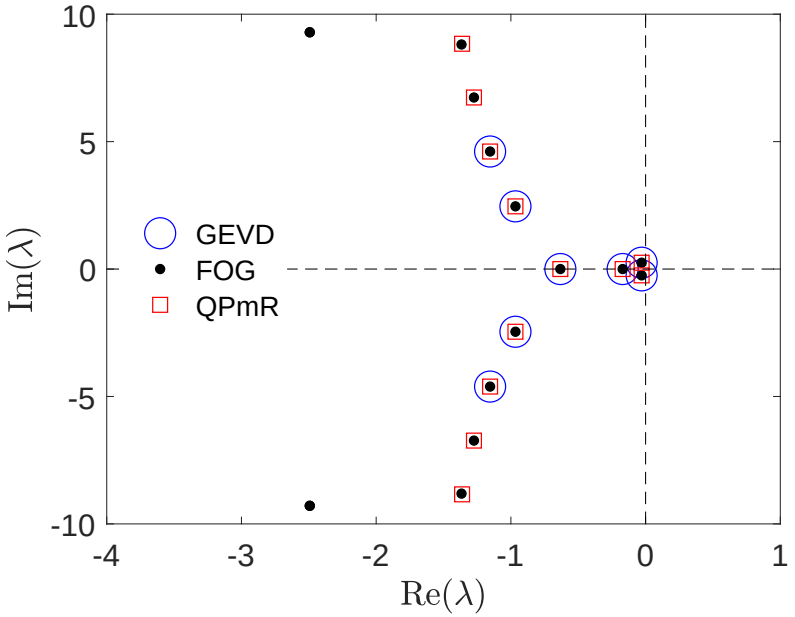

FIGURE 5.6: Roots of Eq. (5.34) using QPmR and spectral-tau methods.

To validate the proposed methodology, Eq. (5.34) is subjected to two different types of sinusoidal inputs of the form $\mathbf{r}(t) = [f(t), 0, 0]^T$. First is a pure sinusoidal input with $f(t) = 10\sin(t)$; second is a combination of multi-frequency sinusoidal waveform with non-commensurate frequencies, i.e, $f(t) = 7\sin(0.1266t) + 10\sin(2.3041t)$.

Figure 5.7 shows the response of the system represented by Eq. (5.34) for a sinusoidal input of the form $\mathbf{r}(t) = [f(t), 0, 0]^T$ with $f(t) = 10\sin(t)$. Figures 5.7[(a) – (c)] show the response of x_1, x_2 and x_3 respectively. For $f(t) = 10\sin(t)$, a close agreement in the time responses of the TDS (Eq. (5.34)) obtained by direct numerical simulation and the 8^{th}-order GEVD system (Eq. (5.22)) and can be observed in Fig. 5.7. For $f(t) = 10\sin(t)$, Figs. 5.7[(d) – (f)] show the error in the response of x_1, x_2 and x_3 respectively obtained using the 54^{th}-order FOG and 8^{th}-order GEVD systems.

Figures 5.7[(d) – (f)] are the error plots for the system responses obtained for the TDS given by Eq. (5.34), 54^{th}-order FOG and 8^{th}-order GEVD systems. For all the state responses, the order of the maximum of $|\xi_1(t)|$ and $|\xi_2(t)|$ are 10^{-2} and 10^{-3}, respectively. It can be interpreted from Figs. 5.7[(a) – (f)] that the stability (characteristic roots) as well as the time response characteristics of the original infinite-dimensional TDS (Eq. (5.34)) are effectively captured by the 54^{th}-order FOG and the 8^{th}-order GEVD systems (constructed from r eigenvalues).

Now, $f(t) = 7\sin(0.1266t) + 10\sin(2.3041t)$ is considered. From Figs. 5.8[(a) – (c)], it can be inferred that the time response of the TDS (Eq. (5.34)) obtained by direct numerical simulation and the 8^{th}-order GEVD system (Eq. (5.22)) for $f(t) = 7\sin(0.1266t) + 10\sin(2.3041t)$ are once again in close agreement. The error plots with $f(t) = 7\sin(0.1266t) + 10\sin(2.3041t)$ obtained for Eq. (5.34) are presented in Figs. 5.8[(d) – (f)]. The order of the maximum of $|\xi_1(t)|$ and $|\xi_2(t)|$ are 10^{-1} and 10^{-2}, respectively, for all state responses.

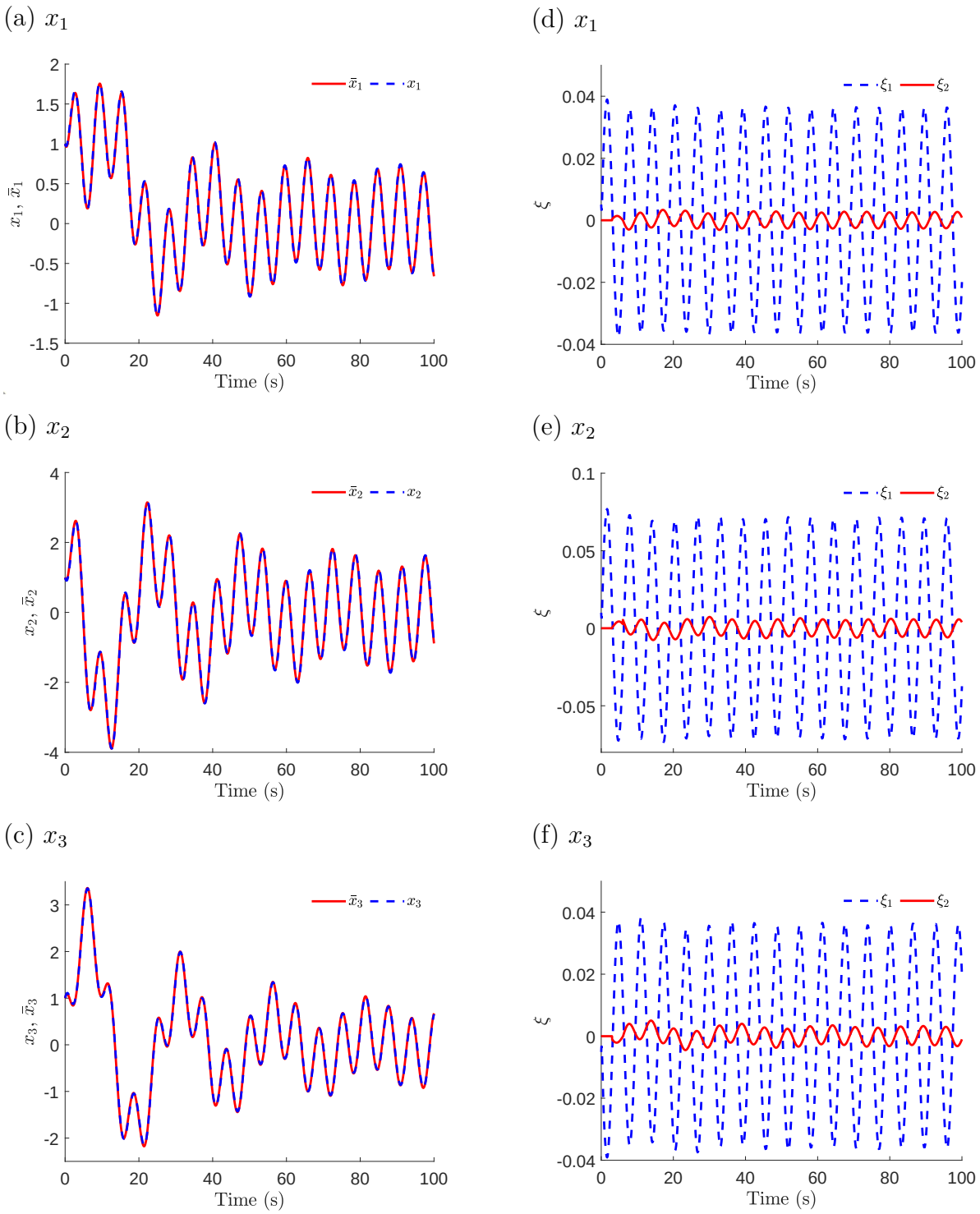

FIGURE 5.7: System responses and error plots of Eq. (5.34) with $\mathbf{r}(t) = [10\sin(t),\ 0,\ 0]^T$.

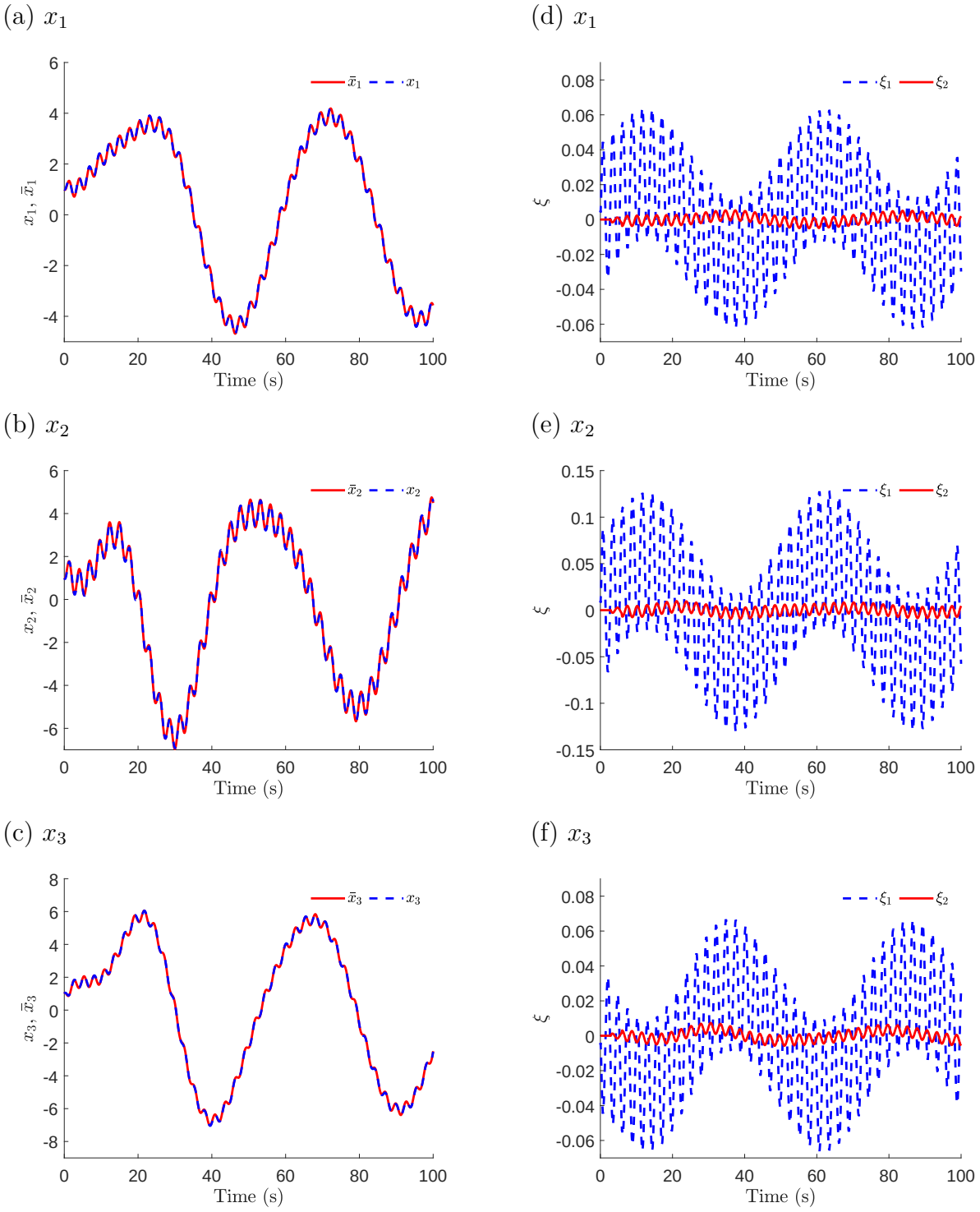

FIGURE 5.8: System responses and error plots of Eq. (5.34) for $\mathbf{r}(t) = [7\sin(0.1266t) + 10\sin(2.3041t),\ 0,\ 0]^T$.

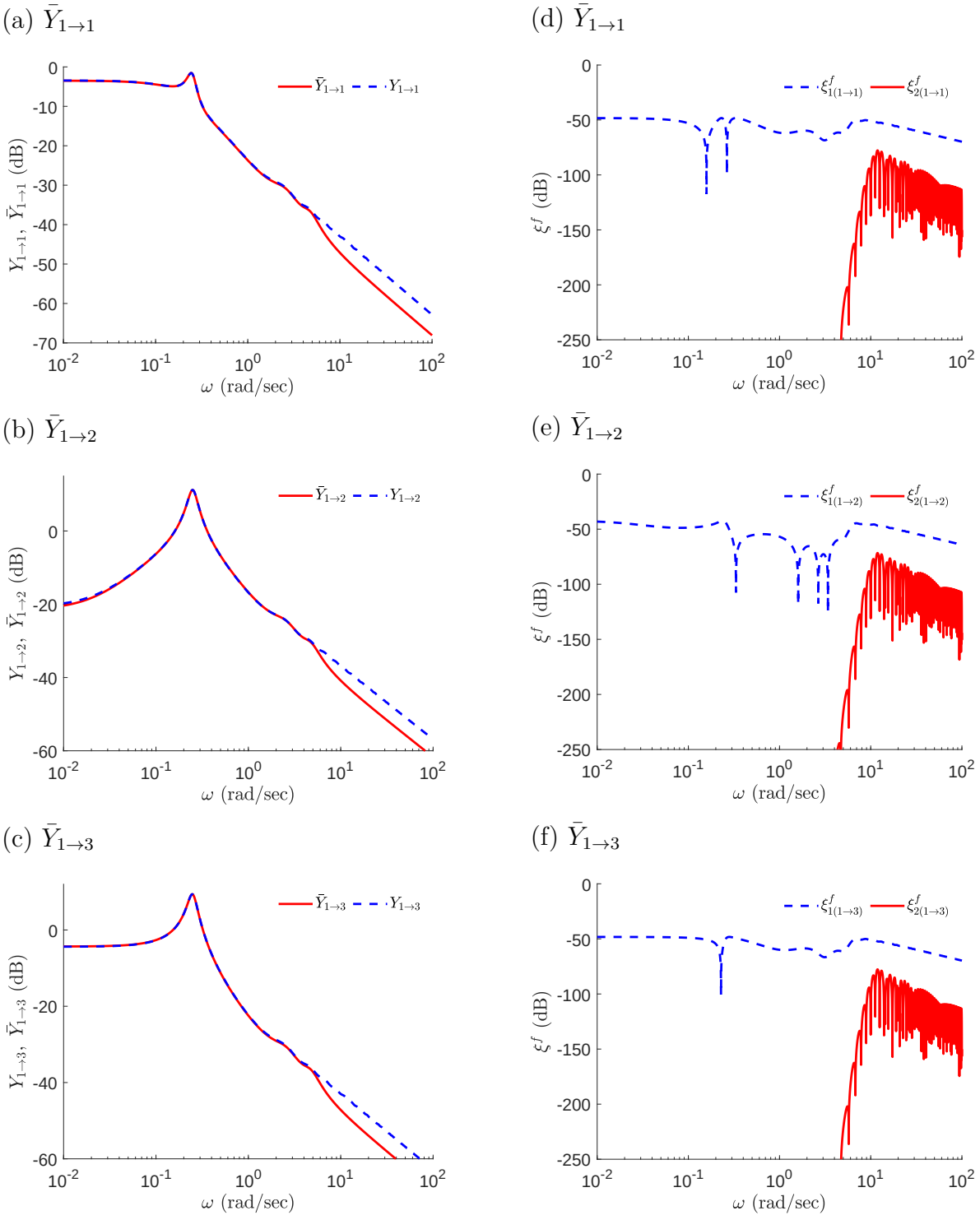

FIGURE 5.9: Frequency response and error plots of GETFs given in Eqs. (5.36a – 5.36c).

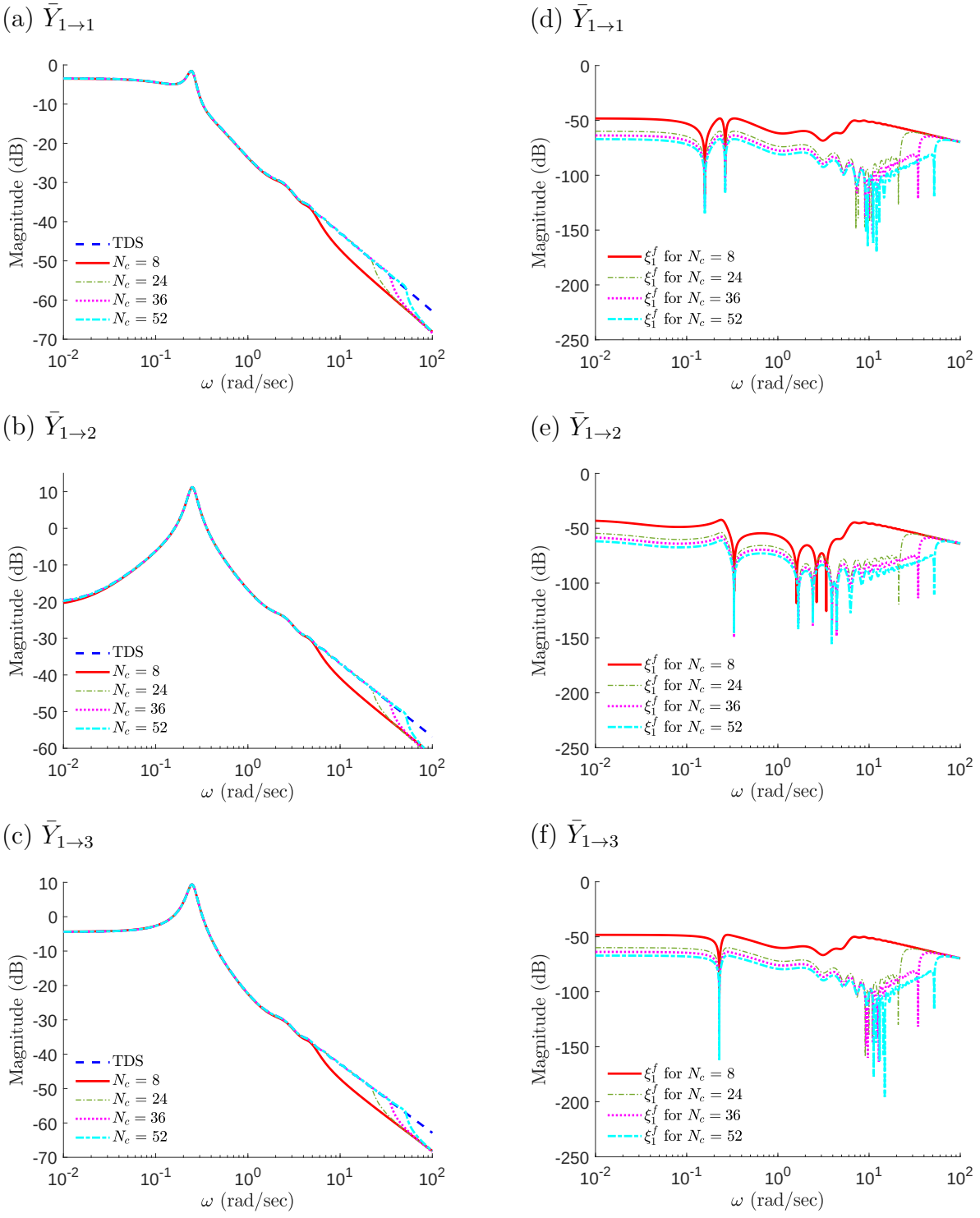

FIGURE 5.10: Frequency response plots and the associated error plots for different degrees of GETFs.

Next, the frequency responses of the ROMs are compared with that of the TDS given by Eq. (5.34). The transfer functions of each output channel with respect to a single input $f(t)$ are obtained. The notations $Y(s)_{i\to o}$, $\hat{Y}(s)_{i\to o}$ and $\bar{Y}(s)_{i\to o}$ are

the transfer functions from input $f(t)$ to output channel o. The GETFs are given as follows:

$$\bar{Y}(s)_{1\to1} = \frac{n(s)_{1\to1}}{d(s)}, \tag{5.36a}$$

$$\bar{Y}(s)_{1\to2} = \frac{n(s)_{1\to2}}{d(s)}, \tag{5.36b}$$

$$\bar{Y}(s)_{1\to3} = \frac{n(s)_{1\to3}}{d(s)}. \tag{5.36c}$$

where

$$n(s)_{1\to1} = 0.0628s^7 + 0.507s^6 + 3.011s^5 + 9.349s^4 + 17.56s^3 + 13.54s^2 - 1.03s + 1.134,$$
$$n(s)_{1\to2} = 0.13059s^7 + 1.087s^6 + 6.616s^5 + 21.55s^4 + 43.63s^3 + 41.62s^2 + 8.143s + 0.1451,$$
$$n(s)_{1\to3} = -0.06238s^7 - 0.4983s^6 - 2.947s^5 - 8.993s^4 - 16.29s^3 - 10.64s^2 + 4.841s + 1.028,$$
$$d(s) = 1.59s^8 + 8.122s^7 + 60.35s^6 + 143.4s^5 + 345.5s^4 + 240.5s^3 + 60.45s^2 + 14.86s + 1.695.$$

Figures 5.9[(a) – (c)] show the frequency response of the TDS given by Eq. (5.34) and the 8^{th}-order GETFs obtained in Eqs. 5.36a – 5.36c. The error plots associated with the frequency responses in Figs. 5.9[(a) – (c)] are given in Figs. 5.9[(d) – (f)]. It can be seen that the 54^{th}-order FOTF and the 8^{th}-order GETF reveal an approximation error of less than -72 dB and -43 dB, respectively, for all frequencies.

As mentioned in Section 5.1, to increase r, N should be increased. Based on the user requirements, r can be chosen and the corresponding N can be obtained. By increasing r, the order of the GETF is increased and the frequency response for the same is shown in Figs. 5.10[(a) – (c)] along with that of the TDS. By increasing r, it can be seen in Figs. 5.10[(a) – (c)] that more natural frequencies of the system can be included in the GETF depending upon the requirement. Figures 5.10[(d) – (f)] shows the corresponding error plot. From Figs. 5.10[(a) – (c)], it can be inferred that, to increase the operating frequency range of the GETF, r should be increased and, correspondingly, N should be increased. Therefore, it can be said that the proposed methodology of ROM satisfactorily captures the time as well as frequency domain characteristics of the TDS.

5.3 Experimental validation

The time responses obtained using the proposed GEVD-based ROM methodology are experimentally validated using a 3D hovercraft, manufactured by Quanser Inc.

Example: 3D hovercraft:

The experimental setup of the 3D hovercraft is shown in Fig. 5.11. The setup consists of a quadrotor mounted on a 3-degree-of-freedom pivot joint. The pivot joint allows the hovercraft to rotate freely about the yaw, pitch and roll axes. The 3D hovercraft is a fully actuated system, which means that the angular movements about the yaw, pitch and roll axes can be controlled with the voltage input being given to the motors. The resolution of the encoder is 0.0439°, and the setup can be directly connected to a computer with the USB interface.

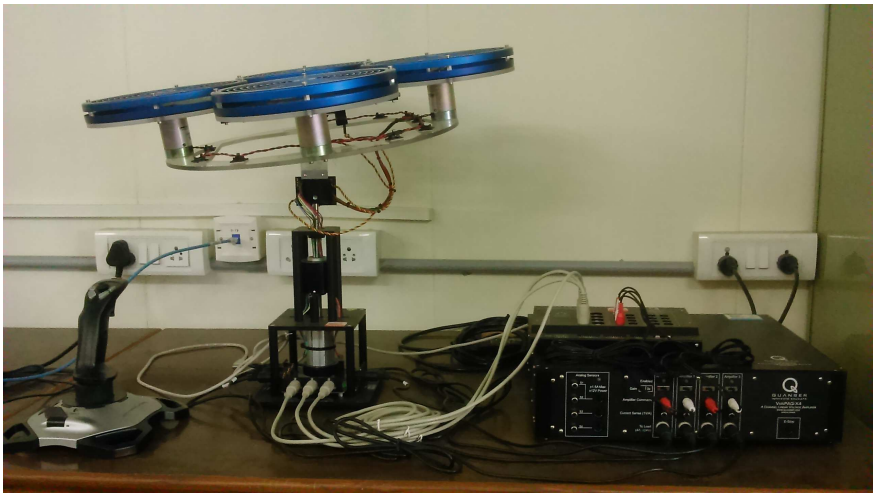

FIGURE 5.11: 3D hovercraft apparatus, manufactured by Quanser Inc. [1].

The state-space model of the 3D hovercraft with a delay in the system is given by Eq. (5.38):

$$\dot{\mathbf{x}}(t) = \mathbf{A}\mathbf{x}(t) + \mathbf{B}u(t), \tag{5.38a}$$

$$u(t) = \mathbf{K}^T[\mathbf{r}(t) - \mathbf{x}(t-\tau)], \quad \tau > 0, \tag{5.38b}$$

where $\mathbf{x} \triangleq [\theta_y, \theta_p, \theta_r, \dot{\theta}_y, \dot{\theta}_p, \dot{\theta}_r]^T$, $u(t) = V(t)$, θ_y,θ_p and θ_r are the yaw, pitch and roll angular positions respectively. The $\mathbf{A}$, $\mathbf{B}$ and $\mathbf{K}$ matrices are given as follows:

$$\mathbf{A} = \begin{bmatrix} 0 & 0 & 0 & 1 & 0 & 0 \\ 0 & 0 & 0 & 0 & 1 & 0 \\ 0 & 0 & 0 & 0 & 0 & 1 \\ 0 & 0 & 0 & 0 & 0 & 0 \\ 0 & 0 & 0 & 0 & 0 & 0 \\ 0 & 0 & 0 & 0 & 0 & 0 \end{bmatrix}, \mathbf{B} = \begin{bmatrix} 0 & 0 & 0 & 0 \\ 0 & 0 & 0 & 0 \\ 0 & 0 & 0 & 0 \\ -b_1 & -b_1 & b_1 & b_1 \\ b_2 & -b_2 & 0 & 0 \\ 0 & 0 & b_2 & -b_2 \end{bmatrix}, \mathbf{K} = \begin{bmatrix} -k_1 & -k_1 & k_1 & k_1 \\ k_2 & -k_2 & 0 & 0 \\ 0 & 0 & k_2 & -k_2 \\ -k_3 & -k_3 & k_3 & k_3 \\ k_4 & -k_4 & 0 & 0 \\ 0 & 0 & k_4 & -k_4 \end{bmatrix}, \tag{5.39}$$

where $b_1 = 0.0326$, $b_2 = 0.4235$, $k_1 = 111.8034$, $k_2 = 132.2876$, $k_3 = 41.4128$ and $k_4 = 36.2268$. Considering $r = 12$, we require $N = 15$.

For any delay (τ), with the given $\mathbf{A}$, $\mathbf{B}$, $\mathbf{K}$ and considering $N = 15$ in the series solution (Eq. (5.6)), Eq. (5.38) is converted into a system of ODEs of the form given by Eq. (5.14), where $\mathbf{L} \in \mathbb{R}^{90\times 90}$. Figure 5.12 shows the eigenvalues of Eq. (5.38) obtained using QPmR [91], eigenvalues of the 90$^{\text{th}}$-order FOG system given by Eq. (5.14) and the 12$^{\text{th}}$-order GEVD system given by Eq. (5.22) for $\tau = 20$ ms and $\tau = 25$ ms, respectively. For both $\tau = 20$ ms and $\tau = 25$ ms, the number of rightmost roots of the TDS obtained using QPmR and the rightmost eigenvalues of the FOG system shown in Figs. 5.12(a) and 5.12(b) are 17 and 15, respectively. For some of the roots, though, it appears from Fig. 5.12 that the roots obtained using QPmR are close to the eigenvalues of the FOG system, but in fact, only 6 rightmost roots converged with a tolerance of $\epsilon < 10^{-4}$. For both $\tau = 20$ ms and $\tau = 25$ ms, for $r = 12$, the corresponding $N = 15$.

(a) $\tau = 20$ ms (b) $\tau = 25$ ms

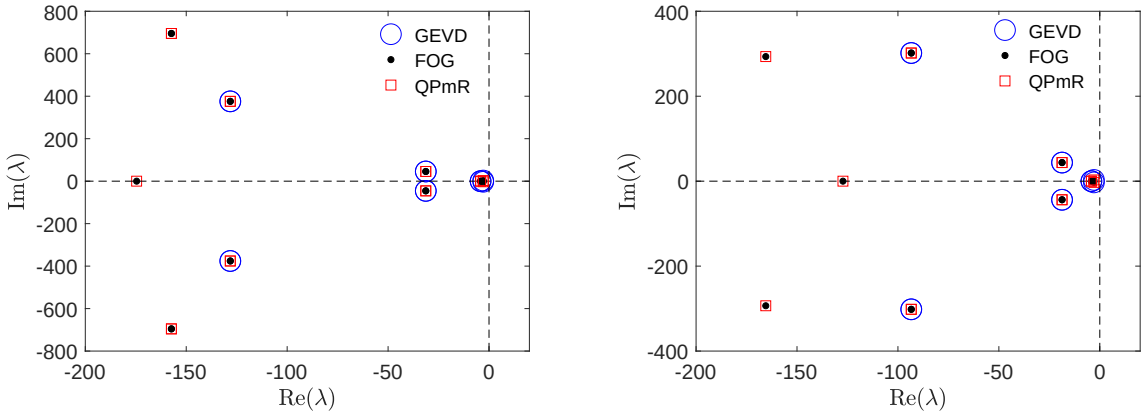

FIGURE 5.12: Roots of Eq. (5.38) using QPmR and spectral methods.

Experiments were performed for different kinds of reference trajectories, $\mathbf{r}(t)$, with $\tau = 20$ ms and $\tau = 25$ ms. The reference signal is considered as $\mathbf{r}(t) = [f(t),\ f(t),\ f(t),\ 0,\ 0,\ 0]^T$, where the first was a sinusoidal input of the form $f(t) = 0.2\sin(2t)$, second was of the form $f(t) = 0.2\sin(2t) + 0.1\sin(\pi t)$, third was a square wave input of the form $f(t) = 0.2(\text{sgn}(\sin(0.25t)))$ and fourth was of the form $f(t) = 0.2(\text{sgn}(\sin(0.25t))) + 0.1(\text{sgn}(\sin(1/\pi t)))$.

First the experiments were performed with $f(t) = 0.2\sin(2t)$ and with $\tau = 20$ ms. Figures 5.13[(a) – (c)] show $\theta_y(t)$, $\theta_p(t)$ and $\theta_r(t)$ obtained using the 12^{th} order GEVD system and experimentally. It can be observed that for a sinusoidal input of the form $f(t) = 0.2\sin(2t)$, the predicted trajectories of $\theta_y(t)$, $\theta_p(t)$ and $\theta_r(t)$ using the 12^{th} order GEVD system match closely with that of the experimentally obtained $\theta_y(t)$, $\theta_p(t)$ and $\theta_r(t)$. Next, for the same delay i.e., $\tau = 20$ ms, experiments were performed with a combination of sinusoidal waveforms with non-commensurate frequencies of the form $f(t) = 0.2\sin(2t) + 0.1\sin(\pi t)$. Figures 5.14[(a) – (c)] show $\theta_y(t)$, $\theta_p(t)$ and $\theta_r(t)$ obtained using the 12^{th} order GEVD system and experimentally. It can be observed that for a combination of sinusoidal waveforms with non-commensurate frequencies of the form $f(t) = 0.2\sin(2t) + 0.1\sin(\pi t)$, the predicted trajectories of $\theta_y(t)$, $\theta_p(t)$ and $\theta_r(t)$ using the 12^{th} order GEVD system match closely with that of the experimentally obtained $\theta_y(t)$, $\theta_p(t)$ and $\theta_r(t)$.

Next, delay in the system is increased to $\tau = 25$ ms. With $\tau = 25$ ms, two sets of experiments were performed with first a sinusoidal input of the form $f(t) = 0.2\sin(2t)$ and then a combination of sinusoidal waveforms with non-commensurate frequencies of the form $f(t) = 0.2\sin(2t) + 0.1\sin(\pi t)$. Figures 5.13[(d) – (f)] show the 12^{th} order GEVD system predicted and the experimentally obtained trajectories for $\theta_y(t)$, $\theta_p(t)$ and $\theta_r(t)$ for $f(t) = 0.2\sin(2t)$ for $\tau = 25$ ms. Figures 5.14[(d) – (f)] show the 12^{th} order GEVD system predicted and the experimentally obtained trajectories for $\theta_y(t)$, $\theta_p(t)$ and $\theta_r(t)$ for $f(t) = 0.2\sin(2t) + 0.1\sin(\pi t)$ for $\tau = 25$ ms.

To validate the proposed reduced order model for different kinds of inputs, two different square waveforms were considered for both the delays i.e., $\tau = 20$ ms and $\tau = 25$ ms. Figures 5.15[(a) – (c)] show $\theta_y(t)$, $\theta_p(t)$ and $\theta_r(t)$ obtained using the 12^{th} order GEVD system and experimentally for the square waveform of the form $f(t) = 0.2(\text{sgn}(\sin(0.25t)))$ for a delay of $\tau = 20$ ms. It can clearly be seen from Figures 5.15[(a) – (c)] that the predicted trajectories of $\theta_y(t)$, $\theta_p(t)$ and $\theta_r(t)$ using the 12^{th} order GEVD system match closely with that of the experimentally obtained $\theta_y(t)$, $\theta_p(t)$ and $\theta_r(t)$. Figures 5.16[(a) – (c)] show $\theta_y(t)$, $\theta_p(t)$ and $\theta_r(t)$ obtained using the 12^{th} order GEVD system and experimentally for a

combination of square waveforms with noncommensurate frequencies of the form $f(t) = 0.2(\text{sgn}(\sin(0.25t))) + 0.1(\text{sgn}(\sin(1/\pi t)))$ with $\tau = 20$ ms. It can once again be seen that the trajectories of $\theta_y(t)$, $\theta_p(t)$ and $\theta_r(t)$ predicted using the 12^{th} order GEVD system are in close agreeemtn with the same obtained experimentally.

Now, the delay is increased to $\tau = 25$ ms. With $\tau = 25$ ms, two sets of experiments were performed with first a square waveform input of the form $f(t) = 0.2(\text{sgn}(\sin(0.25t)))$ and then a combination of square waveforms with noncommensurate frequencies of the form $f(t) = 0.2(\text{sgn}(\sin(0.25t))) + 0.1(\text{sgn}(\sin(1/\pi t)))$. Figures 5.16[(d) – (f)] show the 12^{th} order GEVD system predicted and the experimentally obtained trajectories for $\theta_y(t)$, $\theta_p(t)$ and $\theta_r(t)$ for $f(t) = 0.2(\text{sgn}(\sin(0.25t)))$ for $\tau = 25$ ms. Figures 5.16[(d) – (f)] show the 12^{th} order GEVD system predicted and the experimentally obtained trajectories for $\theta_y(t)$, $\theta_p(t)$ and $\theta_r(t)$ for $f(t) = 0.2(\text{sgn}(\sin(0.25t))) + 0.1(\text{sgn}(\sin(1/\pi t)))$ for $\tau = 25$ ms.

One of the most important observations that can be inferred from Figs. 5.13 – 5.16 is that, even as the delay in the system is increased, the approximated system (i.e., the 12^{th}-order GEVD system) appears to capture the trajectories of $\theta_y(t)$, $\theta_p(t)$ and $\theta_r(t)$ and the dynamics of the original system closely. Also, it should be noted that the 12^{th}-order GEVD system predicts very closely the trajectories of $\theta_y(t)$, $\theta_p(t)$ and $\theta_r(t)$ even for single and multi-frequency sinusoidal as well as square waveform inputs to the original system.

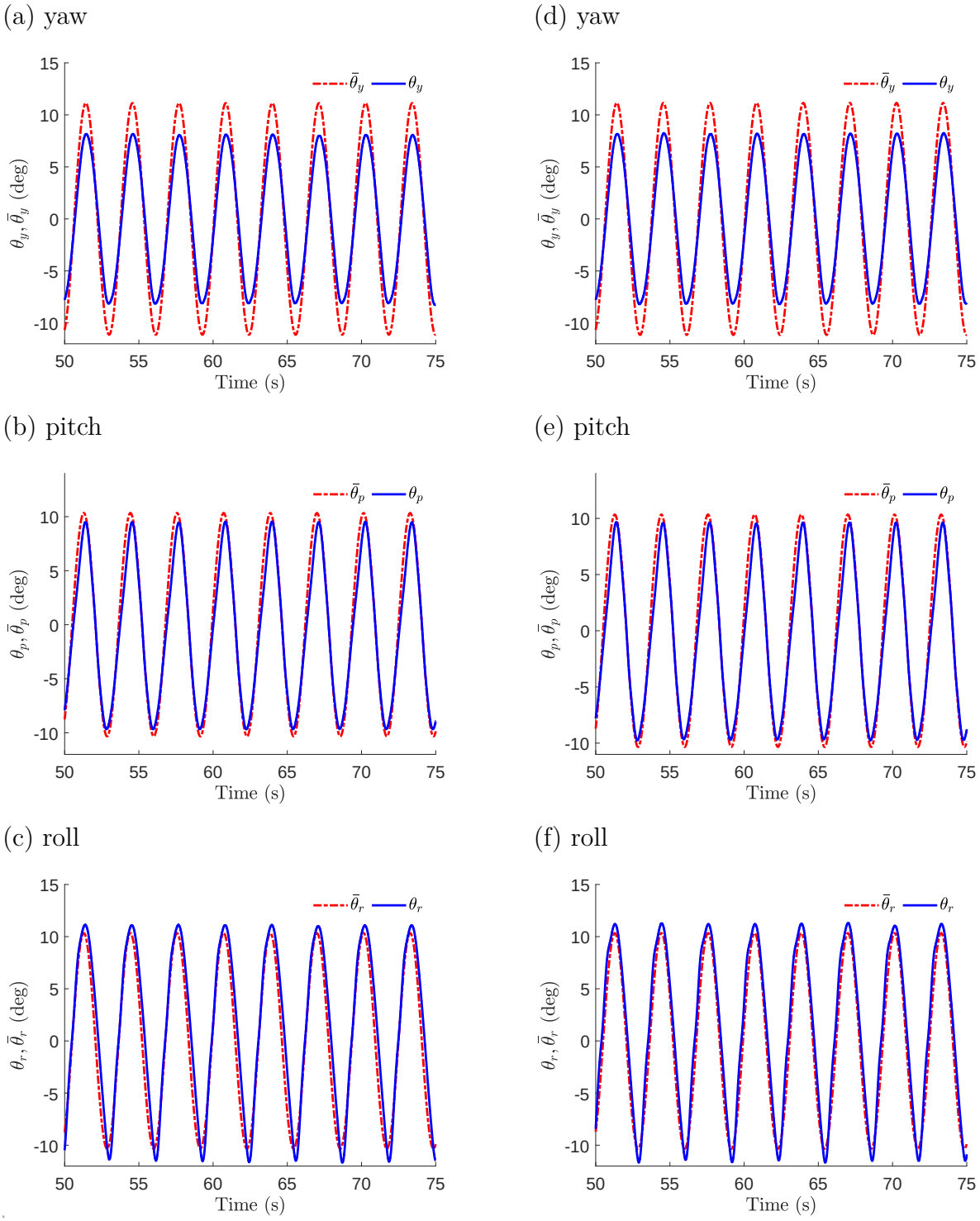

FIGURE 5.13: Trajectories for $f(t) = 0.2\sin(2t)$ and [(a),(b),(c)]: $\tau = 20$ms, and [(d),(e),(f)]: $\tau = 25$ms.

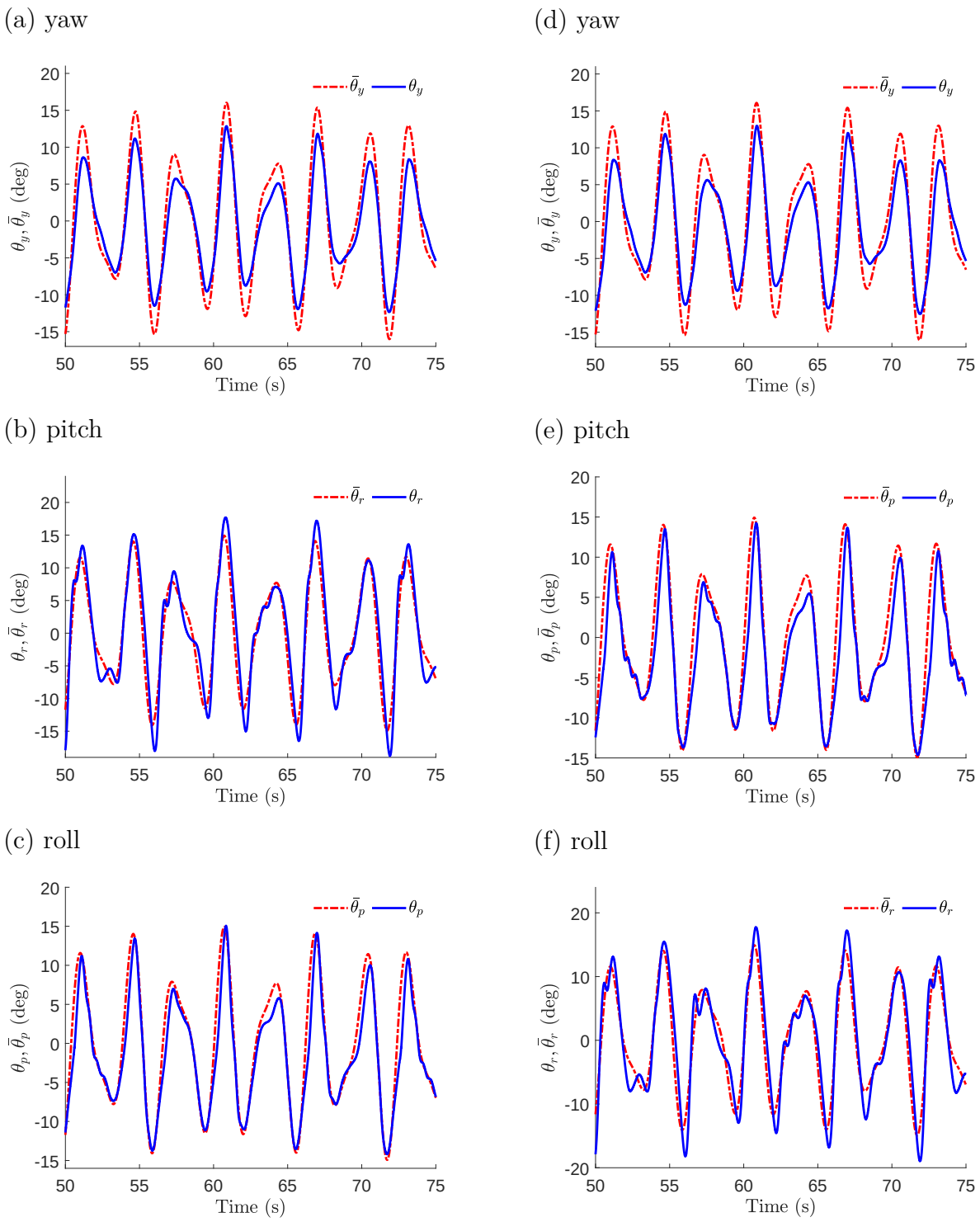

FIGURE 5.14: Trajectories for $f(t) = 0.2\sin(2t) + 0.1\sin(\pi t)$ and [(a),(b),(c)]: $\tau = 20$ms, and [(d),(e),(f)]: $\tau = 25$ms.

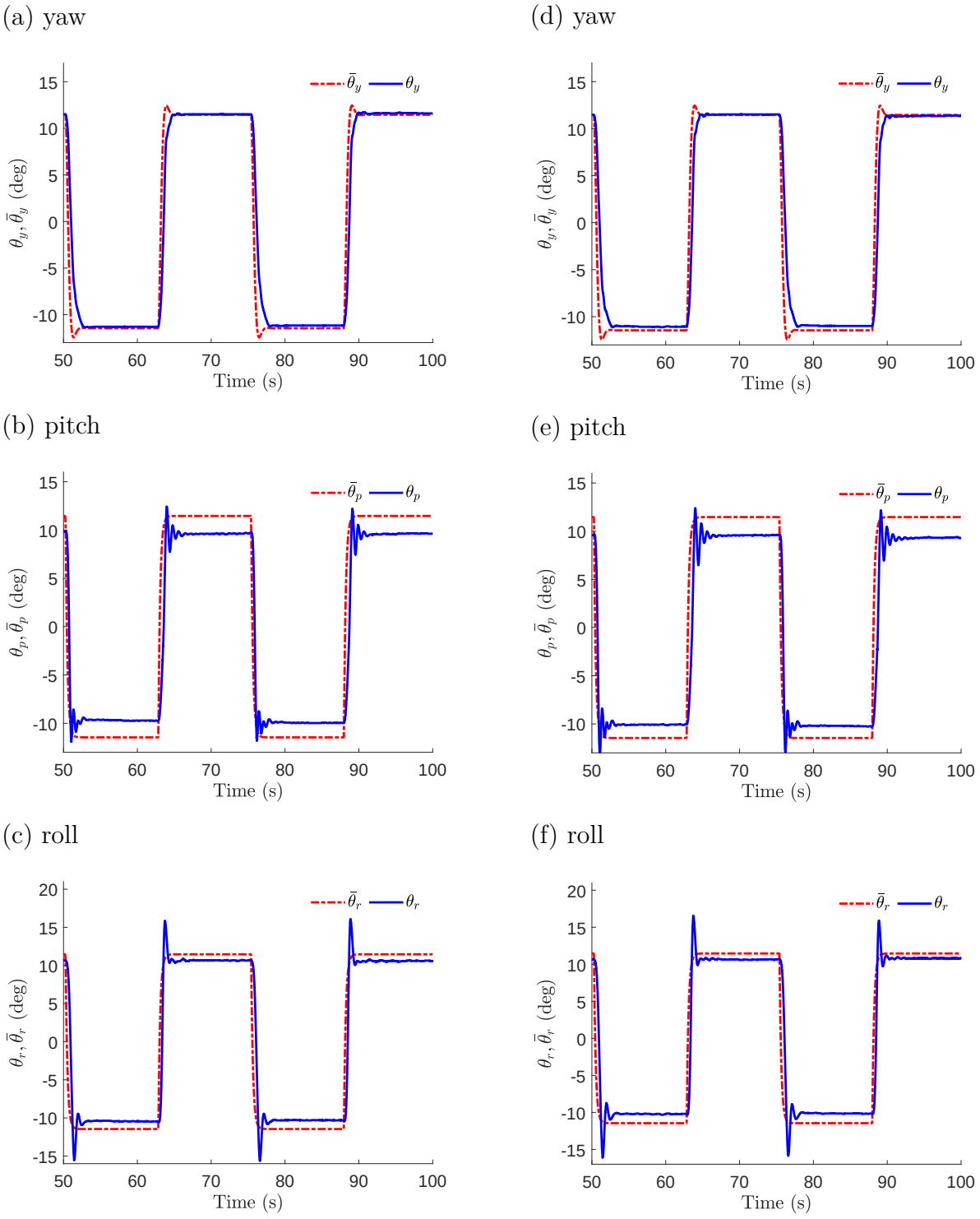

FIGURE 5.15: Trajectories for $f(t) = 0.2(\text{sgn}(\sin(0.25t)))$ and [(a),(b),(c)]: $\tau =$ 20ms, and [(d),(e),(f)]: $\tau = 25$ms.

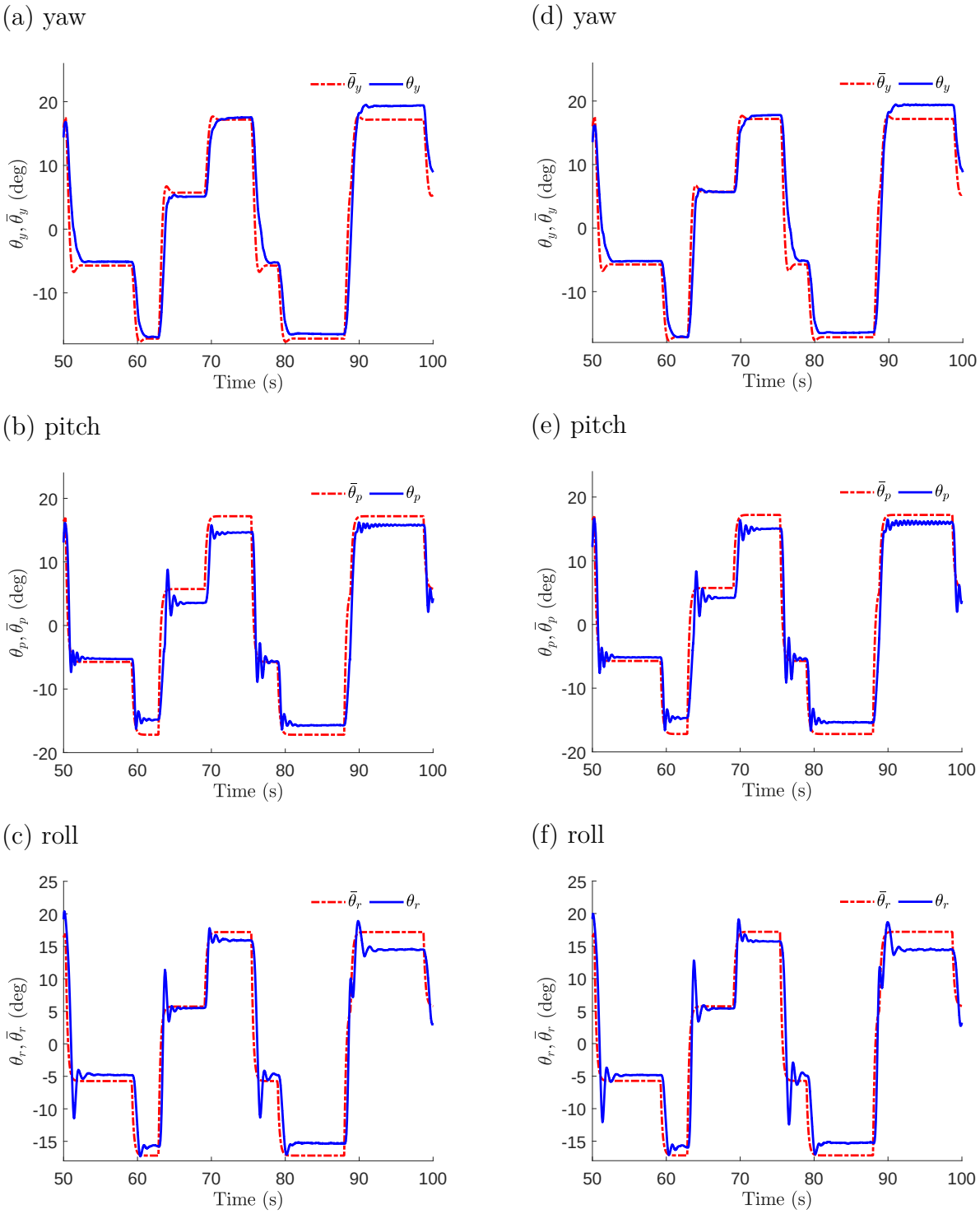

FIGURE 5.16: Trajectories for $f(t) = 0.2(\text{sgn}(\sin(0.25t))) + 0.1(\text{sgn}(\sin(1/\pi t)))$ and [(a),(b),(c)]: $\tau = 20$ms, and [(d),(e),(f)]: $\tau = 25$ms.

5.4 Chapter summary

In this chapter, we developed a method to obtain the ROMs for TDS using Galerkin approximations and EVD. An empirical relationship for N_c as a function of N and ϵ is obtained for a first-order DDE with 25 delays. The FOG as well as the GEVD systems capture the behavior of the TDS very well. Time and frequency responses obtained using the proposed reduced-order modelling technique are in very close agreement with the original TDS models considered in this work. The effectiveness of the proposed reduced-order modelling technique was demonstrated by performing experiments on a 3D–hovercraft. The results obtained using the proposed reduced-order modelling technique were in close agreement with the results obtained experimentally. With the proposed reduced-order modelling approach, a lower-dimensional model can be developed that satisfactorily retains the characteristics of the original TDS.

Chapter 6

Conclusions and future work

Pole placement and reduced-order modelling of TDS using the Galerkin approximations has been investigated in this thesis. Based on the results presented in Chapters 2–5, the following important conclusions are made:

- Spectral methods, such as the Galerkin approximation, have superior convergence properties and are hence favourable for obtaining the spectrum of DDEs.
- The "second-order Galerkin" formulation produces spurious roots at the origin that are not the characteristic roots of the DDE. These spurious roots do not influence stability studies but nevertheless add to the computation time and complexity of the pole placement and reduced-order modelling of TDS.
- A refined mathematical model called the "first-order Galerkin" formulation avoids spurious roots, thus eliminating the need for additional computation to determine the location of the rightmost root.
- A simpler mathematical derivation, called the pseudoinverse-based Galerkin approximation method, for obtaining the spectrum of DDEs was developed. It was observed that, on average, more roots converge using the proposed Galerkin method than the pseudospectral differencing method.
- A Galerkin approximation-based optimization framework was proposed for the pole placement of DDEs with constant/discrete delays, which was then successfully validated using numerical examples from the literature.
- A rotary inverted pendulum system with inherent and deliberate state feedback delays was used to experimentally validate the proposed Galerkin approximation-based optimization framework for the pole placement of TDS.

- Using a simple optimization strategy for the pole placement of DDEs, the time-delay stability margin is increased.
- The optimization-based pole-placement technique gives the precise information about the rightmost root of the DDE; however, the rightmost root is not always placed at the desired location.
- A hybrid pole-placement technique was developed by combining the strengths of the method of receptances (MoR) approach with an optimization-based strategy to address the limitations of the MoR.
- The proposed hybrid MoR and optimization-based technique expands the range of TDS to which pole-placement technique can be applied.
- The proposed hybrid pole-placement technique was experimentally validated using a 3D hovercraft apparatus with a deliberately introduced delay.
- The spectrum of DDEs obtained using Galerkin approximations contain the information of both the converged and unconverged roots.
- A new method to obtain reduced-order models for TDS using Galerkin approximations and EVD was developed that eliminates the information of unconverged roots obtained using the Galerkin approximations.
- The effectiveness of the proposed reduced-order modelling technique was demonstrated by comparing the results of the reduced-order model with experiments on a 3D hovercraft apparatus.

6.1 Open problems and future work

This thesis has touched upon some of the challenges associated with the pole placement and reduced-order modelling of TDS. Based on these studies, a few open problems that are yet to be addressed are the following:

- Investigating the stability of linear DDEs using Floquet theory and, in particular, the presence of spurious Floquet multipliers.
- Reducing the computation time to obtain stability charts using numerical techniques, such as Galerkin approximations, by combining them with analytical tools.

- Experimental validation of Galerkin approximations for TDS with periodic coefficients and/or delays.
- Extension of the proposed pole-placement technique to incorporate systems with the time-periodic coefficients and/or delays.
- Constrained optimization problem for pole placement that handles limits on controller gains, balances the increase in the stability margin with minimizing the control effort, and/or limits actuator energy usage.
- Extension of the proposed pole-placement technique to obtain time-varying feedback gain parameters.
- Extension of the method of receptances to handle higher-order systems, time-varying delays, and constraints imposed by system parameters, actuator saturation, and limits on feedback gains.
- Study the effects of time-varying delays, and constraints imposed by system parameters, actuator saturation, and limits on feedback gains on the system stability by incorporating them into the optimization-based technique.
- Investigation of the effects of delays in the output equations.
- Extension of the proposed optimization strategy to include the frequency component of the spectrum of the DDEs for control.
- Further the experimental validation of the various control strategies for the systems governed by DDEs.

References

[1] J. Apkarian and M. Lévis, *Laboratory Guide: 3 DOF Hover Experiment for MATLAB/Simulink Users*. Quanser Inc., 2013.

[2] J. Apkarian, M. Lévis, and P. Martin, *Instructor Workbook: QUBE-Servo 2 Experiment for MATLAB/Simulink Users*. Quanser Inc., 2016.

[3] N. S. Nise, *Control Systems Engineering*. New York, NY, USA: John Wiley & Sons, 2000.

[4] E. Fridman, *Introduction to Time-Delay Systems: Analysis and Control*. Switzerland: Springer, 2014.

[5] S. Yi, P. W. Nelson, and A. G. Ulsoy, *Time-Delay Systems: Analysis and Control Using the Lambert W function*. Hackensack, NJ, USA: World Scientific, 2010.

[6] T. Insperger and G. Stépán, "Act-and-wait control concept for discrete-time systems with feedback delay," *IET Control Theory & Applications*, vol. 1, no. 3, pp. 553–557, 2007.

[7] S. Yi, P. W. Nelson, and A. G. Ulsoy, "Eigenvalue assignment via the Lambert W function for control of time-delay systems," *Journal of Vibration and Control*, vol. 16, no. 7–8, pp. 961–982, 2010.

[8] T. Insperger, "Stick balancing with reflex delay in case of parametric forcing," *Communications in Nonlinear Science and Numerical Simulation*, vol. 16, no. 4, pp. 2160–2168, 2011.

[9] T. Insperger, J. Milton, and G. Stépán, "Acceleration feedback improves balancing against reflex delay," *Journal of the Royal Society Interface*, vol. 10, no. 79, p. 20120763, 2013.

[10] T. Insperger and J. Milton, "Sensory uncertainty and stick balancing at the fingertip," *Biological Cybernetics*, vol. 108, no. 1, pp. 85–101, 2014.

[11] T. Insperger, J. Milton, and G. Stépán, "Semidiscretization for time-delayed neural balance control," *SIAM Journal on Applied Dynamical Systems*, vol. 14, no. 3, pp. 1258–1277, 2015.

[12] Z. Ahsan, T. K. Uchida, A. Subudhi, and C. P. Vyasarayani, "Stability of human balance with reflex delays using galerkin approximations," *Journal of Computational and Nonlinear Dynamics*, vol. 11, no. 4, p. 041009, 2016.

[13] A. P. Dowling and A. S. Morgans, "Feedback control of combustion oscillations," *Annual Review of Fluid Mechanics*, vol. 37, pp. 151–182, 2005.

[14] A. P. Dowling, "Nonlinear self-excited oscillations of a ducted flame," *Journal of Fluid Mechanics*, vol. 346, pp. 271–290, 1997.

[15] N. Olgac, R. Cepeda-Gomez, U. Zalluhoglu, and A. S. Kammer, "Parametric investigation of thermoacoustic instability (TAI) in a Rijke tube: a time-delay perspective," *International Journal of Spray and Combustion Dynamics*, vol. 7, no. 1, pp. 39–68, 2015.

[16] N. Olgac, U. Zalluhoglu, and A. S. Kammer, "Predicting thermoacoustic instability: a novel analytical approach and its experimental validation," *Journal of Propulsion and Power*, vol. 30, no. 4, pp. 1005–1015, 2014.

[17] S. S. Kandala, A. Maduri, and C. P. Vyasarayani, "Galerkin approximations for thermoacoustic instability in a Rijke's tube," *Procedia IUTAM*, vol. 22, pp. 168–175, 2017.

[18] G. Stépán, *Retarded Dynamical Systems: Stability and Characteristic Functions*. New York, NY, USA: Longman Scientific & Technical, 1989.

[19] B. Balachandran, "Nonlinear dynamics of milling processes," *Philosophical Transactions of the Royal Society of London. Series A: Mathematical, Physical and Engineering Sciences*, vol. 359, no. 1781, pp. 793–819, 2001.

[20] T. Kalmár-Nagy, G. Stépán, and F. C. Moon, "Subcritical Hopf bifurcation in the delay equation model for machine tool vibrations," *Nonlinear Dynamics*, vol. 26, no. 2, pp. 121–142, 2001.

[21] N. K. Chandiramani and T. Pothala, "Dynamics of 2-dof regenerative chatter during turning," *Journal of Sound and Vibration*, vol. 290, no. 1-2, pp. 448–464, 2006.

[22] A. Chanda, A. Fischer, P. Eberhard, and S. K. Dwivedy, "Stability analysis of a thin-walled cylinder in turning operation using the semi-discretization method," *Acta Mechanica Sinica*, vol. 30, no. 2, pp. 214–222, 2014.

[23] G. Urbikain, D. Olvera, L. L. de Lacalle, and A. Elías-Zúñiga, "Spindle speed variation technique in turning operations: Modeling and real implementation," *Journal of Sound and Vibration*, vol. 383, pp. 384–396, 2016.

[24] M. Paidoussis and G. X. Li, "Cross-flow-induced chaotic vibrations of heat-exchanger tubes impacting on loose supports," *Journal of Sound and Vibration*, vol. 152, no. 2, pp. 305–326, 1992.

[25] J. De Bedout, M. Franchek, and A. Bajaj, "Robust control of chaotic vibrations for impacting heat exchanger tubes in crossflow," *Journal of Sound and Vibration*, vol. 227, no. 1, pp. 183–204, 1999.

[26] K. Pyragas, "Continuous control of chaos by self-controlling feedback," *Physics Letters A*, vol. 170, no. 6, pp. 421–428, 1992.

[27] J. Sun, "Delay-dependent stability criteria for time-delay chaotic systems via time-delay feedback control," *Chaos, Solitons & Fractals*, vol. 21, no. 1, pp. 143–150, 2004.

[28] J. Park and O. Kwon, "A novel criterion for delayed feedback control of time-delay chaotic systems," *Chaos, Solitons & Fractals*, vol. 23, no. 2, pp. 495–501, 2005.

[29] X. Guan, G. Feng, C. Chen, and G. Chen, "A full delayed feedback controller design method for time-delay chaotic systems," *Physica D: Nonlinear Phenomena*, vol. 227, no. 1, pp. 36–42, 2007.

[30] Y. Kuang, *Delay Differential Equations: With Applications in Population Dynamics*, vol. 191. San Diego, CA, USA: Academic press, 1993.

[31] I. Kubiaczyk and S. Saker, "Oscillation and stability in nonlinear delay differential equations of population dynamics," *Mathematical and Computer Modelling*, vol. 35, no. 3-4, pp. 295–301, 2002.

[32] D. Xu and Z. Yang, "Impulsive delay differential inequality and stability of neural networks," *Journal of Mathematical Analysis and Applications*, vol. 305, no. 1, pp. 107–120, 2005.

[33] J. Bélair, S. A. Campbell, and P. van den Driessche, "Frustration, stability, and delay-induced oscillations in a neural network model," *SIAM Journal on Applied Mathematics*, vol. 56, no. 1, pp. 245–255, 1996.

[34] S. A. Campbell, S. Ruan, G. Wolkowicz, and J. Wu, "Stability and bifurcation of a simple neural network with multiple time delays," *Fields Institute Communications*, vol. 21, no. 4, pp. 65–79, 1999.

[35] G. Stépán, "Chaotic motion of wheels," *Vehicle System Dynamics*, vol. 20, no. 6, pp. 341–351, 1991.

[36] D. Takács, G. Stépán, and S. J. Hogan, "Isolated large amplitude periodic motions of towed rigid wheels," *Nonlinear Dynamics*, vol. 52, no. 1-2, pp. 27–34, 2008.

[37] D. Takács, G. Orosz, and G. Stépán, "Delay effects in shimmy dynamics of wheels with stretched string-like tyres," *European Journal of Mechanics-A/Solids*, vol. 28, no. 3, pp. 516–525, 2009.

[38] P. S. Addison and D. J. Low, "A novel nonlinear car-following model," *Chaos: An Interdisciplinary Journal of Nonlinear Science*, vol. 8, no. 4, pp. 791–799, 1998.

[39] L. A. Safonov, E. Tomer, V. V. Strygin, Y. Ashkenazy, and S. Havlin, "Multifractal chaotic attractors in a system of delay-differential equations modeling road traffic," *Chaos: An Interdisciplinary Journal of Nonlinear Science*, vol. 12, no. 4, pp. 1006–1014, 2002.

[40] G. Orosz and G. Stépán, "Subcritical Hopf bifurcations in a car-following model with reaction-time delay," *Proceedings of the Royal Society A: Mathematical, Physical and Engineering Sciences*, vol. 462, no. 2073, pp. 2643–2670, 2006.

[41] L. Safonov, E. Tomer, V. Strygin, and S. Havlin, "Periodic solutions of a nonlinear traffic model," *Physica A: Statistical Mechanics and its Applications*, vol. 285, no. 1-2, pp. 147–155, 2000.

[42] F. M. Asl and A. G. Ulsoy, "Analysis of a system of linear delay differential equations," *Journal of Dynamic Systems, Measurement, and Control*, vol. 125, no. 2, pp. 215–223, 2003.

[43] E. Jarlebring and T. Damm, "The Lambert W function and the spectrum of some multidimensional time-delay systems," *Automatica*, vol. 43, no. 12, pp. 2124–2128, 2007.

[44] S. Yi, P. W. Nelson, and A. G. Ulsoy, "Survey on analysis of time delayed systems via the Lambert W function," *differential equations*, vol. 25, p. 28, 2007.

[45] S. Surya, C. P. Vyasarayani, and T. Kalmár-Nagy, "Homotopy continuation for characteristic roots of delay differential equations using the Lambert W function," *Journal of Vibration and Control*, vol. 24, no. 17, pp. 3944–3951, 2018.

[46] P. Wahi and A. Chatterjee, "Asymptotics for the characteristic roots of delayed dynamic systems," *Journal of Applied Mechanics*, vol. 72, no. 4, pp. 475–483, 2005.

[47] P. Wahi and A. Chatterjee, "Galerkin projections for delay differential equations," *Journal of Dynamic Systems, Measurement, and Control*, vol. 127, no. 1, pp. 80–87, 2005.

[48] C. P. Vyasarayani, "Galerkin approximations for higher order delay differential equations," *Journal of Computational and Nonlinear Dynamics*, vol. 7, no. 3, p. 031004, 2012.

[49] A. Sadath and C. P. Vyasarayani, "Galerkin approximations for stability of delay differential equations with distributed delays," *Journal of Computational and Nonlinear Dynamics*, vol. 10, no. 6, p. 061024, 2015.

[50] T. Kalmár-Nagy, "Stability analysis of delay-differential equations by the method of steps and inverse Laplace transform," *Differential Equations and Dynamical Systems*, vol. 17, no. 1-2, pp. 185–200, 2009.

[51] T. Insperger and G. Stépán, *Semi-discretization for Time-Delay Systems: Stability and Engineering Applications*, vol. 178. New York, NY, USA: Springer Science & Business Media, 2011.

[52] E. A. Butcher, H. Ma, E. Bueler, V. Averina, and Z. Szabo, "Stability of linear time-periodic delay-differential equations via Chebyshev polynomials," *International Journal for Numerical Methods in Engineering*, vol. 59, no. 7, pp. 895–922, 2004.

[53] D. Breda, S. Maset, and R. Vermiglio, "Pseudospectral differencing methods for characteristic roots of delay differential equations," *SIAM Journal on Scientific Computing*, vol. 27, no. 2, pp. 482–495, 2005.

[54] Z. Wu and W. Michiels, "Reliably computing all characteristic roots of delay differential equations in a given right half plane using a spectral method," *Journal of Computational and Applied Mathematics*, vol. 236, no. 9, pp. 2499–2514, 2012.

[55] B. P. Mann and B. R. Patel, "Stability of delay equations written as state space models," *Journal of Vibration and Control*, vol. 16, no. 7–8, pp. 1067–1085, 2010.

[56] F. A. Khasawneh and B. P. Mann, "A spectral element approach for the stability of delay systems," *International Journal for Numerical Methods in Engineering*, vol. 87, no. 6, pp. 566–592, 2011.

[57] J. Q. Sun, "A method of continuous time approximation of delayed dynamical systems," *Communications in Nonlinear Science and Numerical Simulation*, vol. 14, no. 4, pp. 998–1007, 2009.

[58] B. Song and J. Q. Sun, "Lowpass filter-based continuous-time approximation of delayed dynamical systems," *Journal of Vibration and Control*, vol. 17, no. 8, pp. 1173–1183, 2011.

[59] T. Koto, "Method of lines approximations of delay differential equations," *Computers & Mathematics with Applications*, vol. 48, no. 1–2, pp. 45–59, 2004.

[60] K. Engelborghs and D. Roose, "On stability of LMS methods and characteristic roots of delay differential equations," *SIAM Journal on Numerical Analysis*, vol. 40, no. 2, pp. 629–650, 2002.

[61] L. Pekař and Q. Gao, "Spectrum analysis of LTI continuous-time systems with constant delays: A literature overview of some recent results," *IEEE Access*, vol. 6, pp. 35457–35491, 2018.

[62] C. P. Vyasarayani, S. Subhash, and T. Kalmár-Nagy, "Spectral approximations for characteristic roots of delay differential equations," *International Journal of Dynamics and Control*, vol. 2, no. 2, pp. 126–132, 2014.

[63] J. Lavaei, S. Sojoudi, and R. M. Murray, "Simple delay-based implementation of continuous-time controllers," in *Proceedings of the American Control Conference*, (Baltimore, MD, USA), pp. 5781–5788, 2010.

[64] G. Orosz, J. Moehlis, and R. M. Murray, "Controlling biological networks by time-delayed signals," *Philosophical Transactions of the Royal Society A: Mathematical, Physical and Engineering Sciences*, vol. 368, no. 1911, pp. 439–454, 2010.

[65] N. Bekiaris-Liberis, M. Jankovic, and M. Krstic, "Adaptive stabilization of LTI systems with distributed input delay," *International Journal of Adaptive Control and Signal Processing*, vol. 27, no. 1–2, pp. 46–65, 2013.

[66] W. Michiels, K. Engelborghs, P. Vansevenant, and D. Roose, "Continuous pole placement for delay equations," *Automatica*, vol. 38, no. 5, pp. 747–761, 2002.

[67] W. Michiels, T. Vyhlídal, and P. Zítek, "Control design for time-delay systems based on quasi-direct pole placement," *Journal of Process Control*, vol. 20, no. 3, pp. 337–343, 2010.

[68] T. Vyhlídal, W. Michiels, and P. McGahan, "Synthesis of strongly stable state-derivative controllers for a time-delay system using constrained non-smooth optimization," *IMA Journal of Mathematical Control and Information*, vol. 27, no. 4, pp. 437–455, 2010.

[69] J. Niu, Y. Ding, L. Zhu, and H. Ding, "Eigenvalue assignment for control of time-delay systems via the generalized Runge–Kutta method," *Journal of Dynamic Systems, Measurement, and Control*, vol. 137, no. 9, p. 091003, 2015.

[70] J. V. Burke, A. S. Lewis, and M. L. Overton, "A robust gradient sampling algorithm for nonsmooth, nonconvex optimization," *SIAM Journal on Optimization*, vol. 15, no. 3, pp. 751–779, 2005.

[71] J. Vanbiervliet, K. Verheyden, W. Michiels, and S. Vandewalle, "A nonsmooth optimisation approach for the stabilisation of time-delay systems," *ESAIM: Control, Optimisation and Calculus of Variations*, vol. 14, no. 3, pp. 478–493, 2008.

[72] S. Yi, P. W. Nelson, and A. G. Ulsoy, "Proportional-integral control of first-order time-delay systems via eigenvalue assignment," *IEEE Transactions on Control Systems Technology*, vol. 21, no. 5, pp. 1586–1594, 2013.

[73] F. Wei, D. Bachrathy, G. Orosz, and A. G. Ulsoy, "Spectrum design using distributed delay," *International Journal of Dynamics and Control*, vol. 2, no. 2, pp. 234–246, 2014.

[74] S. S. Kandala, T. K. Uchida, and C. P. Vyasarayani, "Pole placement for time-delayed systems using galerkin approximations," *Journal of Dynamic Systems, Measurement, and Control*, vol. 141, no. 5, p. 051012, 2019.

[75] Y. M. Ram, A. Singh, and J. E. Mottershead, "State feedback control with time delay," *Mechanical Systems and Signal Processing*, vol. 23, no. 6, pp. 1940–1945, 2009.

[76] Y. M. Ram, J. Mottershead, and M. G. Tehrani, "Partial pole placement with time delay in structures using the receptance and the system matrices," *Linear Algebra and its Applications*, vol. 434, no. 7, pp. 1689–1696, 2011.

[77] T. Insperger, "On the approximation of delayed systems by Taylor series expansion," *Journal of Computational and Nonlinear Dynamics*, vol. 10, no. 2, p. 024503, 2015.

[78] J. M. Pratt, K. V. Singh, and B. N. Datta, "Quadratic partial eigenvalue assignment problem with time delay for active vibration control," in *Proceedings of the 7th International Conference on Modern Practice in Stress and Vibration Analysis, Journal of Physics: Conference Series*, vol. 181, (Cambridge, UK), p. 012092, IOP Publishing, 2009.

[79] H. Ouyang and K. Singh, "Pole assignment for asymmetric systems using state-feedback with time delay," in *Proceedings of ISMA 2010: International Conference on Noise and Vibration Engineering*, (Leuven, Belgium), pp. 383–390, 2010.

[80] K. V. Singh and B. N. Datta, "Zero assignment in a time delayed continuous system for active vibration control," in *Proceedings of the International Conference on Communications, Computing and Control Applications*, (Hammamet, Tunisia), pp. 1–6, IEEE, 2011.

[81] Z. J. Bai, M. X. Chen, and J. K. Yang, "A multi-step hybrid method for multi-input partial quadratic eigenvalue assignment with time delay," *Linear Algebra and its Applications*, vol. 437, no. 7, pp. 1658–1669, 2012.

[82] Z. J. Bai, M. X. Chen, and B. N. Datta, "Minimum norm partial quadratic eigenvalue assignment with time delay in vibrating structures using the receptance and the system matrices," *Journal of Sound and Vibration*, vol. 332, no. 4, pp. 780–794, 2013.

[83] X. T. Wang and L. Zhang, "Partial eigenvalue assignment of high order systems with time delay," *Linear Algebra and its Applications*, vol. 438, no. 5, pp. 2174–2187, 2013.

[84] X. Mao and H. Dai, "Partial eigenvalue assignment with time-delay robustness," *Numerical Algebra, Control and Optimization*, vol. 3, no. 2, pp. 207–221, 2013.

[85] T. X. Li and E. K. W. Chu, "Pole assignment for linear and quadratic systems with time-delay in control," *Numerical Linear Algebra with Applications*, vol. 20, no. 2, pp. 291–301, 2013.

[86] K. V. Singh and H. Ouyang, "Pole assignment using state feedback with time delay in friction-induced vibration problems," *Acta Mechanica*, vol. 224, no. 3, pp. 645–656, 2013.

[87] X. Mao, "Partial eigenvalue assignment problems for time-delayed systems," in *Proceedings of the 26th Chinese Control and Decision Conference*, (Changsha, China), pp. 3173–3177, IEEE, 2014.

[88] K. V. Singh, R. Dey, and B. N. Datta, "Partial eigenvalue assignment and its stability in a time delayed system," *Mechanical Systems and Signal Processing*, vol. 42, no. 1-2, pp. 247–257, 2014.

[89] R. Schmid and T. Nguyen, "Robust eigenvalue assignment for time-delay systems," in *Proceedings of the 53rd Annual Conference on Decision and Control*, (Los Angeles, CA, USA), pp. 2410–2413, IEEE, 2014.

[90] R. Schmid, Q. Gao, and N. Olgac, "Eigenvalue assignment for systems with multiple time-delays," in *Proceedings of the Conference on Control and its Applications*, (Paris, France), pp. 146–152, SIAM, 2015.

[91] T. Vyhlídal and P. Zítek, "QPmR-Quasi-Polynomial Root-finder: Algorithm update and examples," in *Delay Systems: From Theory to Numerics and Applications*, pp. 299–312, Springer, 2014.

[92] L. Zhang, "Multi-input partial eigenvalue assignment for high order control systems with time delay," *Mechanical Systems and Signal Processing*, vol. 72, pp. 376–382, 2016.

[93] X. T. Wang and L. Zhang, "Partial eigenvalue assignment with time delay in high order system using the receptance," *Linear Algebra and its Applications*, vol. 523, pp. 335–345, 2017.

[94] R. Ariyatanapol, Y. P. Xiong, and H. Ouyang, "Partial pole assignment with time delays for asymmetric systems," *Acta Mechanica*, pp. 1–11, 2017.

[95] L. Zhang and F. Shan, "Pole–zero placement problem with time delay for high-order systems," *Circuits, Systems, and Signal Processing*, vol. 36, no. 11, pp. 4354–4364, 2017.

[96] T. L. Santos, J. M. Araújo, and T. S. Franklin, "Receptance-based stability criterion for second-order linear systems with time-varying delay," *Mechanical Systems and Signal Processing*, vol. 110, pp. 428–441, 2018.

[97] J. M. Araújo and T. L. M. Santos, "Control of a class of second-order linear vibrating systems with time-delay: Smith predictor approach," *Mechanical Systems and Signal Processing*, vol. 108, pp. 173–187, 2018.

[98] Z. C. Qin, X. Li, S. Zhong, and J. Q. Sun, "Control experiments on time-delayed dynamical systems," *Journal of Vibration and Control*, vol. 20, no. 6, pp. 827–837, 2014.

[99] N. Olgac, A. F. Ergenc, and R. Sipahi, "Delay scheduling: A new concept for stabilization in multiple delay systems," *Modal Analysis*, vol. 11, no. 9, pp. 1159–1172, 2005.

[100] W. Thomson, "Delay networks having maximally flat frequency characteristics," *Proceedings of the IEE-Part III: Radio and Communication Engineering*, vol. 96, no. 44, pp. 487–490, 1949.

[101] L. Storch, "Synthesis of constant-time-delay ladder networks using bessel polynomials," *Proceedings of the IRE*, vol. 42, no. 11, pp. 1666–1675, 1954.

[102] C. Glader, G. Hognas, P. Makila, and H. Toivonen, "Approximation of delay systems a case study," *International Journal of Control*, vol. 53, no. 2, pp. 369–390, 1991.

[103] G. Gu, P. P. Khargonekar, and E. B. Lee, "Approximation of infinite-dimensional systems," *IEEE Transactions on Automatic Control*, vol. 34, no. 6, pp. 610–618, 1989.

[104] J. Lam, "Convergence of a class of Padé approximations for delay systems," *International Journal of Control*, vol. 52, no. 4, pp. 989–1008, 1990.

[105] J. Lam, "Model reduction of delay systems using Padé approximants," *International Journal of Control*, vol. 57, no. 2, pp. 377–391, 1993.

[106] P. M. Mäkilä, "Approximation of stable systems by Laguerre filters," *Automatica*, vol. 26, no. 2, pp. 333–345, 1990.

[107] P. M. Mäkilä, "Laguerre series approximation of infinite dimensional systems," *Automatica*, vol. 26, no. 6, pp. 985–995, 1990.

[108] J. R. Partington, "Approximation of delay systems by Fourier-Laguerre series," *Automatica*, vol. 27, no. 3, pp. 569–572, 1991.

[109] J. Lam, "Analysis on the Laguerre formula for approximating delay systems," *IEEE Transactions on Automatic Control*, vol. 39, no. 7, pp. 1517–1521, 1994.

[110] M. Yoon and B. Lee, "A new approximation method for time-delay systems," *IEEE Transactions on Automatic Control*, vol. 42, no. 7, pp. 1008–1012, 1997.

[111] P. M. Mäkilä and J. R. Partington, "Laguerre and Kautz shift approximations of delay systems," *International Journal of Control*, vol. 72, no. 10, pp. 932–946, 1999.

[112] P. M. Mäkilä and J. R. Partington, "Shift operator induced approximations of delay systems," *SIAM Journal on Control and Optimization*, vol. 37, no. 6, pp. 1897–1912, 1999.

[113] C. Harkort and J. Deutscher, "Krylov subspace methods for linear infinite-dimensional systems," *IEEE Transactions on Automatic Control*, vol. 56, no. 2, pp. 441–447, 2011.

[114] W. Michiels, E. Jarlebring, and K. Meerbergen, "Krylov-based model order reduction of time-delay systems," *SIAM Journal on Matrix Analysis and Applications*, vol. 32, no. 4, pp. 1399–1421, 2011.

[115] W. Michiels, E. Jarlebring, and K. Meerbergen, "A projection approach for model reduction of large-scale time-delay systems, with application to a boundary controlled PDE," in *Proceedings of the 50^{th} Conference on Decision and Control and European Control Conference*, (Orlando, FL, USA), pp. 3482–3489, IEEE, 2011.

[116] W. Michiels, G. Hilhorst, G. Pipeleers, and J. Swevers, "Model order reduction for time-delay systems, with application to fixed-order H_2 optimal controller design," in *Recent Results on Time-Delay Systems*, pp. 45–66, Springer, 2016.

[117] J. Rommes and N. Martins, "Efficient computation of multivariable transfer function dominant poles using subspace acceleration," *IEEE Transactions on Power Systems*, vol. 21, no. 4, p. 1471, 2006.

[118] J. Rommes and N. Martins, "Efficient computation of transfer function dominant poles using subspace acceleration," *IEEE Transactions on Power Systems*, vol. 21, no. 3, pp. 1218–1226, 2006.

[119] J. Rommes and N. Martins, "Computing transfer function dominant poles of large-scale second-order dynamical systems," *SIAM Journal on Scientific Computing*, vol. 30, no. 4, pp. 2137–2157, 2008.

[120] J. Rommes and G. L. Sleijpen, "Convergence of the dominant pole algorithm and Rayleigh quotient iteration," *SIAM Journal on Matrix Analysis and Applications*, vol. 30, no. 1, pp. 346–363, 2008.

[121] M. Saadvandi, K. Meerbergen, and E. Jarlebring, "On dominant poles and model reduction of second order time-delay systems," *Applied Numerical Mathematics*, vol. 62, no. 1, pp. 21–34, 2012.

[122] Y. Zhang and Y. Su, "A memory-efficient model order reduction for time-delay systems," *BIT Numerical Mathematics*, vol. 53, no. 4, pp. 1047–1073, 2013.

[123] J. Cullum and T. Zhang, "Two-sided Arnoldi and nonsymmetric Lanczos algorithms," *SIAM Journal on Matrix Analysis and Applications*, vol. 24, no. 2, pp. 303–319, 2002.

[124] Q. Wang, Y. Wang, E. Y. Lam, and N. Wong, "Model order reduction for neutral systems by moment matching," *Circuits, Systems, and Signal Processing*, vol. 32, no. 3, pp. 1039–1063, 2013.

[125] G. Scarciotti and A. Astolfi, "Model reduction of neutral linear and nonlinear time-invariant time-delay systems with discrete and distributed delays," *IEEE Transactions on Automatic Control*, vol. 61, no. 6, pp. 1438–1451, 2016.

[126] A. de Jesus Kozakevicius and T. Kalmár-Nagy, "Weak formulation for delay equations," in *Proceedings of the 9th Brazilian Conference on Dynamics, Control and Their Applications*, (Serre Negra, São Paolo, Brazil), pp. 732–736, 2010.

[127] S. Chakraborty, S. S. Kandala, and C. P. Vyasarayani, "Reduced ordered modelling of time delay systems using galerkin approximations and eigenvalue decomposition," *International Journal of Dynamics and Control*, vol. 7, no. 3, pp. 1065–1083, 2019.

[128] D. Breda, S. Maset, and R. Vermiglio, *Stability of Linear Delay Differential Equations: A Numerical Approach with MATLAB*. New York, NY, USA: Springer, 2015.

[129] J. Apkarian, P. Karam, and M. Lévis, *Student Workbook: Inverted Pendulum Experiment for LabVIEW Users*. Quanser Inc., 2012.

[130] T. G. Molnar, D. Hajdu, and T. Insperger, "The Smith predictor, the modified Smith predictor, and the finite spectrum assignment: A comparative study," in *Stability, Control and Application of Time-delay Systems*, pp. 209–226, Elsevier, 2019.

[131] K. Engelborghs, T. Luzyanina, and G. Samaey, "DDE-BIFTOOL: A MATLAB package for bifurcation analysis of delay differential equations," *Tech. Rep. TW 305, Department of Computer Science, Katholieke Universiteit Leuven, Belgium*, 2000.

[132] G. H. Golub and C. F. Van Loan, *Matrix Computations*. Baltimore, MD, USA: Johns Hopkins University Press, 2012.

[133] A. Sadath and C. P. Vyasarayani, "Galerkin approximations for stability of delay differential equations with time periodic delays," *Journal of Computational and Nonlinear Dynamics*, vol. 10, no. 6, p. 061008, 2015.

[134] A. Sadath and C. P. Vyasarayani, "Galerkin approximations for stability of delay differential equations with time periodic coefficients," *Journal of Computational and Nonlinear Dynamics*, vol. 10, no. 2, p. 021011, 2015.

[135] X. S. Yang, *Nature-Inspired Optimization Algorithms*. London, UK: Elsevier, 2014.

[136] D. Lehotzky and T. Insperger, "A pseudospectral tau approximation for time delay systems and its comparison with other weighted-residual-type methods," *International Journal for Numerical Methods in Engineering*, vol. 108, no. 6, pp. 588–613, 2016.

[137] Z. Ahsan, T. K. Uchida, and C. P. Vyasarayani, "Galerkin approximations with embedded boundary conditions for retarded delay differential equations," *Mathematical and Computer Modelling of Dynamical Systems*, vol. 21, no. 6, pp. 560–572, 2015.

[138] R. J. Radke, *A Matlab implementation of the implicitly restarted Arnoldi method for solving large-scale eigenvalue problems*. PhD thesis, Rice University, 1996.

[139] B. Heizer and T. Kalmár-Nagy, "Proper orthogonal decomposition and dynamic mode decomposition of delay-differential equations," *IFAC-PapersOnLine*, vol. 51, no. 14, pp. 254–258, 2018.

[140] W. Michiels, G. Hilhorst, G. Pipeleers, T. Vyhlídal, and J. Swevers, "Reduced modelling and fixed-order control of delay systems applied to a heat exchanger," *IET Control Theory & Applications*, vol. 11, no. 18, pp. 3341–3352, 2017.